Preparation, Morphology and Thermal/Mechanical Properties of Epoxy-Nanoclay Composites

WANG LEI

(B. Sci, University of Science & Technology of China)

A THESIS SUBMITTED

FOR THE DEGREE OF PH. D OF PHILOSOPHY

DEPARTMENT OF MATERIALS SCIENCE

NATIONAL UNIVERSITY OF SINGAPORE

2005

Acknowledgement

I would like to express my deepest gratitude to my supervisors, Dr He Chaobin and Dr Zhang Yongwei, for their continuous care and guidance in the past years. Their advices will be great fortune to me in my future career and life.

It's my pleasure to give my great thanks to all staff and students in IMRE for their help in my work. My hearty appreciation should be given to Dr Liu Tianxi and Dr Wang Ke for discussions and advices in my research. My special thanks are given to Mr Chen Ling, Mr In Yee, Ms Wuiwui and Ms Shen Lu, for their assistance in preparation and characterization of materials. I would also like to show my sincere thanks to Mr Zhao Wei, Mr Poh Chong, Ms Shue Yin and Ms Doreen for their help in experiment.

I want to show my acknowledgement to National University of Singapore and Institute of Material Research and Engineering for providing me with the opportunity to pursue my Ph. D degree as well as facilities to conduct my research.

I am indebted to my wife and parents. Their support and encouragement are important for me to finish this thesis.

Table of contents

Summary

The continuing search for high strength-to-weight ratio polymeric materials that meet performance requirements for demanding applications, yet possess reasonable processability, has until recently been focused on reinforced nanocomposite materials. In the past decade, organic/inorganic nanocomposites have been demonstrated exceptional properties and these materials may supplant some traditional composite materials for a wide variety of structural and high temperature applications. Polymer-nanoclay composites with exfoliated clay nano-platelets have exceptionally high modulus compared to those consisting of conventional micro-sized fillers of the same chemical composition. In addition, such materials also exhibit a range of highly desirable physical properties, such as outstanding flame retardant and barrier properties.

In the preparation of polymer-clay nanocomposites, organoclays are the most commonly used fillers, which have been showing great success in thermoplastic materials. However, for high temperature epoxy system (thermoset system) where high thermal mechanical property is critical for its application, organoclays have many disadvantages. The large amounts of surfactants (30-40 wt%) employed in preparing organoclays affect the thermal mechanical properties of the resulted nanocomposites and increase cost of the products. The aim of this research is to synthesize highly exfoliated epoxy-clay nanocomposites with reduced or eliminated clay surface modifiers, and systematically study the effect of clay on the morphology and thermal/mechanical properties of the nanocomposites.

In this thesis, three types of clay exfoliation approaches, using different amount of surfactant, have been employed. Among the three approaches, two innovated methods are developed to prepare epoxy-clay nanocomposites with reduced/eliminated surfactants as compared to the normally used commercial organoclay, the southern clay 93A, which is widely used with 30 wt% of alkyl-ammonium ions surfactant modifier. Self-modified raw clay with 5 wt% silane surfactant and raw clay with no surface modifier are used as comparisons. The epoxy resin used is bifunctional diglycidyl ether of bisphenol-A (DGEBA) cured with diethyltoluene diamine (DETDA).

The effects of different approaches to the morphology of the composites were studied by using optical microscopy (OM), wide angle X-ray scattering (WAXS) and transmission electron microscopy (TEM). The effects of different clays on the mechanical properties of the nanocomposites were studied by using tensile (ASTM D638) and 3-point bend tests (ASTM D5045), and the thermal properties of the cured systems were studied using dynamic mechanical analysis (DMA). The deformation and fracture behavior of the nanoclay composites were investigated based on the scanning electron microscopy (SEM) observations on the fracture surfaces of neat epoxy and the nanocomposites. In addition, the hydrothermal effects on the thermal/mechanical properties of the highly exfoliated epoxy-clay nanocomposites were also investigated.

It has been found that morphologies of the composites were significantly influenced by different preparation methods, which also lead to a dramatic change in their thermal and mechanical properties of the resulting nanocomposites. The relations between the

morphologies and properties were discussed and possible reinforcing mechanisms were proposed.

List of tables

List of figures

List of symbols

Abbreviation	Annotation
AFM	Atomic Force Microscopy
DGEBA	Diglycidyl Ether of Bisphenol A
DMA	Dynamic Mechanical Analysis
EDTDA	Diethyltoluene Diamine
E	Young's Modulus
E′	Storage Modulus
E″	Loss Modulus
FTIR	Fourier Transform InfraRed
G_{IC}	Energy Release Rate
K_{IC}	Model I Critical Stress Intensity Factor
OM	Optical Microscopy
SEM	Scanning Electron Microscopy
TEM	Transmission Electron Microscopy
Tg	Glass Transition Temperature
ToF-SIMS	Time-of-Flight Secondary Ion Mass Spectrometry
WAXS	Wide Angle X-ray Scattering
θ	Incident Angle
λ	Wave Length

List of publications

1. Wang K, Wang L, Wu JS, Chen L, He CB. ***Preparation of highly exfoliated epoxy-clay nanocomposites by "hydro-compounding" technique: process and mechanisms.*** *Langmuir*, 2005; 21: 3613-3618.
2. Wang L, Liu TX, Tjiu WC, Teh SF, He CB. ***Fracture and toughening behavior of Aramid fiber-epoxy composites.*** *Polym. Compos.*, 2005; 26: 333-342.
3. Wang L, Liu TX, Tjiu WC, He CB. ***Preparation, characterization, and mechanical properties of epoxy-clay nanocomposites.*** *Scientific Israel - Technological Advantages (SITA-Journal)*, 2005; Vol. 7, invited paper.
4. Teh SF, Liu TX, Wang L, He CB. ***Fracture behavior of poly(ethylene terephthalate) fiber toughened epoxy composites***. *Composite A*, 2005; 36: 1167-1173.
5. Wang L, Wang K, Chen L, Zhang YW, He CB. ***Prepartion, morphology and thermal/mechanical properties of epoxy-nanoclay composite.*** *Composite A*, in press.
6. Wang L, Wang K, Chen L, Zhang YW, He CB. ***Hydrothermal effects on the thermal/mechanical properties of high performance epoxy-clay nanocomposites.*** *Polym. Eng. Sci.*, 2006; 46: 215-221.
7. Wang L, Wang K, Chen L, Wu JS, He CB. ***Microwave-assisted exfoliation and mechanical properties of epoxy-raw clay nancomposites.*** *Polymer*, submitted.
8. Shen L, Wang L, He CB, Liu TX. ***Nanoindentation and morphological study of epoxy-organoclay nanocomposites.*** *Nanotechnology*, submitted.

Chapter 1. Introduction

Cured epoxy is known to exhibit excellent properties for engineering application, such as high stiffness and strength, creep resistance and chemical resistance. However, like most of the thermoset plastics, epoxy is intrinsically brittle, which limits its wider application. Consequently, enormous effort has been paid to improve the fracture toughness of epoxy while still maintaining their desirable properties.

One approach to toughen epoxy is to add a second phase of polymeric particles, such as rubbers and thermoplastics. But the addition of soft particles often results in a significant loss of modulus and stiffness. And the addition of large mount of thermoplastic modifier can cause a significant decrease in some of the other desirable properties, such as glass transition temperature and solvent resistance.

Another approach in epoxy toughening is to use fiber as the reinforcement. Fiber reinforced composite materials consist of fibers of high strength and modulus embedded in or bonded to a matrix with distinct interface between them. In this form, both fiber and matrix retain their physical and chemical properties. They produce a combination of properties that cannot be achieved by either of the component alone. Fibers incorporated into the matrix could be of continuous length or discontinuous length. Discontinuous fiber reinforced composite have lower strength and modulus than continuous fiber composites. However, with random orientation of fibers, it is possible to obtain nearly equal mechanical and physical properties in all direction.

Addition of nano-fillers is a new type of reinforcing method. Nanocomposite is a new kind of composites that are particle filled polymers for which at least one dimension of the dispersed phase is in nanometer range. Materials with feature of nanometer scale often exhibit superior properties as compared to their macro-scale counterparts, such as strength, stiffness, thermal stability, and barrier properties. Another unique benefit of nanocomposite is the lack of trade-offs. For the first time, there is an opportunity to design materials without trade-off that is typically found in conventional polymer composites. In general, nanocomposites consist of a nanometer scale phase combined with another phase. Classified by nano-filler dimension, there are a number of types of nanocomposites, such as zero dimension (nanoparticle), one dimension (nanotube or whisker), two dimension (clay or layered silicate) and three dimension (polyhedral oligomeric silsesquioxane (POSS)).

Nanoclay reinforced polymers are just one example of the large variety of new materials with nano-scale fillers and inorganic/organic hybrid materials, which are being developed and investigated. Clays have been recognized as potential useful filler in polymer composites because of their high aspect ratio and platy morphology. Since the pioneer work by Toyota research group **(1-4)**, many research activities have been focusing on polymer-clay nanocomposites. It has been demonstrated that nanocomposites consisting of nanometer-sized, exfoliated clay layers have exceptionally high modulus as compared to conventional composites filled with micron-sized fillers of the same composition **(5-7)**. Such materials also exhibit other desirable physical properties, such as flame retardant and gas barrier properties **(8-9)**.

However, since clays are hydrophilic and do not have good compatibility with the hydrophobic polymer matrix to achieve good dispersion, surface modification by ion exchange is often applied to the clay before incorporating into polymer matrix, which renders the layer surface hydrophobic and increases the interlayer spacing to facilitate polymer penetrating. But this modification also leads to negative effects. Many alkyl-ammonium chains are introduced to the layer surface, which cause the interface between the layers and polymer matrix to be very complex and affect the composite properties. The existence of organic modification lowers the reinforcing effect of clay, and makes it difficult to understand the underlying mechanism. The influence of organoclay on the α- and β-transition of the composite has been reported by Simon **(10)**. It is likely that the motions of polymer chains can be affected by organoclay. Indeed, Pinnavaia and Beall **(9)** claim that in thermoplastic materials, for a concentration of 5% exfoliated clay, some 50% of polymer chains are affected by the organoclay surface. On the other hand, the modification also increases the cost of the product.

Therefore, there is a need to develop new approaches to disperse clay with reduced or eliminated surface modification into polymer matrix. It's the purpose of this work to achieve well-exfoliated epoxy-clay nanocomposites with reduced/eliminated surfactant and investigate the origin of the reinforcement effect, the fracture behavior of these materials and a rational way to toughen them.

The objectives of this research are:

i) to achieve a better exfoliation of clay in the polymer matrix. This will include clay modification and also processing optimization;

ii) to investigate the effect of clay on the mechanical properties of the resulting nanocomposites, in particular the fracture mechanisms of a series of nanocomposites, and to investigate possible approaches to toughening.

In this research, new processing techniques were developed to facilitate exfoliation of clay in the preparation of epoxy-clay nanocomposite. The morphology of the nanocomposites was characterized with optical microscopy (OM), wide angle X-ray scattering (WAXS) and transmission electron microscopy (TEM). The mechanical properties and fracture behavior of the nanocomposites were studied by tensile and 3-point bend tests. Microscopic mechanisms for deformation and fracture were investigated on several length scales ranging from the macroscopic to the nanometer levels. These mechanisms were related to the morphology and nanostructure of the materials. After an introduction of current status in polymer-clay nanocomposites research in Chapter 2, Chapter 3 will describe the materials and the characterization techniques used in this research in detail.

Clay exfoliation is the crucial step in this study. Different approaches will be developed to achieve exfoliation, which will be described in Chapters 4, 5 and 6. Chapter 4 will describe our research based on commercially available organoclay system, while Chapter 5 and 6 will focus on our new approaches based on “microwave-assisted exfoliation” and

"solvent-assisted silane-modified clay system" respectively. In these researches, morphology of the nanocomposites was studied by OM, WAXS, SEM and TEM from different scales. Experiments were conducted to investigate the thermal/mechanical properties of the blends, and possible relationships between the morphology and properties of nanocomposites were studied. In addition, hydrothermal effect on the thermal/mechanical properties of fully exfoliated epoxy-clay nanocomposite will also be addressed in Chapter 6. Finally Chapter 7 and Chapter 8 will draw some conclusions and propose future work.

The results of this study could be helpful for industry to achieve composite materials with better properties at lower cost. The mechanisms investigation will illuminate the reinforcing effect and help to design new composite materials with better mechanical properties.

References:

1. Kojima Y, Usuki A, Kawasumi M, Okada A, Kurauchi T, Kamigaito O. *J. Polym. Sci: Polym. Chem.*, 1993; 31: 983-986.
2. Usuki A, Kawasumi M, Kojima Y, Okada A, Kurauchi T, Kamigaito O. *J. Mater. Res.*, 1993; 8: 1174-1178.
3. Usuki A, Kojima Y, Kawasumi M, Okada A, Fukushima Y, Kurauchi T, Kamigaito O. *J. Mater. Res.*, 1993; 8: 1179-1184.
4. Kojima Y, Usuki A, Kawasumi M, Okada A, Fukushima Y, Kurauchi T, Kamigaito O. *J. Mater. Res.*, 1993; 8: 1185-1189.

5. Giannelis EP. *Appl. Organomet. Chem.*, 1998; 12: 675-680.
6. LeBaron PC, Wang Z, Pinnavaia TJ. *Appl. Clay. Sci.*, 1999; 15: 11-29.
7. Gilman JW. *Appl. Clay. Sci.*, 1999; 15: 31-49.
8. Porter D, Metcalfe E, Thomas MJK. *Fire. Mater.*, 2000; 24: 45-52.
9. Pinnavaia TJ, Beal GW (Ed.). *Polymer-Clay Nanocomposites. Chichester: Wiley*, (2000).
10. Becker O, Varley R, Simon G. *Polymer*, 2002; 43: 4365-4373.

Chapter 2. Development of polymer-nanoclay composites

2.1 Background

The term "nanocomposites" describes a two-phase material with one of the phases dispersed in the second one at a nanometer level. This term is commonly used in two distinct areas of materials science: ceramics and polymers. Polymer nanocomposites are commonly based on polymer matrices reinforced by nano-fillers such as silica beads, nanotubes, as well as cellulose whiskers.

Clays are layered silicates with a layer thickness around 1 nm and the lateral dimensions of the layers around several hundred nanometers. They have been recognized as potential useful fillers in polymer composites because of their high aspect ratio and platy morphology. Polymer-clay interactions have been studied for many years but it is only recently that researchers from Toyota **(1)** discovered the possibility to build nanostructures from blending polymer and organophilic clay. Their material based on polyamide-6 and organophilic montmorillonite showed dramatic improvements of mechanical properties and thermal resistance as compared with the pure matrix with only a few percentage of clay content (~ 4 wt%)

Polymer-clay composites can be divided into three general types (Figure 2.1): conventional composites where the clay acts as a conventional filler, intercalated nanocomposites consisting of a regular insertion of the polymer in between the clay

layers and exfoliated nanocomposites where 1 nm-thick layers are dispersed in the matrix forming a monolithic structure on the micro-scale. The latter morphology is of particular interest because it maximizes the polymer-clay interactions. This could lead to dramatic changes in mechanical and physical properties.

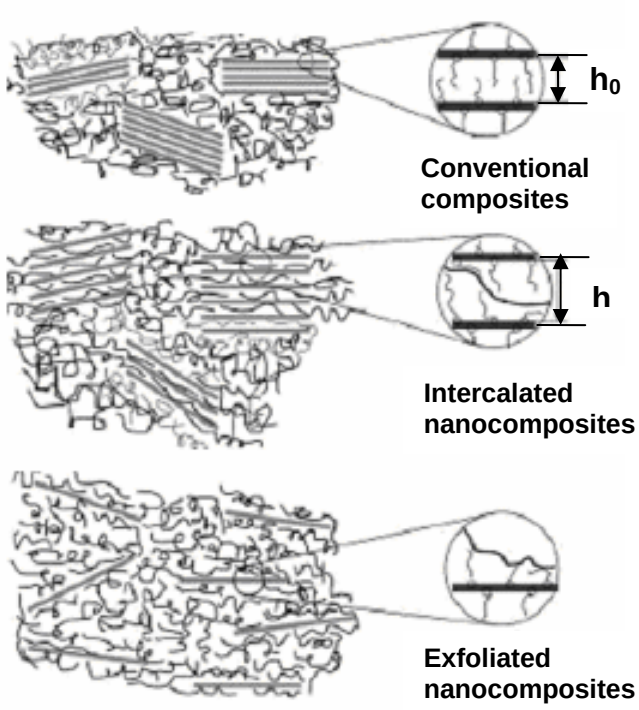

Figure 2.1. The three idealized structures of polymer-clay composites (reproduced from **(2)**).

2.1.1 Clay information

2.1.1.1 Structure of clay

The layered silicates commonly used in nanocomposites belong to the structural family known as the 2:1 phyllosilicates. Their crystal lattice, as shown in Figure 2.2 **(3)**, consists of two fused silica tetrahedral sheets sandwiching an edge-shared octahedral sheet of either aluminum or magnesium hydroxide. The layer thickness is around 1 nm and the

lateral dimensions of these layers may vary from 300 Å to several microns or even larger depending on the particular silicate. These layers organize themselves to form stacks with a regular van der Waals gap in between them called the interlayer or the gallery. Isomorphous substitutions of Si^{4+} for Al^{3+} in the tetrahedral sheet and of Al^{3+} for Mg^{2+} in the octahedral sheet cause an excess of negative charges within the layers. These negative charges are counterbalanced by cations such as Ca^{2+} and Na^{+} situated between the layers. This type of layered silicate is characterized by a moderate surface charge known as the cation exchange capacity (CEC), and generally expressed as Mequiv/100g. This charge is not locally constant, but varies from layer to layer, and must be considered as an average value over the whole crystal. Due to the high hydrophilic nature of the clay, water molecules are usually also present between the layers. The sum of the single layer thickness (0.96 nm) and the interlayer represents the repeat unit of the multiplayer material, also called d-spacing or basal spacing. The d-spacing between the silica-alumina-silica units varies from 0.96 nm to 20 nm when the clay is dispersed from the collapsed state into water solution.

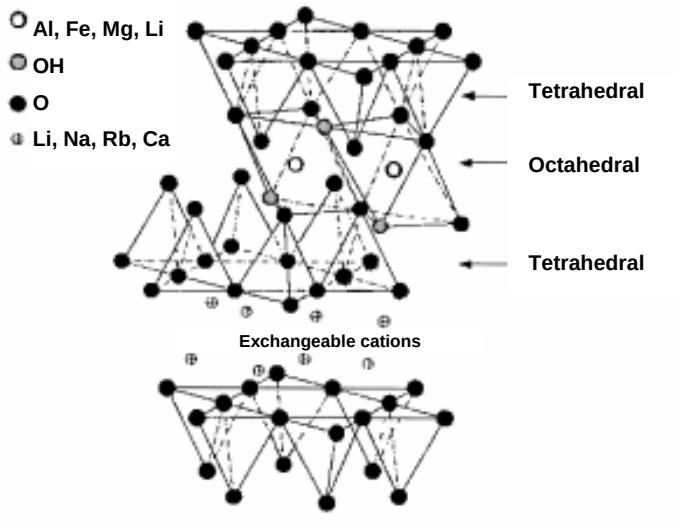

Figure 2.2. Structure of 2:1 phyllosilicates (reproduced from **(3)**).

Montmorillonite (MMT), hectorite, and saponite are the most commonly used layered silicates, which have the same crystal structure yet different chemical formula. Details regarding the structure and chemistry for these layered silicates are provided in Figure 2.2 **(3)** and Table 2.1 respectively.

Table 2.1. Chemical formulas and characteristic parameters of commonly used 2:1 phyllosilicates.

Phyllosilicates	Chemical formula	CEC (mequiv/100g)	Particle length (nm)
Montmorillonite	$M_x(Al_{4-x}Mg_x)Si_8O_{20}(OH)_4$	110	100-150
Hectorite	$M_x(Mg_{6-x}Li_x)Si_8O_{20}(OH)_4$	120	200-300
Saponite	$M_xMg_6(Si_{8-x}Al_x)Si_8O_{20}(OH)_4$	86.6	50-60

M, monovalent cation; x, degree of isomorphous substitution (between 0.5 and 1.3).

2.1.1.2 Clay surface modification and organoclay structures

Since the silicate layers are hydrophilic and do not have good interaction with hydrophobic polymer matrix, clay surface modifications are usually necessary before incorporation with polymer. In order to make the galleries more organophilic, the hydrated cations of the interlayer can be exchanged with cationic surfactants such as alkyl-ammonium or alkyl-phosphonium. The organically modified clay (or organoclay) being organophilic and of a lower surface energy, is more compatible with organic polymers. These polymers may be able to intercalate within the galleries. The most widely used alkyl-ammonium ions are based on primary alkyl-amines, which are put in an acidic medium to protonate the amine function. Their basic formula is CH_3-$(CH_2)_n$-

NH_3^+ where n is between 1 and 18. It is noted that the length of the ammonium ions has a strong impact on the resulting structure of nanocomposites. Lan et al **(4)** showed that alkyl-ammonium ions with chain length larger than eight carbon atoms favor the synthesis of delaminated nanocomposites whereas alkyl-ammonium ions with shorter chains lead to the formation of intercalated nanocomposites.

The replacement of inorganic exchange cations by organic onium ions on the gallery surfaces of clays not only serves to match the clay surface polarity with the polarity of the polymer, but also expand the clay galleries. This facilitates the penetration of the gallery space by either the polymer precursors or preformed polymer. Depending on the charge density of clay and onium ion surfactant, different arrangements of the onium ions are possible. In general, the longer the surfactant chain length, and the higher the charge density of the clay, the further apart the clay layers will be forced. This is expected since both of these parameters contribute to increasing the volume occupied by the intragallery surfactant. Depending on the charge density of the clay, the onium ions may lie parallel to the clay surface as a monolayer, a lateral bilayer, a pseudo-trimolecular layer, or an inclined paraffin structure as illustrated in Figure 2.3 **(5)**.

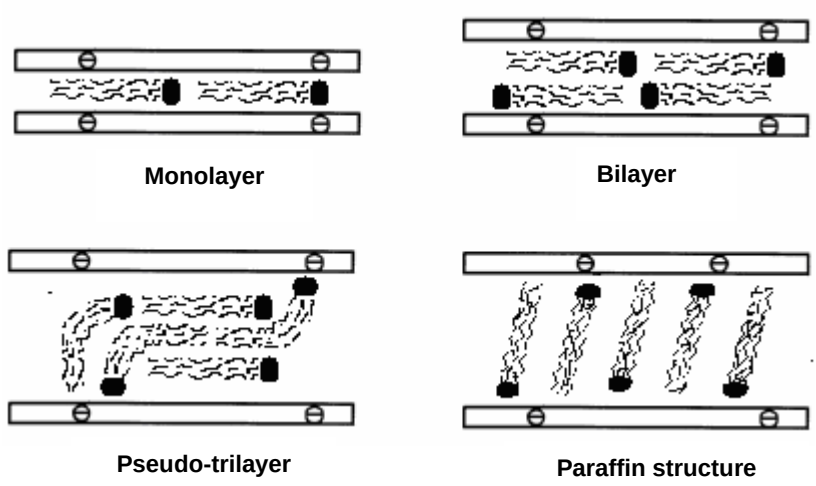

Figure 2.3. Orientations of alkyl-ammonium ions in the galleries of layered silicates with different layer charge densities (adapted from **(5)**).

2.1.1.3 Synthetic organoclay

The main incentive for using synthetic clays is that several interesting clay minerals are not available in sufficient quantities in their natural form (e.g. beidellite). Another aim lies in designed materials applications. Variables such as purity, composition, reproducibility, and specifically designed features can be better controlled in this way than by using natural clay specimens which typically contain impurities. Synthetic montmorillonite typically requires high temperatures, in the 300-400^{o}C range, and autogenous pressure conditions to afford the best purity and crystallinity in reasonable time frames. Hectorite on the other hand, which forms at low temperatures and pressures in nature, is amenable to crystallization under much less rigorous conditions. Kloprogge discussed these conditions for many types of clay in his review article **(6)**.

2.1.2 Properties of polymer-clay nanocomposites

Delamination of a relatively low amount of clay can trigger a tremendous properties improvement of the polymers in which they are dispersed. Significant increase in Young's modulus **(7)**, thermal stability **(8)**, fire resistance **(9)**, and barrier properties **(10)** has been achieved at low clay concentration.

2.1.2.1 Tensile properties

It was first reported by the Toyota researchers that the tensile strength of polyamide-6 was increased by 55% and the modulus by 90% with the addition of only 4 wt% of delaminated clay **(11)**. Later, Lan and Pinnavaia **(12)** reported more than a ten-fold increase in strength and modulus in a rubbery epoxy matrix with only 15 wt% of delaminated organoclay.

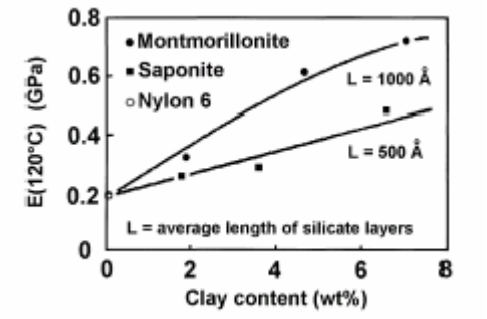

Figure 2.4. Dependence of tensile modulus E at 120^{o}C on clay content for organo-modified montmorillonite and saponite-based nanocomposites (reproduced from **(13)**).

Kojima et al **(13)** investigated the dependence of Young's modulus measured at 120^{o}C for exfoliated nylon-6-clay nanocomposites with various clay contents. As shown in Figure 2.4, the dependence clearly indicates that the ability of dispersed silicate layers to increase the Young's modulus of nylon-6-based nanocomposites can be directly related to

the average length of the layers, hence to the aspect ratio of the dispersed nanoparticles. Moreover, the degree of delamination of the clay in the polymer matrix, which increases the interaction between the clay layers and the polymer, strongly influences the measured Young's modulus values **(7)**. All these observations are furthermore confirmed in Figure 2.5 that presents the evolution of the Young's modulus of nylon-6 nanocomposites in function of filler weight content measured at room temperature **(14)**.

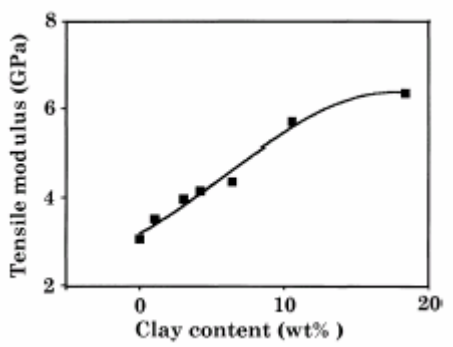

Figure 2.5. Effects of clay content on tensile modulus, measured at room temperature, of organo-modified montmorillonite-nylon-6-based nanocomposites obtained by melt intercalation (reproduced from **(14)**).

The results indicate that the exfoliated layers are the main factor responsible for the stiffness improvement, while intercalated particles, having a smaller aspect ratio, play a minor role. Several explanations have been given about the reinforcement properties of polymer-clay hybrids based on interfacial properties and restricted mobility of the polymer chains. Shi et al **(15)** proposed interfacial effects, where the direct binding of the polymer to the clay layers, would be the dominant factor. Usuki et al **(16)** also suggested that the strong ionic interaction between polyamide-6 and silicate layers could generate some crystallinity at the interface, explaining part of the reinforcement effect. As mentioned previously, Kojima et al **(13)** also proposed an explanation describing the formation of a constrained region in the vicinity of the clay layers. In their concept, the

contribution of a constrained region where the polymer chains have a restricted mobility could be used to describe the improvement of tensile modulus in polyamide-6-clay hybrid.

2.1.2.2 Fracture

Although the delaminated nanocomposite structure brings a substantial increase of modulus, it lowers the fracture toughness. A study **(17)** performed on polyamide-6-clay nanocomposites shows that the fracture energy G_C is lowered by more than 10 times with the addition of only 4 wt% of delaminated clay. It is thought that the reduction in the extent of plastic deformation in the constrained polymer matrix increases the brittleness of the nanocomposites. In contrast, in the presence of micro-scale aggregates, significant plastic deformation could be observed, leading to a toughness improvement.

On the other hand, the opposite phenomena were also observed in other clay-based systems, that is, adding a small amount of clay into polymer matrix gave rise to higher fracture toughness. Kornmann et al **(18)** reported a toughness improvement of a partially delaminated unsaturated polyester-clay nanocomposite. The non-delaminated clay aggregates might act as stress concentrators and induce plastic deformation around them, permitting an improvement of the fracture toughness. Zerda and Lesser **(19)** studied the fracture behavior of epoxy-clay nanocomposites. The fracture toughness data was given in Figure 2.6. It was notable that the trend at low clay content (less than 5 wt%) is similar to the previous study **(18)**, but further increasing clay content decreased the fracture

toughness. This may be due to the poor clay dispersion at high concentration, which results in the formation of big clusters of clay.

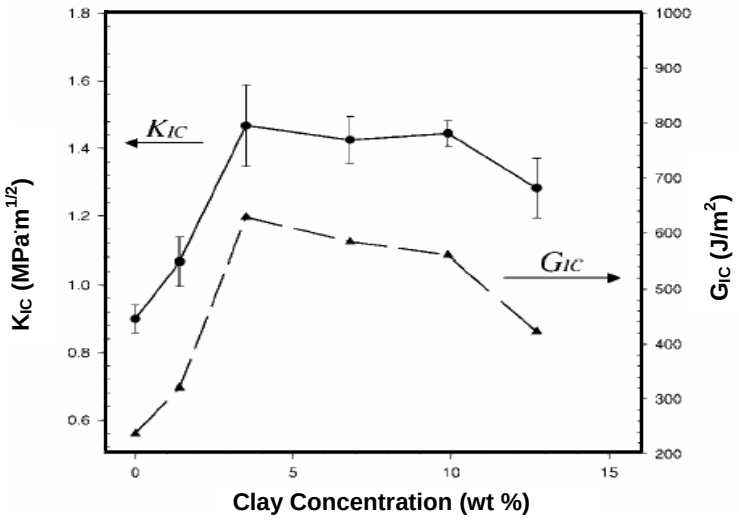

Figure 2.6. Changes in fracture toughness with increasing clay concentration (reproduced from **(19)**).

An attempt to determine the fracture mechanisms at micro-scale for polymer-layered silicate nanocomposites reveals that the failures are located mainly at the polymer/silicate interface **(20)**. The main conclusion of this work is that toughness of nanocomposites should be improved through strengthening of the polymer/surface binding.

2.1.2.3 Dynamic mechanical properties

DMA measures the response of a given material to an oscillatory deformation as a function of temperature. DMA results are expressed by three main parameters: (i) the storage modulus (E′), corresponding to the elastic response to the deformation; (ii) the loss modulus (E″), corresponding to the plastic response to the deformation; (iii) tanδ, the

ratio (E′/E″), useful for determining the occurrence of molecular mobility transitions, such as the glass transition temperature (Tg).

Temperature dependences of the dynamic mechanical spectra (the storage modulus, loss modulus and loss factor tanδ) of polymer upon nanocomposite formation under different experimental conditions have been extensively studied using dynamic mechanical analysis (DMA) **(21-28)**. Laus compared the values of the storage modulus for two sets of samples for which the filler content is varied form 0 to 30 wt% **(21)**. The first series displays the values recorded for nanocomposites filled with organo-modified clay and the second one shows the results obtained for composites prepared by melt-blending the SBS matrix and Na-montmorillonite under the same conditions (microcomposites). As shown in Figure 2.7, remarkable increase in elastic modulus for nanocomposites is achieved while microcomposites do not present any improvement, whatever the filler content is. The influence of clay dispersion and clay surface modification was further investigated by Choi et al **(22)**, where the researchers synthesized exfoliated polyacrylonitrile (PAN)/Na-MMT nanocomposites via emulsion polymerization. It was observed that the storage modulus increased up to 20 wt% of Na-MMT, while the major effect occurs less than 5 wt% of silicate in other nanocomposites. The authors interpreted that exfoliated morphology in the composite has the strongest effect on modulus increase. Meanwhile, pristine silicate and polarity of PAN also affect the enhancement because strong negative C≡N groups in PAN will interact with exfoliated layers of hydrophilic Na-MMT.

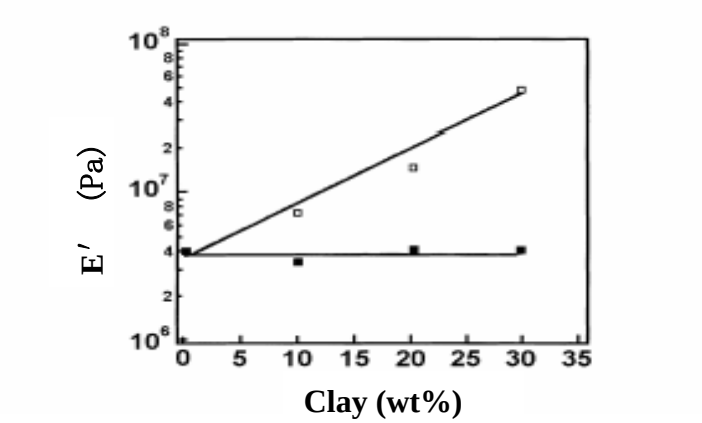

Figure 2.7. Trend of the storage modulus at 25°C for SBS-based nanocomposites (□□) and microcomposites (■■) as a function of the filler level (reproduced from **(21)**).

Figure 2.8 shows the temperature dependences of E′, E″ and tanδ for PP-clay nanocomposites and corresponding PP matrix **(23)**. For the PP-clay nanocomposites, there is a strong enhancement of the modulus over the investigated temperature range, which indicates that the plastic and elastic responses of PP towards deformation are strongly influenced in the presence of organoclay. When the silicate layers are exfoliated/intercalated and thoroughly dispersed in the polymer matrix, the rigid silicate layers directly enhance the stiffness of the polymer-clay nanocomposites. Therefore, the storage modulus of the nanocomposites might exceed that of pure polymer. The loss modulus of the nanocomposites also increases with clay content, because the exfoliation/intercalation of the silicate layers increases the friction between the silicate layers and the polymer molecules as the temperature increases.

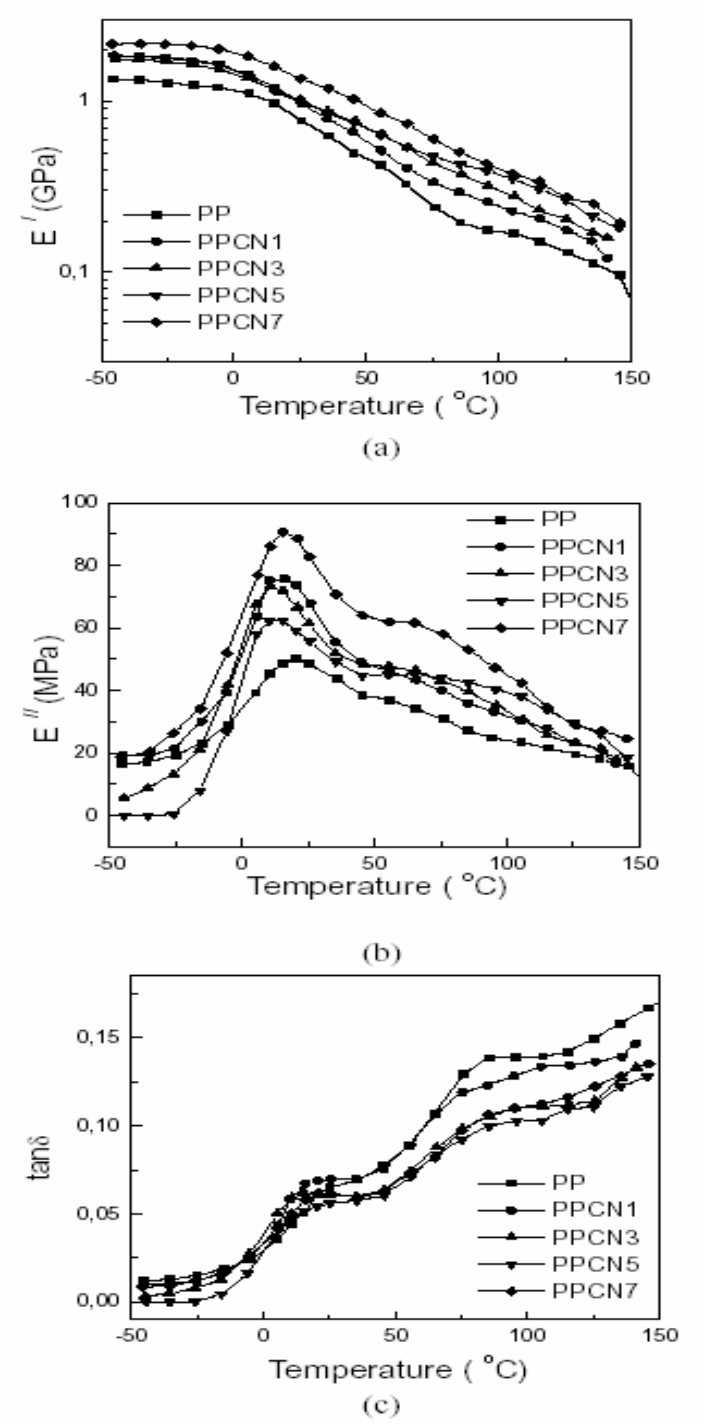

Figure 2.8. Dynamic mechanical spectra ((a) storage modulus; (b) loss modulus; (c) loss factor tanδ) as a function of temperature for PP and PPCN (reproduced from **(23)**).

The loss modulus is useful to elucidate the effect of silicate layers on the α-transition and β-transition of the nanocomposites. The α-transition is related to the Brownian motion of

the main-chains at the transition from the glassy to the rubbery state, which determines the glass transition temperature of the nanocomposites. The β-transition occurs at a lower temperature and is related to the crankshaft rotation of the backbones in the glassy state. When a polymer goes through one of these relaxations, tanδ, the ratio of energy dissipated to energy stored, shows a maximum and provides a very sensitive technique of analyzing the α- and β-relaxations. Figure 2.8(c) shows typical relaxation peaks for PP-clay nanocomposites. It was found that the trend of glass transition temperature (Tg) is not obvious as a function of clay concentration. The glass transition temperatures of polymer-clay nanocomposites were investigated widely **(21-36)**. Both increase and decrease cases have been reported. The segment motion of polymers in the composites was retarded by the delaminated silicate sheets, leading to an increased Tg. However, lack of surrounding entanglements and the small surfactant molecules introduced to clay surface might cause a lower Tg. The mechanism of how the addition of clay affects the Tg of polymer-clay nanocomposites needs to be studied further.

2.2 Synthesis of polymer-layered silicate nanocomposites

Processing techniques are crucial in preparing polymer-clay nanocomposite. To achieve a better nanocomposite, the mineral must be well dispersed into polymer matrix. Similar to polymer blends, any mixture of polymer and clay does not necessarily lead to a nanocomposite. In most cases, the incompatibility of the hydrophobic polymer and the hydrophilic silicate leads to a phase separation similar to that of macroscopically filled systems. In contrast, by using surface-modified silicates, as mentioned earlier, one can fine-tune their surface energy and render them miscible (or compatible) with different

polymers. This concept was first realized by researchers from Toyota who discovered the possibility to build a nanocomposite from polyamide-6 and organophilic clay. Their new material showed dramatic improvements in mechanical and physical properties. Numerous other researchers later used this concept for nanocomposites based on epoxies **(26, 32, 37)**, unsaturated polyester **(18)**, poly (ε-caprolactone) **(38)**, poly (ethylene oxide) **(39)**, silicone rubber **(40, 41)**, polystyrene **(42)**, polyimide **(10)**, polypropylene **(43)**, poly (ethylene terephthalate) **(44)** and polyurethane **(45)**.

Several methods have been used to prepare polymer layered silicate nanocomposites. They include three main processes:

1. In-situ intercalation: a suitable monomer is intercalated into the layers so that the polymerization can occur between the intercalated layers, thus resulting in an intercalated or exfoliated structure;
2. Solution intercalation: the layered silicate is exfoliated into single layers by a polymer dissolved in a solvent. The layered silicate is dispersed in an adequate solvent, and the polymer absorbs onto the delaminated layers. When the solvent evaporated, the layers sandwich the polymer, forming a well-ordered multilayers;
3. Melt intercalation: the layered silicate is mixed with the polymer matrix in the molten stated with or without shear forces. Depending on the compatibility of polymer and layer surface, polymer can crawl into the galleries, producing either an intercalated or an exfoliated nanocomposite.

2.2.1 In-situ polymer-clay nanocomposites

In-situ polymerization was the first method used to synthesize polymer-clay nanocomposites based on polyamide-6 **(11)**. Nowadays, it is the conventional process used to synthesize thermoset-clay nanocomposites. The strategy is illustrated schematically in Figure 2.9.

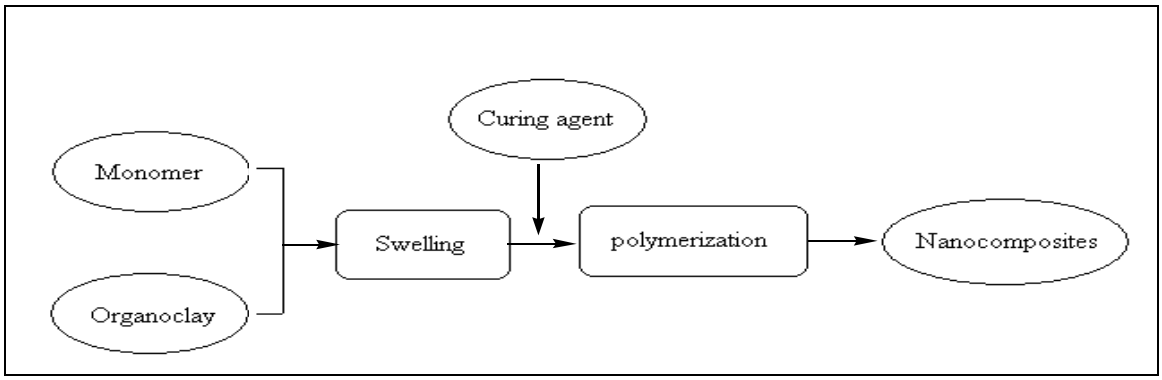

Figure 2.9. Flowchart presenting the different steps of the in-situ polymerization approach.

The key is to control the polymerization occurring between the layers (intragallery polymerization). If the cure kinetics between the layers is lower than outside the layers, then delamination of the clay is embedded. Therefore, one needs to find ways to favor the intragallery polymerization as compared with extragallery polymerization **(46)**.

The driving force for the "in-situ polymerization" method is linked to the polarity of the monomer molecules and the mechanism is believed to be the following. During the swelling phase, the high surface energy of the clay attracts polar monomer molecules so that they diffuse between the clay layers. When certain equilibrium is reached the diffusion stops and the clay is swollen in the monomer to a certain extent corresponding

to a perpendicular orientation of the alkyl-ammonium ions. When the polymerization is initiated, the monomer starts to react with the curing agent. This reaction lowers the overall polarity of the intercalated molecules and displaces the thermodynamic equilibrium so that more polar molecules are driven into between the clay layers. As this mechanism occurs, the organic molecules can eventually delaminate the clay. Polymer-clay nanocomposites based on epoxy **(4)**, polyurethanes **(45)** and polyethylene terephthalate **(44)** have been synthesized by this method.

2.2.2 Solution intercalation

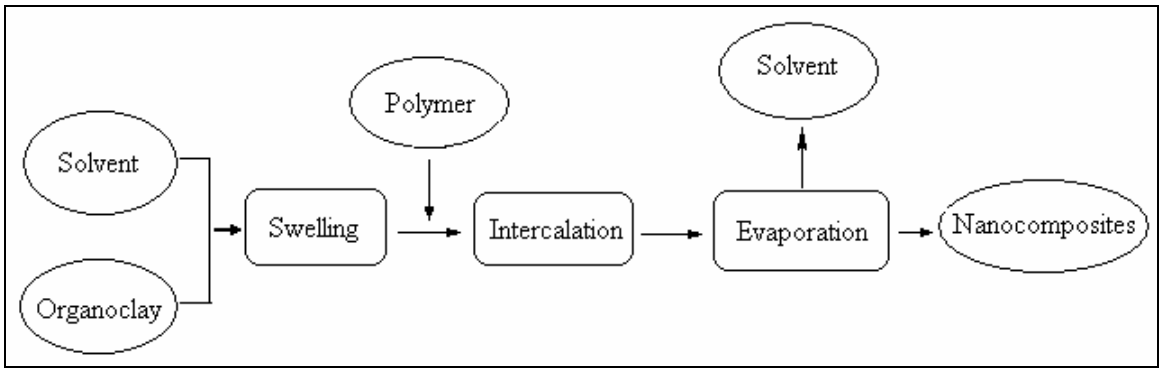

Figure 2.10. Flowchart presenting the different steps of the solution approach.

Polar solvents can be used to synthesize intercalated polymer-clay nanocomposites. The strategy is similar to the one used in the in-situ polymerization approach. The organoclay is first swollen in the solvent. Then, the polymer, dissolved in the solvent, is added to the solution and intercalates between the clay layers. The last step consists in removing the solvent by evaporation usually under vacuum. Figure 2.10 is the schematic description of the process.

The driving force for polymer intercalation from solution is the entropy gained by desorption of solvent molecules. The major advantage of this method is that it offers the possibilities to synthesize intercalated nanocomposites based on polymers with low or even no polarity. Nanocomposites based on high-density polyethelene **(47)**, polyimide **(10)** and nematic liquid crystal polymers **(48)** have been synthesized by this method.

2.2.3 Melt intercalation

The melt intercalation process was first reported by Vaia et al **(42)** in 1993. The strategy consists of blending a molten thermoplastic with an organoclay in order to optimize the polymer-clay interactions. The mixture is then annealed at a temperature above the glass transition temperature of the polymer and forms a nanocomposite (Figure 2.11).

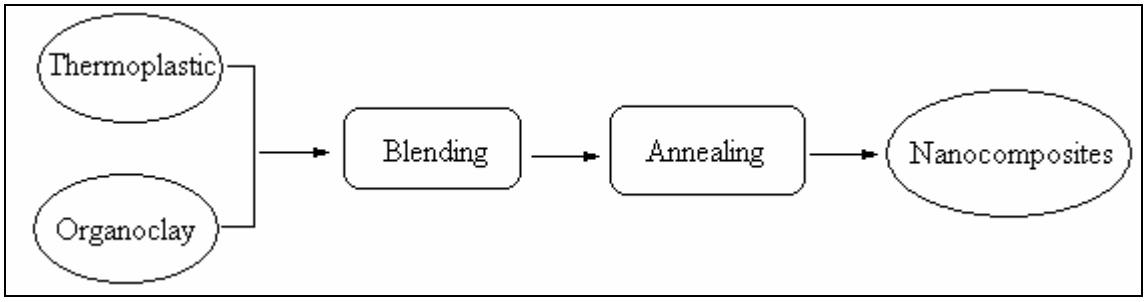

Figure 2.11. Flowchart presenting the different steps of the melt intercalation approach.

Because the unperturbed radius of gyration of the polymer is roughly an order of magnitude greater than the interlamallar spacing **(49)**, the polymer chains experience a dramatic loss of conformational entropy during the intercalation. The proposed driving

force for this mechanism is the important enthalpic contribution of the polymer-organoclay interactions during the blending and annealing steps.

The melt intercalation process has become increasingly popular because of its great potential for application in industry. Indeed, the traditional method such as extrusion can be used for melt intercalation **(50)**. A wide range of thermoplastics, from strongly polar polyamide-6 **(14, 51)** to polystyrene **(52)** has been intercalated between clay layers.

2.3 Polymer-clay nanocomposites

It has been proven in recent years that polymer-based nanocomposites reinforced with a small amount of nano-sized clay particles significantly improve the mechanical, thermal and barrier properties of the pure polymer matrix **(53-57)**. These composites are now being considered for a wide range of applications including packaging, coating, electronics, automotive and aerospace industries. It is generally believed that the improvement of the properties of clay nanocomposites is directly related to the completed exfoliation of silicate layers in the polymer matrix. Layered silicate-based polymer nanocomposites have become an attractive set of organic-inorganic materials not only for their obvious potential as technological materials, but also for providing a convenient macroscopic system to study fundamental scientific issues concerning confined and tethered polymers. Studying the formation, structure and dynamics of these nanocomposites can lead to a better understanding of organic-inorganic hybrids, polymers in a confined environment or at a solid interface and polymer brushes. Although the high aspect ratio of silicate nanolayers is ideal for both industry and scientific fields, the nanolayers are not easily dispersed in most polymers due to their

preferred face-to-face stacking in agglomerated tactoids. In view of this, great efforts have been made to achieve full exfoliation and homogeneous dispersion of clay into polymer matrix **(58-80)**.

2.3.1 Thermoplastic-clay nanocomposites

Clay exfoliation was first achieved in a thermoplastic, nylon-6, matrix **(13, 58, 59)**. Polyamide has been successfully reinforced by addition of fillers such as glass fiber. Compared with these conventional composites, in which polymer and fillers are not homogeneously dispersed on the microscopic scale, clay reinforced nanocomposites exhibit further improved properties. Due to the strong tendency of clay nanoparticles to agglomerate and the intrinsic incompatibility of hydrophilic layered-silicates and the hydrophobic engineering plastics, dispersion of the tactoids into discrete monolayers is greatly hindered. However, as was first demonstrated by the Toyota group **(57)**, the replacement of the inorganic exchange cations in the galleries of the native clay by alkyl-ammonium surfactants can compatibilize the surface chemistry of the clay and hydrophobic polymer matrix. ε-caprolactam was polymerized in the interlayer gallery region of the organoclay to form a true nylon-6-clay nanocomposite **(13, 58, 59)**. Individual silicate layers of montmorillonite were completely exfoliated and homogeneously dispersed in nylon-6 matrix, as revealed by WAXS and transmission electron microscopy (TEM). There are significant improvements in the properties of nylon-6-clay nanocomposites containing 4.2 wt% clay compared with pure nylon-6. The modulus doubled, the strength increased more than 50% and the heat distortion temperature increased 80^{o}C compared to pristine nylon-6. Exfoliated nylon-6-organoclay

nanocomposites also demonstrated significant improvements in dimensional stability, barrier properties and flame retardant properties.

Since the pioneering work on nylon-6-clay nanocomposites by the Toyota group, many investigations on preparation and characterization have been followed **(13-16, 25)**, and great success has been achieved. Liu et al prepared nylon-11-organoclay nanocomposites via melt-compounding method using a Brabender twin-screw extruder at 220^{o}C with a screw speed of 80 rpm **(25)**. The clay dispersion within nylon-11 matrix was characterized by both WAXS and TEM. Figure 2.12 shows the WAXS patterns for neat nylon-11 and its organoclay nanocomposites with different clay concentrations. The basal plane of clay disappears after incorporating with nylon-11 by melt-compounding, indicating the delamination and dispersion of the clay nanolayers within the nylon-11, i.e. the formation of an exfoliated nanostructure with clay loading levels up to 8 wt%.

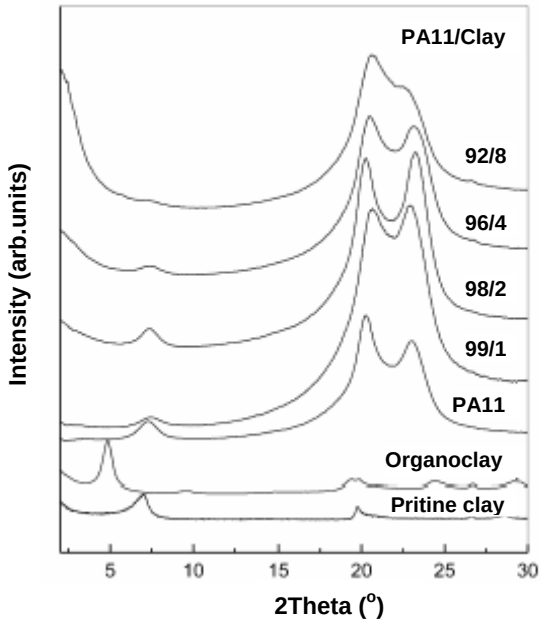

Figure 2.12. WAXS patterns of the pristine and modified clay; neat PA-11 and its organoclay nanocomposites (reproduced from **(25)**).

TEM observations (Figure 2.13) illustrate typical but different clay dispersions for nylon-11 nanocomposites containing organoclay of 2 and 8 wt%. It can be seen that the clay platelets (separated dark lines) with thickness of about 1nm are individually and homogeneously dispersed in the polymer matrix in both cases. The nanolayer spacing of high clay concentration nanocomposite (Figure 2.13) is just 10 nm or more, which could be due to too much clay in the matrix.

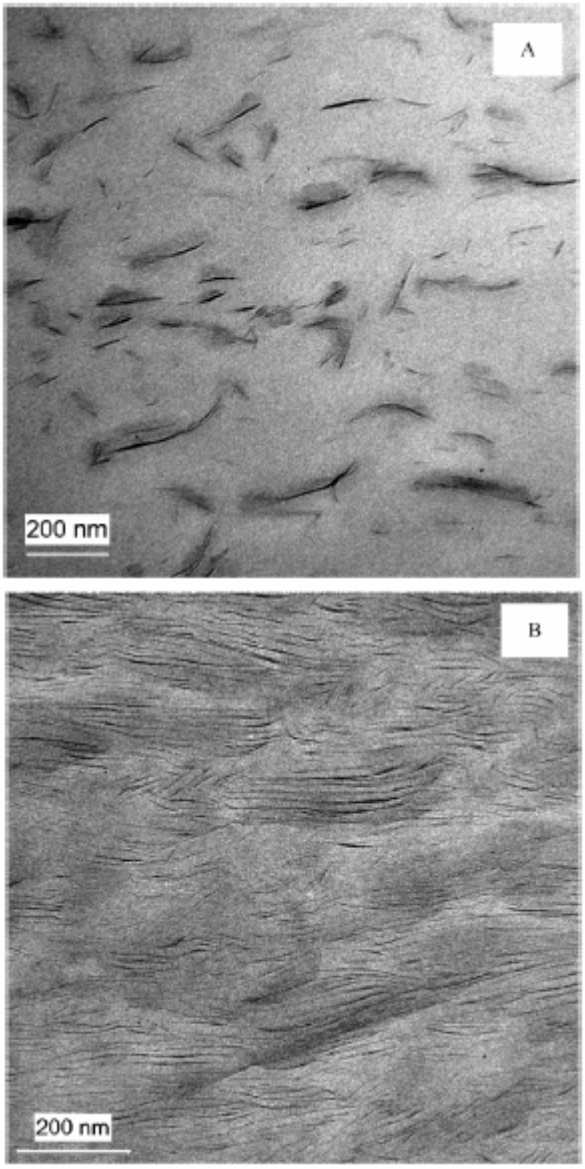

Figure 2.13. Bright field TEM images of PA-11-clay nanocomposites. PA-11-clay: (A)98/2; (B) 92/8 (reproduced from **(25)**).

Morgan and Gilman synthesized nylon-6-clay nanocomposites using a combined method **(60)**. The PA-6 sample was prepared with an in-situ polymerization approach with an MMT treated with a 12-amino-1-dodecanoic acid ammonium salt (AcidC12-MMT). Specifically, the clay was dispersed in the monomer before polymerization, and the polymerization process expanded the clay layers. However, this sample was subjected to shear after the polymerization process via processing in a twin-screw extruder to pelletize it after synthesis in a polymer reactor. As shown in Figure 2.14, the resulted nanocomposite was observed to adopt a highly exfoliated and disordered structure.

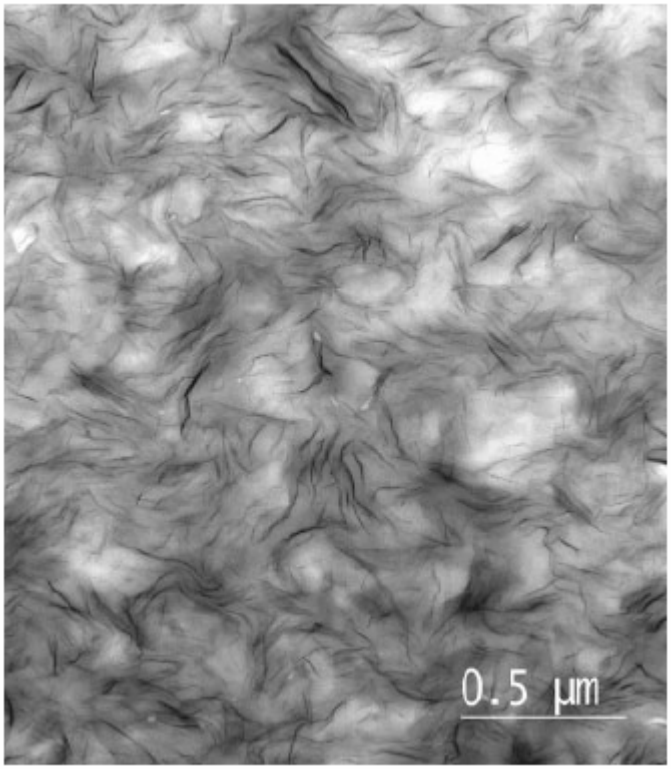

Figure 2.14. Low magnification TEM image of an exfoliated PA-6 nanocomposite (mass fraction = 5% AcidC12-MMT) (reproduced from **(60)**).

Paul et al systematically investigated the effects of clay source **(61)** and matrix molecular weight **(62)** on nylon-6-clay nanocomposites. The effect of sodium montmorillonite

source on the morphology and properties of nylon-6 nanocomposites was examined using equivalent experimental conditions. Sodium montmorillonite samples were two well-known mines, Yamagata, Japan (YM), and Wyoming, USA (WY), were ion exchanged with the same alkyl-ammonium chloride compound ($(HE)_2M_1R_1$) to form the organoclays designated as $(HE)_2M_1R_1$-YM and $((HE)_2M_1R_1$-WY. Nanocomposites were produced by melt mixing each organoclay with high molecular weight (HMW) nylon-6 using a twin-screw extruder. Quantitative analysis of TEM photomicrographs of the two nanocomposites (Figure 2.15) revealed that the Yamagata clay is comprised of platelets that are slightly larger than those of the Wyoming clay. The larger average particle length and slightly higher degree of platelet exfoliation observed for Yamagata clay nanocomposite translates into a higher particle aspect ratio that observed for Wyoming clay nanocomposite.

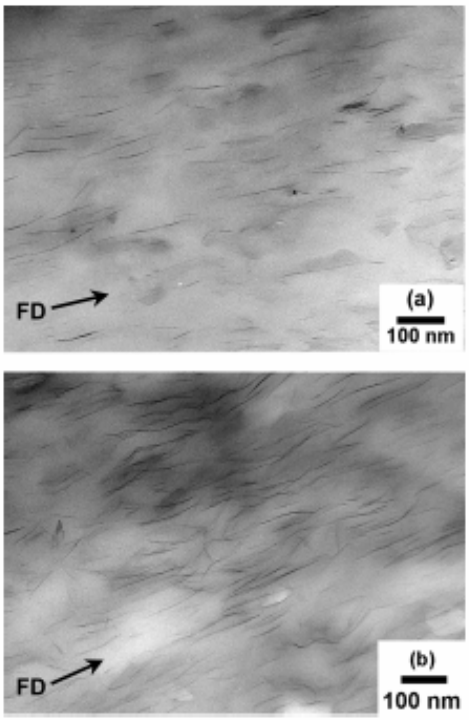

Figure 2.15. TEM micrographs of injection molded HMW nylon-6 nanocomposites based on (a) $(HE)_2M_1R_1$-WY; (b) $(HE)_2M_1R_1$-YM organoclay (reproduced from **(61)**).

The effect of matrix molecular weight was examined with organoclay nanocomposites based on three different molecular weight grades of nylon-6. Nylon-6 of low, medium and high molecular weight (referred to as LMW, MMW and HMW) was melt blended with organoclay using a twin-screw extruder. WAXS (Figure 2.16) and TEM (Figure 2.17) results collectively reveal a mixed structure for the LMW-based nanocomposite, having regions of intercalated and exfoliated clay platelets, while the MMW and HMW composites revealed well-exfoliated structures.

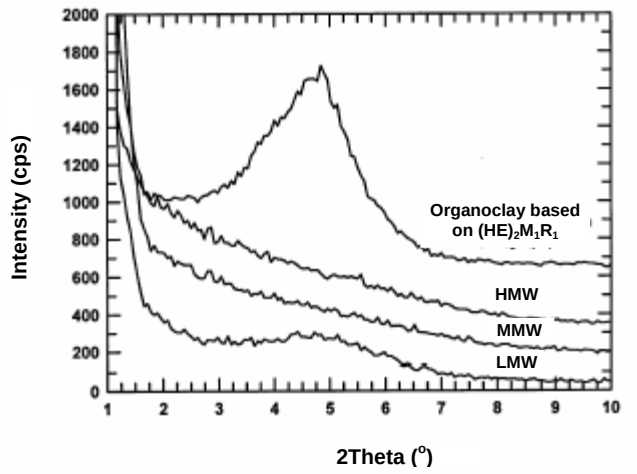

Figure 2.16. WAXS patterns for $(HE)_2M_1R_1$ organoclay and $(HE)_2M_1R_1$ organoclay nanocomposites based on LMW, MMW and HMW nylon-6 matrices containing 1.5 wt% montmorillonite. The curves are vertically offset for clarity (reproduced from **(62)**).

Qualitative TEM observations showed that the average number of platelets per stack decreased with increasing nylon-6 molecular weight. The TEM particle density, which is the average number of silicate particles per μm^2, increased with increasing molecular weight, thereby revealing larger extents of clay platelet exfoliation for the nanocomposites in the order HMW > MMW > LMW composites. Overall, it is imperative to emphasize that the delamination and dispersion of clay is quite good, despite relative differences in morphology between these five systems.

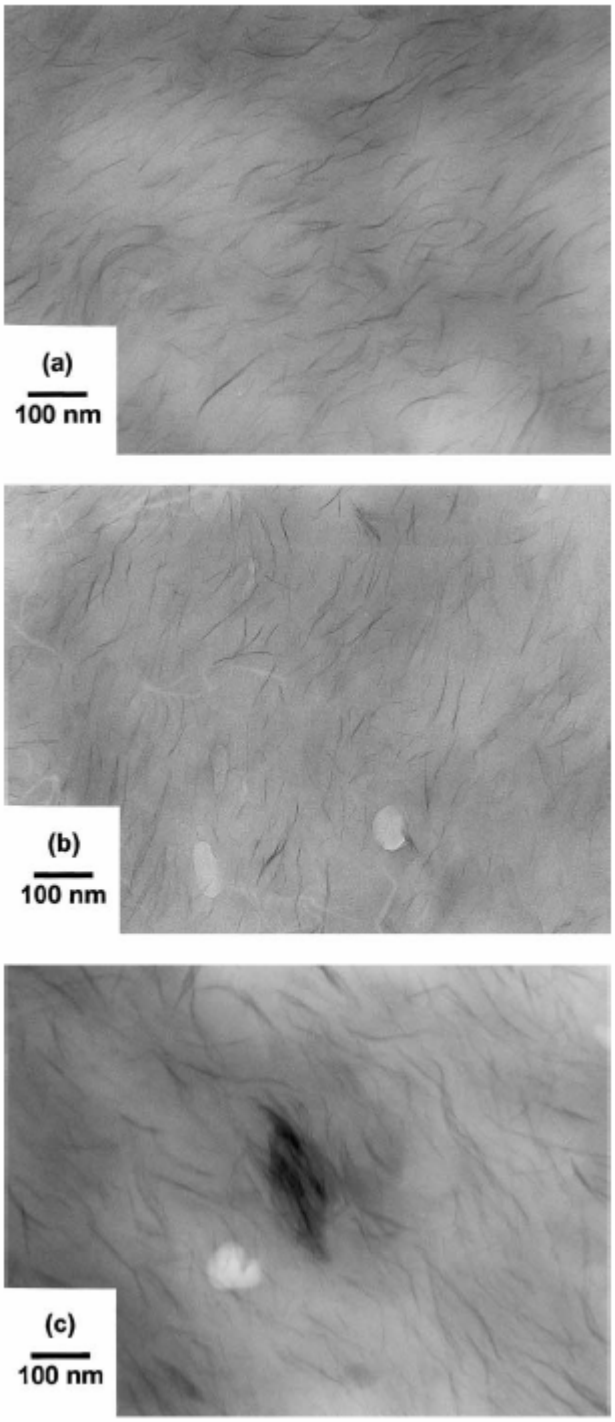

Figure 2.17. TEM micrographs of melt compounded nanocomposites containing 3.0 wt% montmorillonite based on (a) HMW; (b) MMW; (c) LMW nylon-6 (reproduced from **(62)**).

Polypropylene (PP) is one of the most widely used polyolefin polymers. Preparation of PP-clay nanocomposites is difficult since PP lacks polar groups in its backbone. PP modified with polar groups was used for intercalation into clay galleries, followed by melt compounding of organoclay with bulk PP to prepare nanocomposites **(63, 64)**. Only a limited degree of clay exfoliation was observed by this approach. An alternative method was developed later by the Toyota research group **(65-68)**. A mixture of maleic anhydride-modified PP oligomer, homo-PP and stearyl-ammonium-exchanged MMT was melt-blended to obtain PP-clay nanocomposites. The hydrolyzed maleic anhydride PP intercalated into the organoclay, expanding the galleries, and facilitating further intercalation by homo-PP. The PPCNs with three different clay content of 2, 4 and 7.5 wt% (abbreviated as PPCN2, PPCN4 and PPCN7.5) were prepared.

As shown by X-ray scattering (Figure 2.18) and TEM (Figure 2.19) **(68)**, a larger fraction of clay layers was exfoliated. Interestingly, the density of maleic anhydride groups has a significant effect on the final morphology and properties of the nanocomposite. For PPCN2 and PPCN4, a small remnant shoulder was observed around 2.7^{o} and 2.9^{o} respectively, corresponding to the (001) plane of silicate layers in the PP-MA matrix. In the PPCN7.5, the strong scattering peak is observed as a well-defined peak at 3.05^{o} (2.89 nm), implying that the ordered intercalated nanocomposite was formed. TEM described the features clearly. For each PPCN, fine and uniformly dispersed clay layers in the polymer matrix were evidenced. For PPCN4 and PPCN7.5, stacked silicate layers were observed while fully exfoliation was achieved in PPCN2. The nanocomposites exhibit improved storage modulus compared to pristine PP in the temperature range from Tg to

90°C. The impact of clay nanolayer reinforcement in PP nanocomposites is not as dramatic as in nylon-6, probably due to lower degree of exfoliation, weaker interfacial adhesion between polymer matrix and clay nanolayers, and the introduction of a large amount of oligomer.

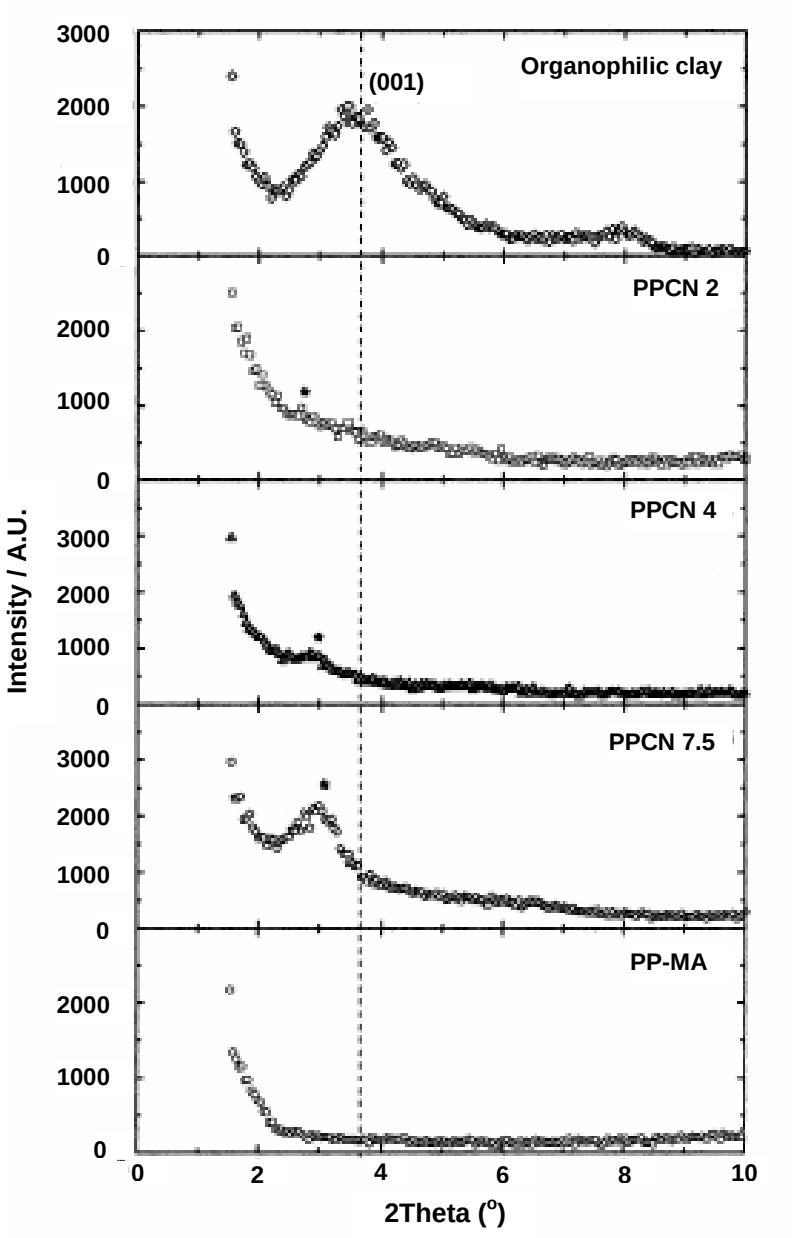

Figure 2.18. WAXS patterns for organophilic clay; PP-MA; PPCNs. The dashed lines indicate the location of the silicate (001) scattering of organophilic clay. The asterisks indicate a remnant shoulder of PPCN2 or a small peak for PPCN4 (reproduced from **(68)**).

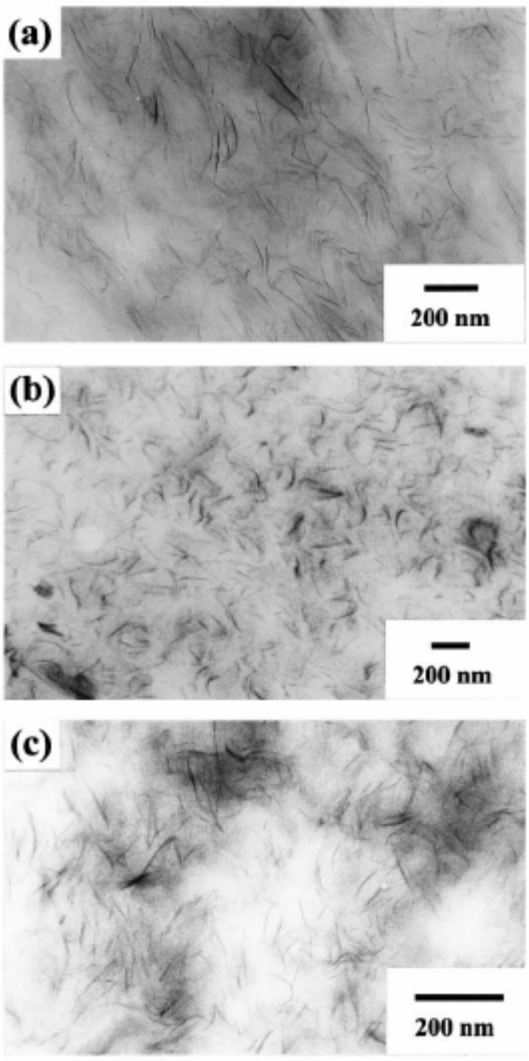

Figure 2.19. TEM micrographs showing PPCNs for: (a) PPCN2; (b) PPCN4; (c) PPCN7.5. The dark lines are the cross-sections of silicate layers and the bright areas are the PP-MA matrix (reproduced from **(68)**).

Since the past decades, abundant publications have been reporting the successful exfoliation of clay in thermoplastic polymers such as nylon **(69)**, PP **(70)**, PS **(71)**, PE **(72)**, PVA **(73)**, ABS **(74)**, PMMA **(75)**, PET **(44)**, SBR **(76, 77)** and so on. By reviewing the literatures, one can conclude that true exfoliation and uniform dispersion of clay are achieved in thermoplastic/elastomeric polymer systems.

2.3.2 Thermoset-clay nanocomposites

Next to all the aforementioned thermoplastic nanocompoistes, approaches have been explored to create thermoset-based nanocomposites. The intercalation and exfoliation chemistry of PA-clay nanocomposites have been transferred to a thermoset polyurethane system **(45, 78)**. The organoclay was swollen in polyols prior to the addition of the diisocyanate prepolymer. Solvation of the organoclays by polyols afforded intercalates with basal spacings that were dependent on the chain length of the gallery onium ion, but independent of the molecular weight of the polyol or the cation exchange capacity of the clay. In-situ polymerization of polyol-isocyanate precursor-organoclay mixtures afforded nanocomposites containing an intercalated clay phase embedded in the cross-linked polyurethane network. It seems that exfoliation of clay in thermosets is more challenge than thermoplastics.

Polyimides are one of the most frequently used polymers in high-temperature insulators and dielectrics owing to their good electrical and thermal properties. Within the field of polyimide (PI)-based nanocomposites, several studies have been focused on the thermoplastic PI systems **(79, 80)**. Yano et al **(79)** have studied PIs-based on pyromellitic dianhydride (PMDA) and 4,4'-diaminophenyl ether in dimethylacetamide. They found that a several-fold reduction in permeability of small gases was achieved, but the clay was not exfoliated, only adopted an intercalated morphology. A parallel study by Lan et al **(80)** confirmed the findings of Yano et al **(79)**. Later, Abdalla et al **(81)** synthesized high temperature, thermoset PMR type PI-clay nanocomposites using conventional organically (OLS) as well as an unmodified clay (LS). The methanol solvent was used to

swell the unmodified clay, resulting in nanocomposite formation, without the use of a modifier. The development in the morphology of the nanocomposites prepared was studied by analyzing WAXS curves of PGV (unmodified clay), PGVC10COOH (modified using 11-aminoundecanoic acid) and PGV12 (modified using dodecylamine), B-stage (imidized) and consolidated (fully cured) nanocomposites.

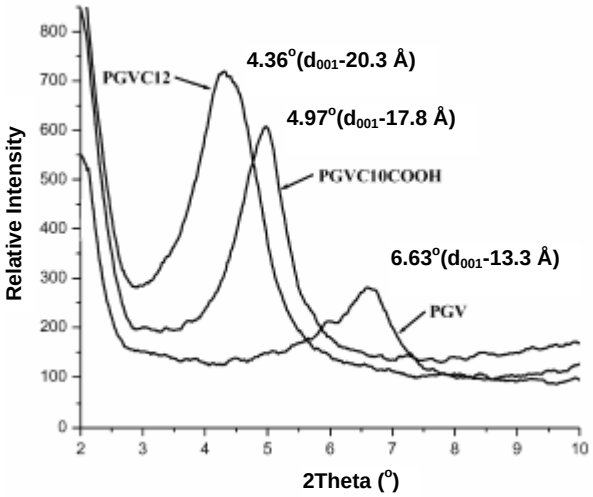

Figure 2.20. WAXS curves of PGV and organically modified clay (reproduced from **(81)**).

By comparing Figure 2.20 and Figure 2.21, one can find that the PMR oligomers diffused and intercalated between the clay layers leading to partial disruption of the clay layer. The reducing and broadening of the peaks for the consolidated PGV and PGVC10COOH/PMR nanocomposites indicated that although further intercalation into the silicate clay layers has occurred, complete exfoliation has not been achieved. TEM of the specimen (Figure 2.22) indicates that intercalated domains are maintained in the sample. The persistence of the intercalated morphology in the consolidated sample is presumably due to the inability of the prepolymer to diffuse into the layers and subsequently delaminate them during the cross-linking stage. This may be due to the relatively large size of the prepolymer. A potential approach to achieve an exfoliated

morphology may be to disperse the clay in the monomeric mixture, before polyamic acid formation. This needs further investigation.

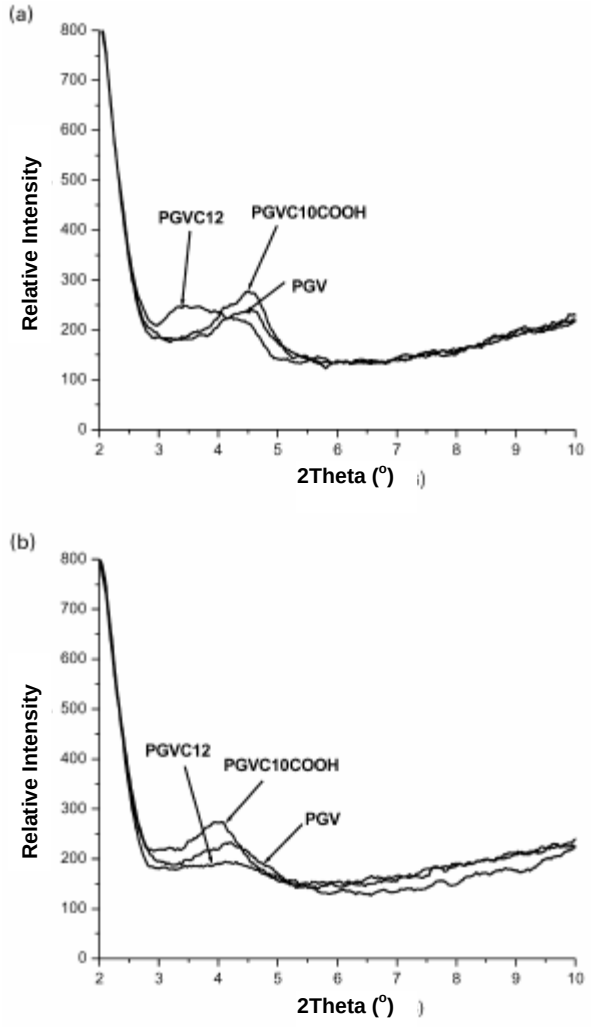

Figure 2.21. (a) WAXS curves of B-staged 5 wt% clay loaded LS and OLS nanocomposites; (b) WAXS curves of consolidated 5 wt% clay loaded LS and OLS nanocomposites (reproduced from **(81)**).

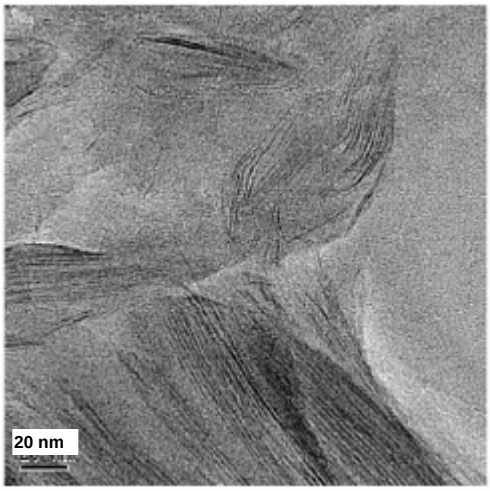

Figure 2.22. TEM micrograph of PGVC12/PMR-15 (1 wt% clay loaded) (reproduced from **(81)**).

Epoxies are among the most important thermosetting engineering polymers. Hence, large portion of research work about thermoset nanocomposits is focused on epoxy system. Messersmith and Giannelis **(26)** first reported the preparation of epoxy resin-based nanocomposites of organoclay. They found that the modified clay dispersed readily in DGEBA when sonicated for a short time period, as determined by the increase in viscosity at relatively low shear rates and the clarity of the suspension changing from opaque to semitransparent. In the subsequent paper, Wang and Pinnavaia **(82)** reported the preparation of nanocomposites using the epoxy DGEBA, and the concomitant delamination of acidic forms of MMT at elevated temperatures using the self-polymerization technique. As shown in Figure 2.23, the clay dispersion is not uniform, although the WAXS (Figure 2.24) shows no scattering peak for the composite with 5 wt% organoclay. Inside the tactoids, clay morphology is more like intercalation rather than exfoliation.

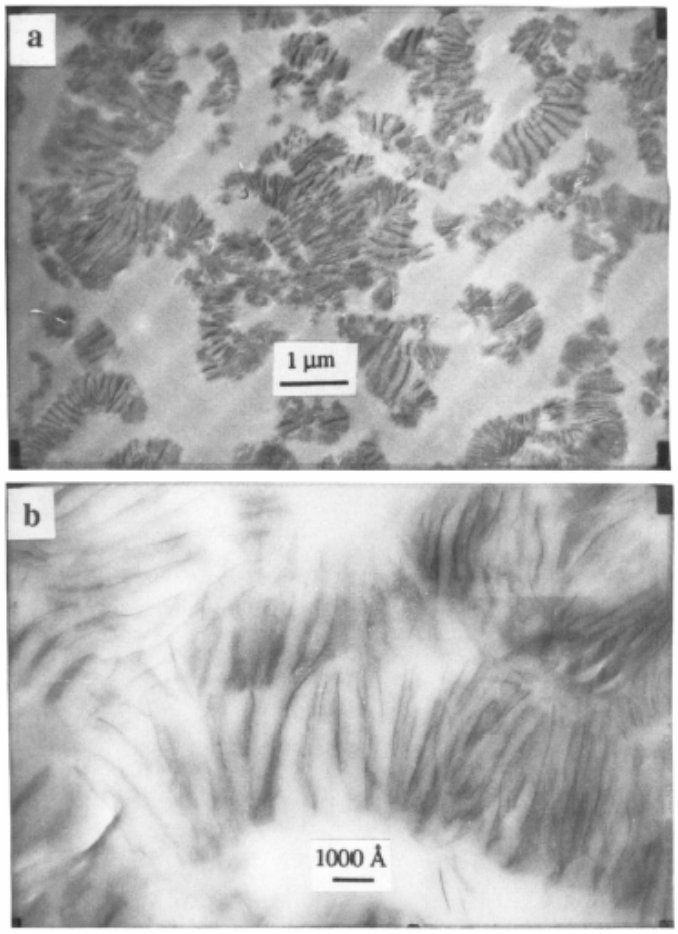

Figure 2.23. Transmission electron micrographs of a clay-polyether nanocomposite containing 5 wt% $[H_3N(CH_2)_{11}COOH]^+$-montmorillonite: (a) ×10000; (b) ×58000 (reproduced from **(82)**).

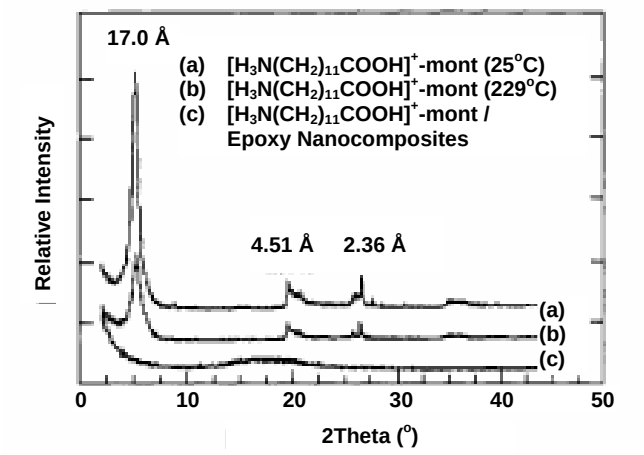

Figure 2.24. WAXS powder patterns for (a) freeze-dried $[H_3N(CH_2)_{11}COOH]^+$-montmorillonite; (b) $[H_3N(CH_2)_{11}COOH]^+$-montmorillonite freeze-dried, then heated at 229°C; (c) clay-polyether nanocomposite containing 5 wt% $[H_3N(CH_2)_{11}COOH]^+$-montmorillonite (reproduced from **(82)**).

A research group from Australia **(30)** reported the morphology, thermal relaxation and mechanical properties of layered silicate nanocomposies of high-functionality epoxy resins, in which typical materials and method were employed to prepare high performance epoxy nanocomposites. Three different types of resins were used: bifunctional DGEBA, trifunctional triglycidyl p-amino phenol (TGAP) and tetrafuncitional tetraglycidyldiamino diphenylmethane (TGDDM). All were cured with diethyltoluene diamine (DETDA). MMT modified with octadecylammonium cation was used for the preparation of nanocomposites. The nanocompoistes were prepared using in-situ intercalative polymerization method.

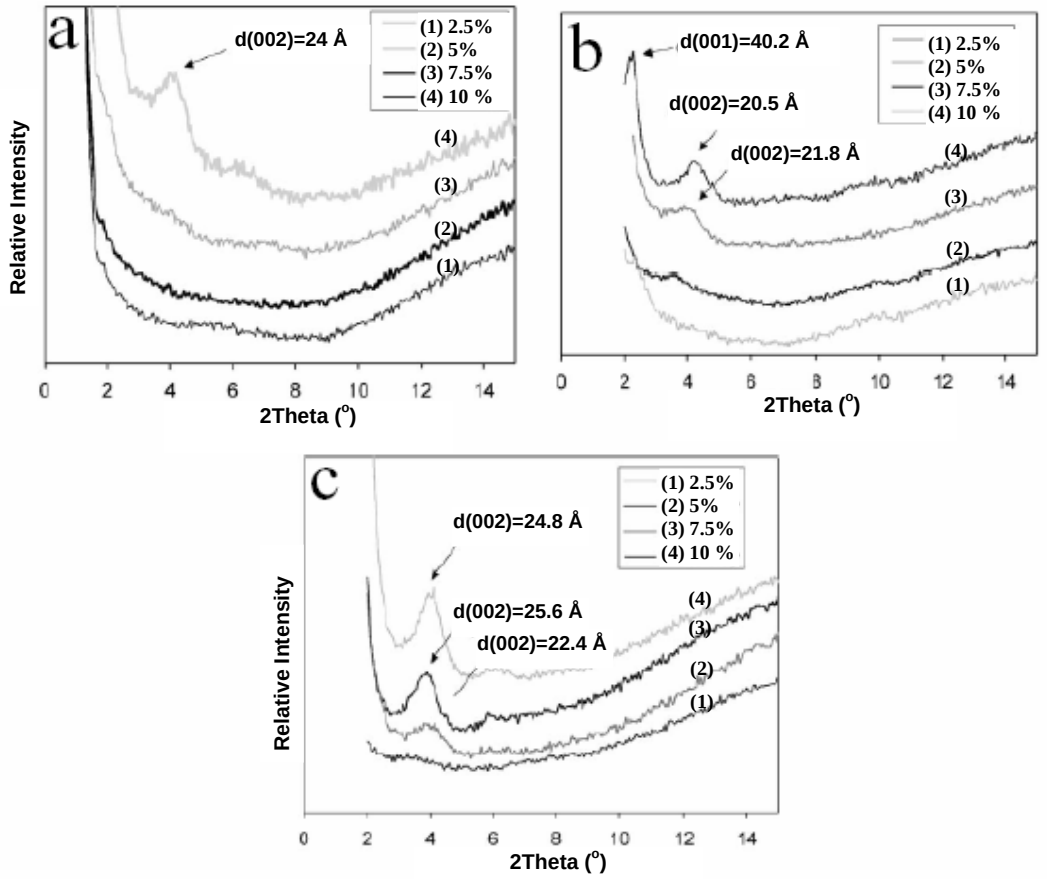

Figure 2.25. WAXS patterns of DETDA cured (a) DGEBA; (b) TGAP; (c) TGDDM nanocomposites containing 0-10 wt% organoclay (adapted from **(30)**).

The morphology of the cured samples was investigated using WAXS and different microscopy techniques. Figure 2.25 represents the WAXS patterns of the MMT concentration series and shows that the organoclay with an initial d-spacing of 2.3 nm is mainly exfoliated in low clay concentration specimen. On the other hand, high content samples show an intercalated structure.

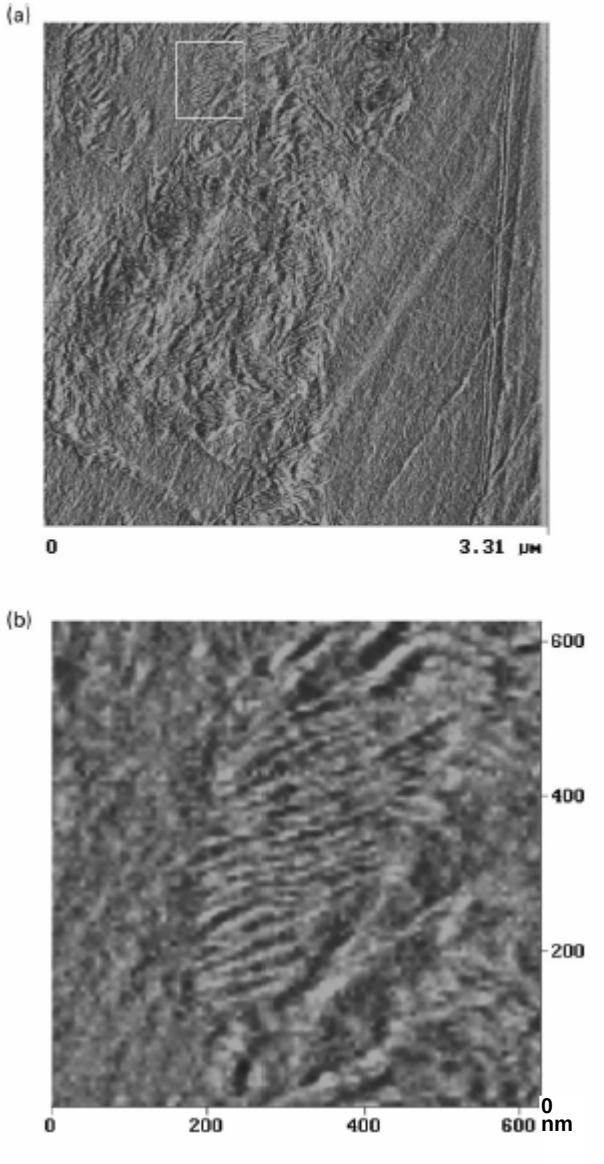

Figure 2.26. Phase contrast AFM images of DETDA cured DGEBA containing 5 wt% organoclay (reproduced from **(30)**).

Part (a) and (b) of Figure 2.26 represent AFM phase contrast images of the DGEBA nanocomposite containing 5 wt% layered silicate. Individual layers cannot be seen by AFM as they usually are by TEM. A striated structure, however, can be seen with increasing phase intervals at the top of the picture. So from AFM images it is established that at least part of the silicate content remains in tactoids or stacking of layers rather than forming a homogenous morphology through the whole material.

Park and Jana **(83)** studied the mechanism of exfoliation of nanoclay in epoxy-clay nanocomposites, which suggested the role of elastic force as the primary force behind clay layer exfoliation in epoxy-nanoclay systems. The elastic force exerted by the cross-linking epoxy molecules inside the clay galleries pushed out the outermost clay layers from the tactoids against the opposing forces arising from electrostatic and van der Waals attraction as well as shear force due to motion of clay sheet during exfoliation. Exfoliation continued until the extragallery epoxy turned into a gel. The formation of gels, on the other hand, was expedited by higher curing temperature and the presence of clay particles. Exfoliated structures were produced even when the rates of intra- and extragallery curing reactions were matched, which obviates the requirement that intragallery polymerization must be faster.

Epoxy is not readily to form exfoliated layered silicate nanocomposites. This may be due to the high viscosity of the resin and the strong tendency of clay nanoparticles to agglomerate **(84)**. It is also reported that the degree of exfoliation depends on the structure of the clay, curing temperature and curing agent **(85)**. The commonly used

techniques for processing epoxy-clay nanocomposites are direct mixing and solution mixing **(19, 85-87)**. However, these techniques produce intercalated or mixed structure of intercalated/exfoliated composites rather than fully exfoliated composites. Vaia et al **(52)** have suggested that the degree of exfoliation can be improved through the aid of conventional shear devices such as extruders, mixers, ultrasonicators, etc. This idea was employed by Yasmin et al **(88)**. In their work, a three-roll mill was used as a means of applying external shearing forces to disperse and exfoliate the silicate clay layers in the epoxy matrix. First, the epoxy resin (DGEBA) was placed between the feed and the center rolls. Once the rolls started moving, the clay particles were spread gradually on the resin to get direct and maximum contact with the rolls. The dispersion was achieved by the shear forces generated between the adjacent rolls. It was observed that the solution became viscous and opaque as the silicate layers dispersed and expanded with time. However, when the dispersion was completed, it produced a clear and transparent solution. The final product from the mill was then collected and mixed with the hardener and cured. The TEM observations were shown in Figure 2.27. The nanocomposites containing 1, 5 and 10 wt% of clay respectively, show homogenous dispersion of nanoparticles throughout the cross-section. The TEM images also show disordered intercalates rather than complete exfoliation for any clay content. The compounding of epoxy-clay nanocomposites with a three-roll mill is appealing. However, it is important to mention that the processing of nanocomposites by shear mixing produces a foamy and viscous solution and makes degassing quite difficult. This, in turn, may leave some nanovoids inside materials as shown in Figure 2.27.

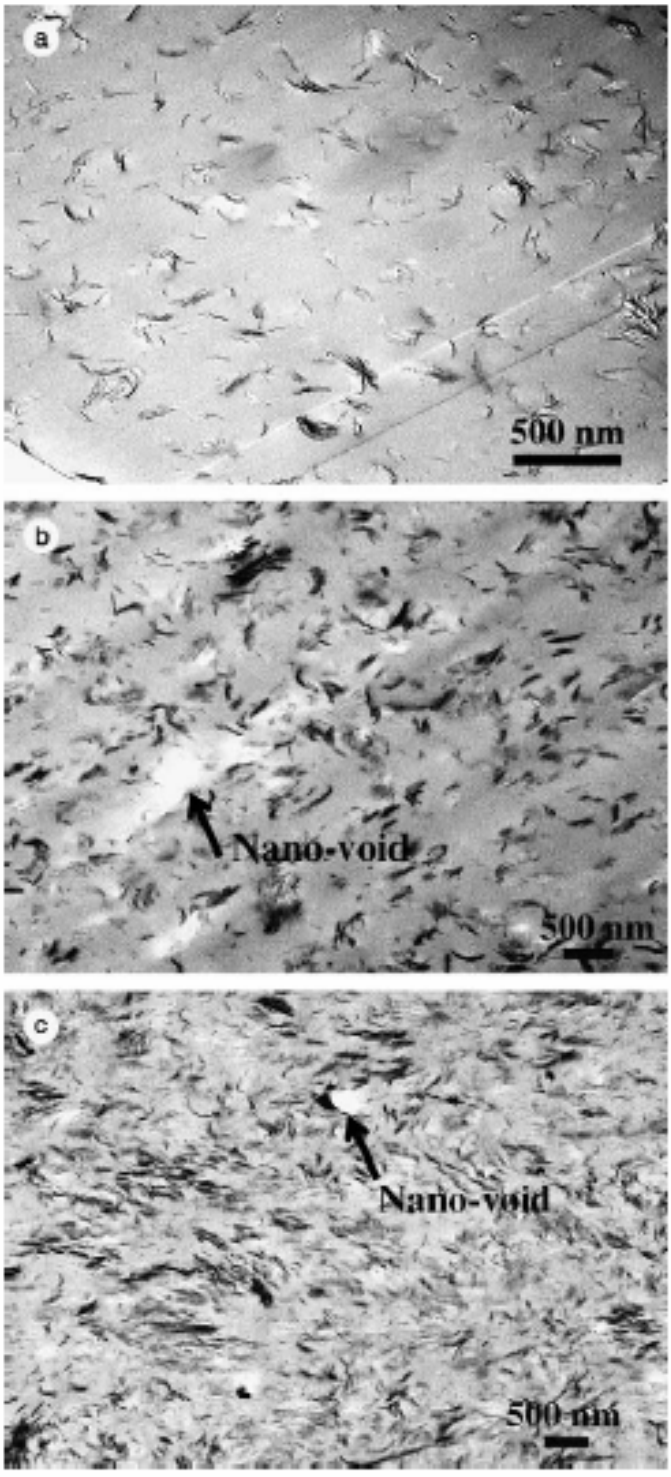

Figure 2.27. TEM images of clay nanocomposites at low magnification: (a) 1 wt%; (b) 5 wt%; (c) 10 wt% (reproduced from **(88)**).

2.4 Conclusions and our proposed research

From the above review, one can find that a processing technique that produces true exfoliation within thermoset epoxy is still a technical challenge. This is in contrast with nylon-6 system in which fully exfoliated structure can be achieved. Moreover, the mechanical property improvement of the epoxy-clay nanocomposites is not so significant as compared with neat epoxy. It is clear that exfoliation and reinforcement is really a challenge in epoxy-organoclay system, which also provides an opportunity for us to address this issue through an innovated approach to modify the approaches (clay and method) in order to achieve better exfoliation.

It is believed that the resistance forces to full exfoliation are extragallery viscous force, attractive force arising from electrostatic attraction between clay layers and van der Waals force, and the driving force to full exfoliation is the elastic force due to the confinement of crossed-linked epoxy chains and the restriction on the conformational entropy increase during epoxy curing **(83, 88)**. To achieve full exfoliation, what we need to do is to overcome the forces or avoid them. Therefore, our research focused on two areas to achieve better-exfoliated epoxy-clay systems:

1) to use microwave as an extra force to overcome the van der Waals force and extragallery viscous force;
2) to use inreactive solvent as an assistant to disperse clay into epoxy matrix, thus avoid the forces.

Normally, clay is treated with organic surfactants to make the surface of clay platelets more organophilic and at the same time to obtain swollen galleries so that the organic polymer chains can diffuse into the galleries and lead to a nanocomposite. This has been shown useful in preparing some thermoplastic nanocomposites such as nylon systems. However, this modification also leads to negative effects. When a high concentration of alkyl-ammonium small molecules is introduced to the layer surface, it leads to a complicated interface between the layers and polymer matrix and poor composite properties **(30, 89)**. In view of this, we will manage to reduce or eliminate the surface modifiers when preparing the nanocomposites.

Based on the project objectives and the above literature study prompted in Chapter 1, our research was proposed to include the following points:

(1) to synthesize better exfoliated epoxy-clay nanocomposites with reduced or eliminated clay surface modifier. In addition, the organoclay nanocomposites will also be prepared for comparison;

(2) to systematically study the effect of the different approach on the morphology of the nanocomposites;

(3) to systematically study the effect of clay on the thermal/mechanical properties of composites;

(4) to investigate the deformation and fracture behavior of the nanoclay composites.

References:

1. Motokatsu M, Takahashi T, Nie HY, Mizutani WH, Tokumoto H. *Polymer*, 1997; 38: 177-182.
2. Krishnamoorti R, Yurekli K. *Current Opinion in Colloid & Interface Science*, 2001; 6: 464-470.
3. Giannelis EP, Krishnamoorti R, Manias E. *Adv. Polym. Sci.*, 1999; 118: 108-147.
4. Lan T, Kaviratna PD, Pinnavaia TJ. *Chem. Mater.*, 1995; 7: 2144-4150.
5. Lagaly G. *Solid State Ionics*, 1986; 22: 43-51.
6. Kloprogge JT. *J. Porous Mater.*, 1998; 5: 5-41.
7. Kojima Y, Usuki A, Kawasumi M, Okada A, Kurauchi T, Kamigaito O. *J. Poly. Sci.: Part A*, 1993; 31: 1755-1758.
8. Takekoshi JT, Giannelis EP. *Mater. Res. Soc. Symp. Proc.*, 1997; 475: 523-528.
9. Gillman JW, *Applied Clay Science*, 1999; 15: 31-49.
10. Yano K, Usuki A, Kurauchi T, Kamigaito O. *J. Poly. Sci.: Part A*, 1993; 31: 2493-2498.
11. Okada A, Kawasumi M, Usuki A, Kojima Y, Kurauchi T, Kamigaito O. *Mater. Res. Soc. Proc.*, 1990; 171: 45-50.
12. Lan T, Pinnavaia TJ. *Chem. Mater.*, 1994; 6: 2216-2219.
13. Kojima Y, Usuki A, Kawasumi M, Okada A, Fukushima Y, Karauchi T, Kamigaito O. *J. Mater. Res.*, 1993; 6: 1185-1189.
14. Liu L, Qi Z, and Zhu X. *J. Appl. Polym. Sci.*, 1999; 71: 1133-1138.
15. Shi D, Lan T, Pinnavaia TJ. *Chem. Mater.*, 1996; 8: 1584-1587.

16. Usuki A, Koiwai A, Kojima Y, Kawasumi M, Okada A, Kurauchi T, Kamigaito O. *J. Appl. Polym. Sci.*, 1995; 55: 119-123.
17. Harcup JP, Yee AF. *ANTEC'99 Comn. Proc.*, 1999; 3: 3396-3398.
18. Kornmann X, Berglund LA, Skerte J, Giannelis EP. *Polym. Eng. Sci.*, 1998; 38: 1351-1358.
19. Zerda AS, Lesser AJ. *J. Polym. Sci.: Part B*, 2001; 39: 1137-1146.
20. Manias E, Han WJ, Jandt KD, Kramer EJ, Giannelis EP. *Mat. Res. Soc. Symp. Proc.*, 1997; 457: 495-500.
21. Laus M, Francesangeli O, Sandrolini F. *J. Mater. Res.*, 1997; 12: 3134-3139.
22. Choi YS, Wang KH, Xu MZ. Chung IJ, *Chem. Mater.*, 2002; 14: 2936-2939.
23. Liu XH, Wu QJ. *Polymer*, 2001; 42: 10013-10019.
24. Nam PH, Maiti P, Okamoto M, Kotaka T, Hasegawa N, Usuki A. *Polymer*, 2001; 42: 9633-9640.
25. Liu TX, Lim KP, Tjiu WWC, Pramoda KP, Chen ZK. *Polymer*, 2003; 44: 3529-3535.
26. Messersmith PB, Giannelis EP. *Chem. Mater.*, 1994; 6: 1719-1725.
27. Yu YH, Lin CY, Yeh JM, Lin WH. *Polymer*, 2003; 44: 3553-3560.
28. Alexandre M, Dubois P, Sun T, Garces JM, Jerome R. *Polymer*, 2002; 43: 2123-2132.
29. Brown JM, Curliss D, Vaia RA. *Chem. Mater.*, 2000; 12: 3376-3384.
30. Becker O, Varley R, Simon G. *Polymer*, 2002; 43: 4365-4373.
31. Lee DC, Jang LW. *J. Appl. Polym. Sci.*, 1997; 68:1997–2005.
32. Kelly P, Akelah A, Qutubuddin S, Moet A. *J. Mater. Sci.*, 1994; 29: 2274–2280.

33. Massam J, Pinnavaia TJ. *Mater. Res. Soc. Symp. Proc.*, 1998; 520: 223-232.

34. Bajaj P, Jha NK, Ananda Kumar R. *J. Appl. Polym. Sci.*, 1990; 40: 203–212.

35. Tak Gam K., Sue HJ. *Preparation and Mechanical Properties of Epoxy-Clay nanocomposites in ACS Spring Meeting*, 2000 San Francisco.

36. Zax D, Yang D, Santos R, Hegemann H, Giannelis H, Manias E. *J. Chem. Phys.*, 2000; 112: 1951–2945.

37. Pinnavaia TJ, Lan T, Wang Z, Shi H, Kaviratna PD. *ACS Symp. Ser.*, 1996; 622: 250-261.

38. Messersmith PB, Giannelis EP. *Chem. Mater.*, 1993; 5:1064-1066.

39. Messersmith PB, Giannelis EP. *J. Polym. Sci.: Polym. Chem.*, 1995; 33: 1047-1057.

40. Burnside S, Giannelis EP. *Chem. Mater.*, 1995; 7: 1597-1600.

41. Wang S, Long C, Wang X, Li Q. *J. Appl. Polym. Sci.*, 1998; 69: 1557-1561.

42. Vaia RA, Ishii H, Giannelis EP. *Chem. Mater.*, 1993; 5: 1694-1696.

43. Usuki A, Kato M, Okada A, Kurauchi T. *J. Appl. Polym. Sci.*, 1997; 63: 137–139.

44. Ke Y, Long C, Qi Z. *J. Appl. Polymer. Sci.*, 1999; 71: 1139-1146.

45. Wang Z, Pinnavaia TJ. *Chem. Mater.*, 1998; 10: 3769-3771.

46. Chin IJ, Thomas TA, Kim KC, Thomas PR, Wang J. *Polymer*, 2001; 42: 5947-5952.

47. Jeon HG, Jung HT, Hudson SD. *Polymer Bulletin*, 1998; 41: 107-113.

48. Kawasumi M, Hasegawa N, Usuki A, Akane O. *Mater. Sci. Eng.: C*, 1998; 6: 135-143.

49. Vaia RA, Jandt KD, Kramer EJ. *Macromolecules*, 1995; 28: 8080-8085.

50. Kojima Y, Usuki A, Kawasumi M, Okada A, Kurauchi T, Kamigaito O, Kaji K. *J. Poly. Sci.: Part B*, 1994; 32: 625-630.

51. Liu TX, Liu ZH, Ma KX, Shen L, Zeng KY, He CB. *Compos. Sci. Technol.*, 2003; 63: 331-337.

52. Vaia RA, Jandt KD, Kramer EJ, Giannelis EP. *Chem. Mater.*, 1996; 8: 2628-2635.

53. Komarneni S. *J. Mater. Chem.*, 1992; 2: 1219-1230.

54. Kojima Y, Fukumori K, Usuki A, Okada A, Kurauchi T. *J. Mater. Sci. Lett.*, 1993; 12: 889-890.

55. Haque E, Armeniades CD. *Polym. Eng. Sci.*, 1986; 26(21): 1524-1530.

56. Giannelis EP. *Adv. Mater.*, 1996; 8(1): 29-35.

57. Fukushima Y, Inagaki S. *J. Inclusion. Phenom.*, 1987; 5: 473-482.

58. Usuki A, Kawasumi M, Kojima Y, Okada A. *J. Mater. Res.*, 1993; 8: 1174-1178.

59. Usuki A, Kojima Y, Kawasumi M, Okada A, Fukushima Y, Kurauchi T. *J. Mater. Res.*, 1993; 8: 1179-1184.

60. Morgan AB, Gilman JW. *J. Appl. Poly. Sci.*, 2003; 87: 1329-1338.

61. Fornes TD, Hunter DL, Paul DR. *Polymer*, 2004; 45: 2321-2331.

62. Fornes TD, Yoon PJ, Keskkula H, Paul DR. *Polymer*, 2001; 42: 9929-9940.

63. Kurokawa Y, Yasuda H, Oya A. *J. Mater. Sci. Lett.*, 1996; 15: 1481–1483.

64. Wang Y, Chen FB, Li YC, Wu KC. *Composite B*, 2004; 35: 111-124.

65. Kawasumi M, Hasegawa N, Kato K, Usuki A, Okada A. *Macromolecules*, 1997; 30: 6333–6338.

66. Kato M, Usuki A, Okada A. *J. Appl. Polym. Sci.*, 1997; 63: 1781–1785.

67. Hasegawa N, Kawasumi M, Kato M, Usuki A, Okada A. *J. Appl. Polym. Sci.*, 1998; 67: 87–92.

68. Nam PH, Maiti P, Okamoto M, Kotaka T, Hasegawa N, Usuki A. *Polymer*, 2001; 42: 9633-9640.

69. Hasegawa N, Okamoto H, Kato M, Usuki A, Sato N. *Polymer*, 2003; 44: 2933-2937.

70. Hasegawa N, Okamoto H, Kato M, Usuki A. *J. Appl. Polym. Sci.*, 2000; 78: 1918-1922.

71. Weiner MW, Chen H, Giannelis EP, Sogah DY. *J. Am. Chem. Soc.*, 1999; 121: 1615-1616.

72. Heinemann J, Reichert P, Thomann R, Mulhaupt R. *Macromol. Rapid. Commun.*, 1999; 20: 423-430.

73. Chang JH, Jang TG, Ihn KJ, Lee WJ, Sur GS. *J. Appl. Polym. Sci.*, 2003; 90: 3208-3214.

74. Wang SF, Hu Y, Zong RW, Tang Y, Chen ZY, Fan WC. *Appl. Clay. Sci.*, 2004; 25: 49-55.

75. Chen GH, Chen XQ, Lin ZY, Ye W. *J. Mater. Sci. Lett.*, 1999; 18: 1761-1763.

76. Ma J, Xu J, Ren JH, Yu ZZ, Mai YW. *Polymer*, 2003; 41: 4619-4624.

77. Wang YQ, Wu YP, Zhang HF, Zhang LQ, Wang B, Wang ZF. *Macromol. Rapid commun.*, 2004; 25: 1973-1978.

78. Zilg C, Thomann T, Mulhaupt R, Finter J. *Adv. Mater.*, 1999; 11: 49-51.

79. Yano K, Usuki A, Okada A, Kurauchi T, Kamigaito O. *J. Polym. Sci. Part A: Polym. Chem.*, 1993; 31: 2493-2498.

80. Lan T, Kaviratna P, Pinnavaia T. *Chem. Mater.*, 1997; 6: 573-575.

81. Abdalla M, Dean D, Campbell S. *Polymer*, 2002; 43: 5887-5893.

82. Wang MS, Pinnavaia TJ. *Chem. Mater.*, 1994; 10: 468-474.

83. Park JH, Jana SC. *Macromolecules*, 2003; 36: 2758-2768.

84. Wei CL, Zhang MQ, Rong MZ, Friedrich K. *Comp. Sci. Technol.*, 2002; 62: 1327-1340.

85. Lv JK, Ke YC, Qi ZN, Yi XS. *J. Polym. Sci: Part B*, 2000; 39: 115-120.

86. LeBaron PC, Wang Z, Pinnavaia TJ. *J. Appl. Clay Sci.*, 1999; 15: 11-29.

87. Kornmann X, Lindberg H, Berglund LA. *Polymer*, 2001; 42: 1303-1310.

88. Yasmin A, Abot JL, Dinia IM. *Scripta Materialia*, 2003; 49: 81-86.

89. Pinnavaia TJ, Beal GW (Ed.). *Polymer-Clay Nanocomposites*. *Chichester: Wiley*, (2000).

Chapter 3. Materials and experiments

The major effort of this research is to achieve exfoliated epoxy-clay nanocomposites and establish processing condition-microstructure-property relationships. Based on this, three approaches were employed to prepare epoxy nanocomposites by using organoclay, microwave-assisted pristine clay and solvent-assisted SMC clay respectively. The resin used in each system is bifunctional diglycidyl ether of bisphenol-A (DGEBA) cured with diethyltoluene diamine (DETDA). The characterization techniques include: morphology characterization techniques such as wide angle X-ray scattering (WAXS), transmission electron microscopy (TEM) and optical microscopy (OM); property characterization methods such as dynamic mechanical analysis (DMA), tensile test and 3-point bend method. In addition, scanning electron microscopy (SEM) was used to observe the fracture surface of 3-point bend sample, thus to interpret the toughening mechanisms.

3.1 Materials

Organoclay: Cloisite 93A, supplied by Southern Clay Products, with methyl dehydrogenated tallow ammonium ion as the cation exchange resin was used after removal of typically 2 wt% of inherently present moisture. The initial interlayer d-space is 23.6 Å. Table 3.1 shows some typical properties of Cloisite 93A.

Table 3.1. Typical properties of Cloisite 93A.

Treatment/Properties	Organic modifier	Modifier concentration	Moisture	% Weight loss on ignition
Cloisite 93A	M2HT	90 meq/100g clay	< 2 wt%	40 wt%

Where HT is Hydrogenated Tallow (~65% C18; ~30% C16; ~5% C14), Anion: HSO_4, M2HT: methyl, dehydrogenated tallow ammonium.

Pristine Clay: Nanomer PGW, provided by Nanocor Inc., is a high purity aluminosilicate mineral with a level greater than 98% montmorillonite. Admixture minerals are generally those with specific gravities similar to montmorillonite and include albite, calsite, dolomite, orthoclase and quartz. Typical physical properties are shown in Table 3.2.

Table 3.2. Typical physical properties of PGW.

Physical properties:	CEC (meq/100g)	Aspect ratio	Specific gravity	Moisture	Avg. dry particle size (μm)
PGW	145	200-400	2.6	< 12 wt%	16-22

Silane: 3-aminopropyl-trimethoxysilane provided by Sigma-Aldrich Chemical was used to chemically modify the clay surfaces. Acetone was selected as the inactive solvent to facilitate clay modification and dispersion.

Epoxy Resins: In order to obtain materials with high Tg, an aromatic epoxy, diglycidyl ether of bisphenol A (DGEBA) in the form of DER 332 of Dow Chemical, was chosen

for the study. This epoxy resin offered epoxide equivalent weight of 171-175, viscosity of 4-6 Pa·s and specific gravity of 1.16 at 25°C.

Curing Agents: The curing agent, Ethacure 100LC of Albemarle Corp. is an aromatic diethyltoluene diamine (DETDA), which is widely used in high performance epoxy resin systems. Ethacure 100LC is a mixture of two DETDA isomers, containing 75-81% 2,4 isomer and 18-20% 2,6 isomer. The structures of the resin and amine are showed in Figure 3.1.

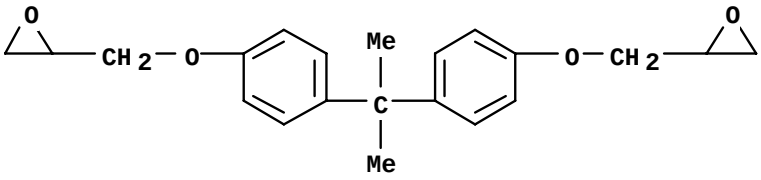

DER 332: Diglycidyl ether of bisphenol A

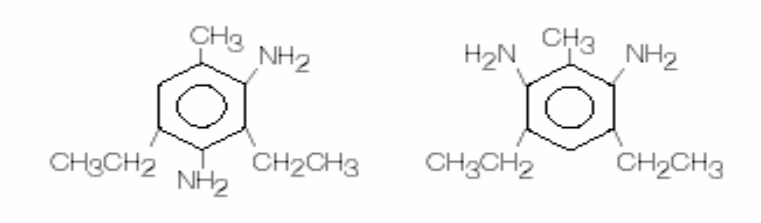

3,5-diethyltoluene-2, 4-diamine, 3,5-diethyltoluene-2, 6-diamine

Diethyltoluene diamine (DETDA)

Figure 3.1. Chemical structures of the resin and amine used for the nanocomposite synthesis.

3.2 Preparation of epoxy-clay nanocomposites

3.2.1 Benchmark organoclay system

Following most of the literatures, in-situ polymerization method was used to prepare organoclay nanocomposites. A mixed structure of intercalation and exfoliation is a typical morphology in this system. The synthesis and characterization will be described in Chapter 4.

3.2.2 Microwave-assisted pristine clay system

A new method was employed for this preparation, which involves microwave treatment of epoxy-raw clay mixtures. Unique domain structure was observed in the nanocomposites. This system will be shown in Chapter 5.

3.2.3 Solvent-assisted silane-modified clay (SMC) system

A novel approach assisted with water and acetone solvent, called "hydro-compounding" technique, was developed to disperse clay into epoxy matrix. Exfoliation and uniform dispersion were achieved with this approach. The detailed description will be illustrated in Chapter 6. In addition, studies were also carried out to investigate the hydrothermal effects on the thermal/mechanical properties of epoxy-nanoclay composites based on this system, which will also be elucidated in Chapter 6.

3.3 Nanocomposite characterization

There are mainly two methods to characterize the morphology of polymer-clay nanocomposites. The most straightforward way is X-ray scattering because it is a good way to evaluate the spacing between the clay layers. However, one needs to be very careful with the interpretation of the results. Lack of sensitivity of the analysis and limits of the equipment can lead to wrong conclusions about the nanocomposite structure. Therefore, transmission electron microscopy is a necessary complement to X-ray scattering. TEM gives a direct measure of the spatial distribution of the layers but it requires substantial skills in specimen preparation and analysis.

3.3.1 Optical microscopy (OM)

To examine the size of clay aggregates in the sample and any extrinsic defects such as air bubbles, which may be induced during processing and which could have a significant impact on the property of the resulting matrix. OM may also be used to examine the fracture morphology of the nanocomposite samples to gain a better understanding of the fracture mechanism. Optical microscopy was performed using an Olympus optical microscope and the samples were finely polished before investigation.

3.3.2 Wide angle X-ray scattering (WAXS)

Figure 3.2 shows the diffraction from two scattering planes (i.e. two consecutive clay layers or other crystallographic planes of the layers themselves) that are separated by a distance d (i.e. interlamellar spacing or d-spacing) and intercept X-rays of wavelength λ at the incident angle θ. A constructive interference occurs when:

$$n \cdot \lambda = 2 \cdot d \cdot \sin\theta$$

This equation is known as the Bragg Law.

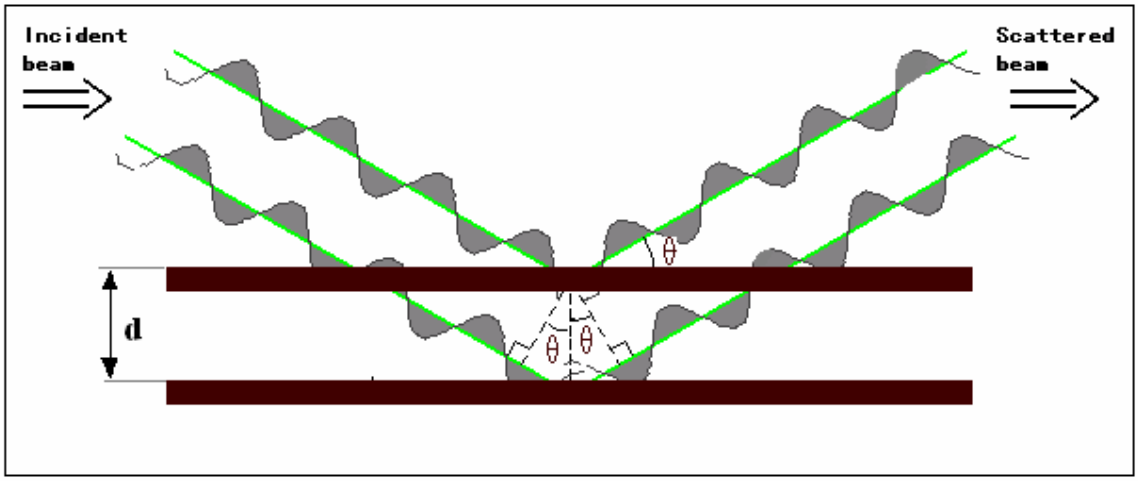

Figure 3.2. Principle of X-ray scattering.

The analysis is performed at low angle ($2\theta < 9^{o}$, i.e. d > 9.8Å) in order to detect the (001) scattering and evaluate the d-spacing between the clay layers. In intercalated nanocomposites, the repetitive multiplayer structure is well preserved, allowing the interlayer spacing to be determined. The intercalation of the polymer chains usually increases the interlayer spacing, which is reflected by a shift of the X-ray scattering peak towards lower angle values. As far as exfoliated structure is concerned, no more scattering peaks are visible at low angle (less than 10°) in the WAXS pattern either because of a much too large spacing between the layers (i.e. exceeding 8 nm in the case of ordered exfoliated structure) or because the clay layer does not present ordering anymore.

WAXS was performed with a Bruker X-ray Diffractometer fitted with a 2-D detector using nickel-filtered Cu-$K_{\alpha 1}$ radiation source (λ = 0.15418 nm) under a voltage of 40 kV and a current of 40 mA. For clay/water suspension and clay/acetone slurry, glass capillaries (Hampton Research, HR6-194) were used to carry the liquid samples.

3.3.3 Transmission electron microscopy (TEM) analysis

Transmission electron microscopy is a powerful technique to study structures at and below the nanometer scale. It allows a precise observation of nanostructures with an exceptional resolution (about 0.2 nm). Therefore, TEM provides a most direct way to examine the states of clay exfoliation as this technique can image materials on the nanometer scale. The states of clay exfoliation, such as whether the clay is intercalated or exfoliated, can be observed directly. It can be used as a complementary tool to confirm results obtained by WAXS regarding the organization of clay layers in the nanocomposite. In TEM, image formation is due to the scattering of electrons as the electron beam passes through the sample, so the specimens need to be sufficiently thin.

Ultrathin films (with thickness of about 80 nm) for transmission electron microscopy (TEM) observation were prepared by cutting from the trimmed surface perpendicular to flow direction using a diamond knife with Leica Ultracut UCT microtome. The sections were collected on carbon coated copper grids. A Philips CM300-FEG TEM operating at an accelerating voltage of 300 kV was used to examine the morphology.

3.4 Fourier transform infrared (FTIR) spectroscopy

Fourier transform infrared (FTIR) spectroscopy was carried out using a Perkin-Elmer 2000 spectrometer to characterize the possible reaction between the clay surface and silane. For FTIR testing, the modified clay was washed with acetone and centrifuged 5 times, and the resulting solid was dried at 80^{o}C for 24 h. KBr discs were prepared after mixing (0.5%) each of the test samples with dry KBr. Analyses were performed in the transmission mode in the 400-4000 cm^{-1} range, with a resolution of 2 cm^{-1} and accumulation of 16 scans.

3.5. Time-of-flight secondary ion mass spectrum (ToF-SIMS)

ToF-SIMS was employed to trace the silane in the silane-modified clay, which could have been bonded onto the clay surface during the clay surface modification. The ToF-SIMS measurements were done with an ION-ToF-SIMS IV instrument. The accelerating voltage of the primary ion source of Ar^{+} is 10 keV. The pressure in the analysis chamber was maintained at 7.6×10^{-9} Torr (1×10^{-6} Pa) or lower during each measurement. Dry powders of pristine clay and modified clay were compressed into discs and the analyzed area was $200\times200\ \mu m^{2}$.

3.6 Mechanical test

Both tensile and fracture toughness tests were performed, following the ASTM standards, to learn how the mechanical properties differ between the neat and modified epoxy

nanocomposites. The testing results were correlated with the morphology and toughening mechanisms of the nanocomposites.

Uniaxial tensile tests were performed according to ASTM D638 to measure the modulus of the composites. Samples were cut and further machined into dog-bone tensile specimens with dimension of 50 × 13 × 3 mm^3 (Figure 3.3(A)). An Instron Model 5567 computer-controlled testing machine was used at a crosshead speed of 5 mm/min at room temperature. For modulus of elasticity measurement, an Instron Model 2630-105 extensometer with a maximum strain error of 0.0002 mm/mm was used to automatically continuously record the strain. At least six specimens of each composition were tested. The modulus was calculated by using the initial linear portion of the stress-strain curve (strain range 0.5%-1%), dividing the difference in stress by the corresponding difference in strain.

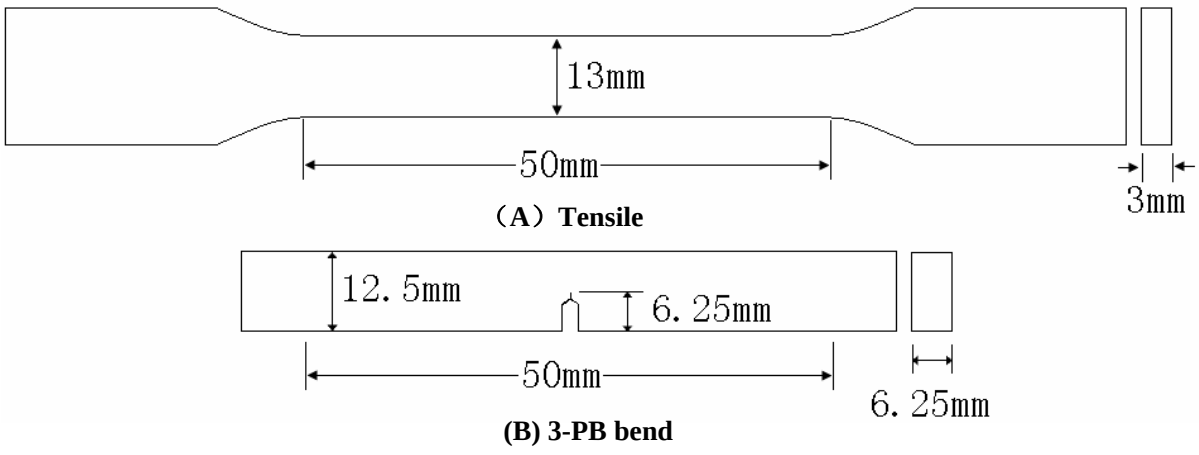

Figure 3.3. Specimen dimensions of (A) tensile and (B) 3-point bend tests.

The Mode I fracture toughness, as quantified by the critical stress intensity factor (K_{IC}), was determined using the 3-point bend test. Single-edge-notched (SEN) type specimens were prepared for the experiment. As shown in Figure 3.3(B), specimen thickness (B) and width (W) are 6.25 mm and 12.5 mm respectively. This specimen geometry satisfies the requirement for the plane strain condition (ASTM D5045). A sharp notch was introduced by tapping a hammer on a razor blade inserted into the sample. The tip of the crack was created by the wedging action of the razor. A screw-driven Instron machine was used at a crosshead speed of 2 mm/min. At least six specimens of each composition were tested. The K_{IC} values were determined using the following relationship **(1)**

$$K_{IC} = Y \frac{3PS\sqrt{a}}{2BW^2}$$

$$Y = 1.93 - 3.07(a/W) + 14.53(a/W)^2 - 25.11(a/W)^3 + 25.80(a/W)^4$$

where Y is a shape factor, P the load at failure, S the length of the span and a the crack length.

3.7 Scanning electron microscopy (SEM)

The toughening mechanisms of the clay filled nanocomposites were investigated by analyzing the fracture surface of SEN-3PB specimens. A JEOL-JSM-5600 scanning electron microscopy (SEM) was used to image the fracture surface (coated with a thin layer of gold-palladium) under the accelerating voltage of 5 kV.

3.8 Dynamic mechanical analysis (DMA)

The storage modulus and glass transition temperature (Tg) of the samples were measured using a DMA 2980 dynamic mechanical analyzer in single cantilever mode. The conditioned samples were machined into rectangular of $30 \times 10 \times 3$ mm^3 and scanned from 30^oC to 300^oC at a heating rate of 3^oC/min using a frequency of 1 Hz.

References:

1. Hertzberg RW. *Deformation and fracture mechanics of engineering materials*. *New York: Wiley*, (1989).

Chapter 4. Benchmark organoclay system

4.1 Background

Polymer-clay nanocomposite was first achieved by incorporating organoclay into nylon matrix in 1993 **(1)**. Afterwards, this concept was transferred to epoxy systems, but the exfoliation was not promising. Nevertheless, epoxy-organoclay nanocomposites showed good performance in improving the thermal/mechanical properties of the matrix. In our research, organoclay system was investigated as a benchmark for comparison.

4.2 Preparation of epoxy-clay nanocomposites

Epoxy and clay were dried for 12 h at 80°C under vacuum oven prior to sample preparation. The clay was dispersed in the resin at 70°C using a homogenizer at 10000 rotations per minute (rpm). After mixed for 1 h, the resin/clay blend was further treated with ultrasonicator at 60°C for 1 h. Then the curing agent was added and mixed under vacuum until no more bubbles gave out. The blends were then poured into a preheated and vertically mounted glass mold in an oven and cured for 2 h at 100°C followed by a post curing for 5 h at 180°C. After that, the oven was switched off and the cured resin was allowed to cool slowly to room temperature in the oven. The resulted nanocomposite plates with thickness of 3 mm and 6.25 mm were then machined to different dimensions for thermal or mechanical tests.

4.3 Morphology

A wide range of epoxy nanocomposites containing 0, 1, 2.5, 5 and 7.5 wt% organoclay were prepared. The morphology of the cured samples was investigated using OM, WAXS and TEM.

Before investigating the microstructure of the nanocomposites, optical microscopy was first applied to observe the finely polished bulk surface of the nanocomposites. Optical micrograph as shown in Figure 4.1 for the nanocomposites containing 5 wt% organoclay, shows numerous well-dispersed clay aggregates with size of about 5 μm. Inside these particulate phases, the clay may exist in intercalated or exfoliated states. However, these aggregates indicate that not all clay particles are uniformly dispersed in the polymer phase.

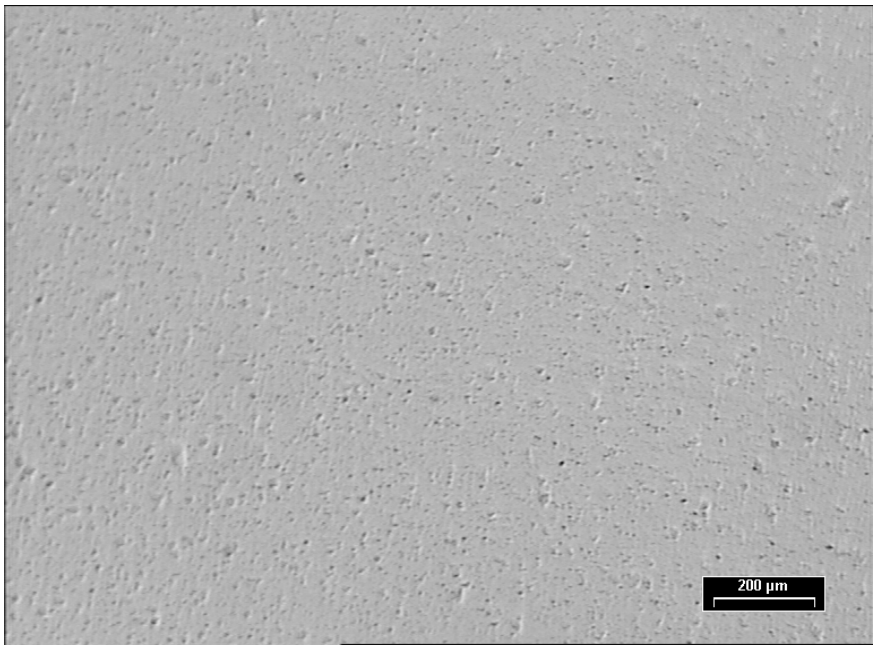

Figure 4.1. Optical micrograph of epoxy-clay nanocomposites (5 wt%) with clay aggregations (The scale bar is 200 μm).

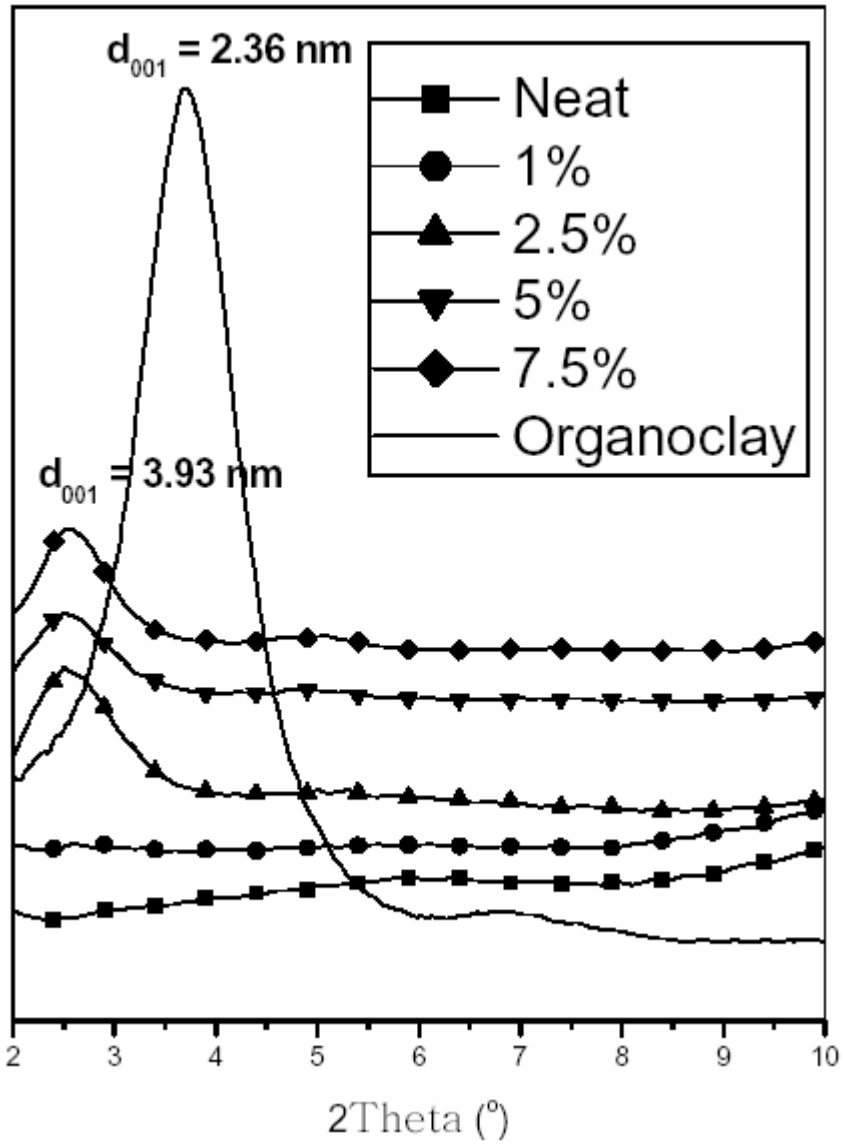

Figure 4.2. WAXS of epoxy-clay nanocomposites containing 0-7.5 wt% organoclay.

The WAXS patterns of the organoclay, neat epoxy and the nanocomposites containing different clay concentrations are shown in Figure 4.2. For organoclay, the scattering peak at d-spacing = 2.36 nm is assigned to the (001) basal plane, which corresponds to an interlayer spacing of the clay. The absence of basal scattering in the sample with 1 wt% clay suggests the possible formation of exfoliated clay structure after in-situ

polymerization. However, a small peak at d-spacing = 3.93 nm was observed for the samples with 2.5, 5 and 7.5 wt% clay, probably indicating that the clay platelets are not fully exfoliated but intercalated throughout the matrix. It is worth noting however that a WAXS pattern may not reveal the true level of exfoliation. The packing structure of layered silicates is similar to the structure of smectic liquid crystals. A disruption of ordered layer structure without any exfoliation could also lead to weakening of the scattering peak since the "structure factor" is lost. As a result, WAXS data is only a useful approximation to the nanostructure. It should be accompanied by TEM observations, which provide direct visualization of the morphology and spatial distribution of clay platelets.

The clay morphology within epoxy is shown in Figure 4.3 for the nanocomposite sample containing 5 wt% clay. At lower magnification, clay aggregation is evident as presented in Figure 4.3(A). The amount of aggregation is dependent on the clay content. At higher loading level, more clay clusters would be expected. By probing an aggregate at higher magnification (Figure 4.3(B)), it can be seen that the clay platelets retain much of their face-to-face alignment but cluster together in large domains. In addition to the regular stacking arrangement, some other regions where completely delaminated clay sheets dispersed individually can also be seen. Since a disorientation and delamination of the clay platelets represents exfoliation, the observed morphology may be considered as a mixture of intercalated and exfoliated clay sheets. Although the majority retains their face-to-face orientation, TEM indicates that a small amount of clay is indeed exfoliated.

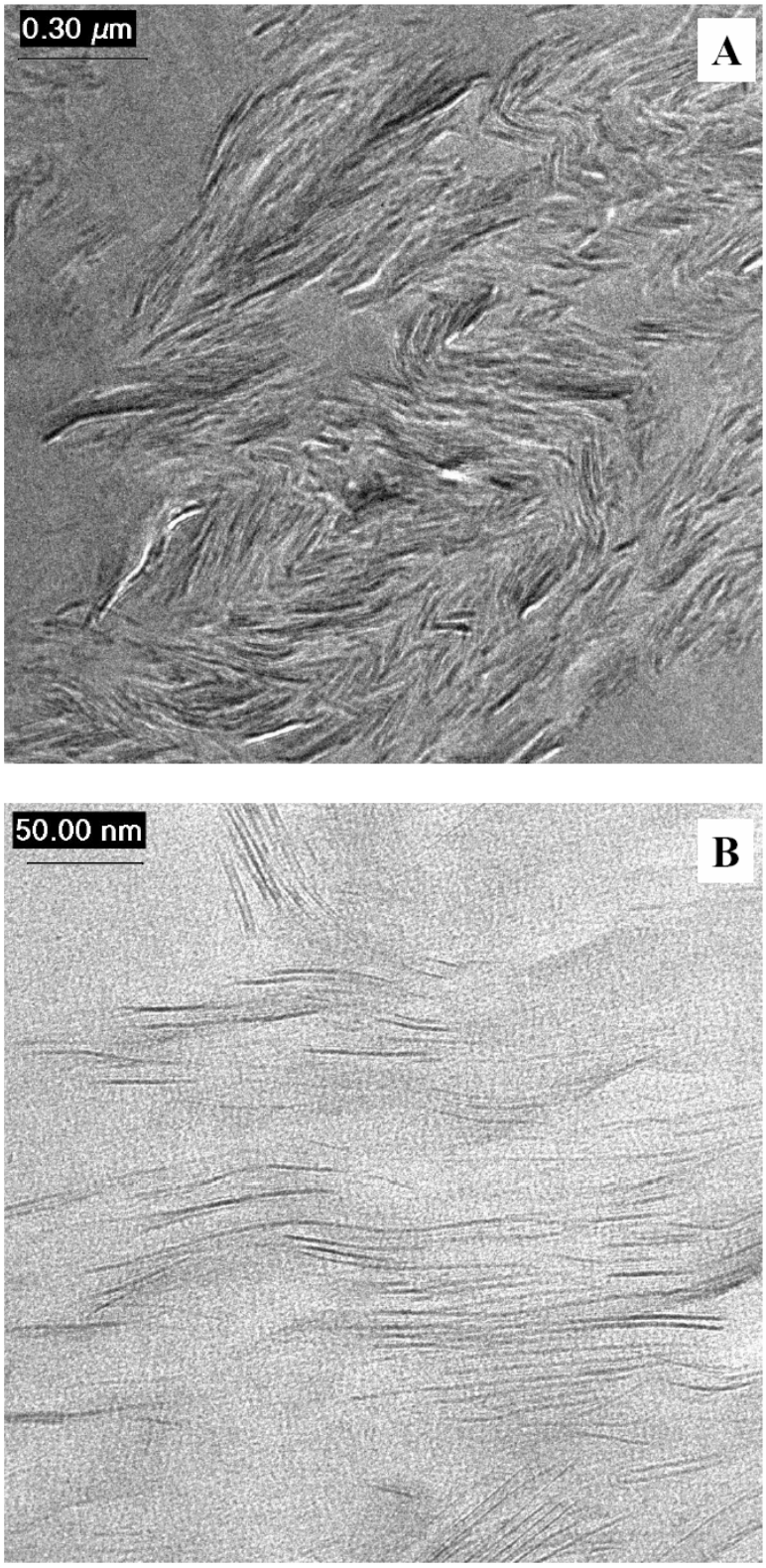

Figure 4.3. Low/high magnification TEM images of epoxy-clay nanocomposites (5 wt%): (A) intercalated morphology; (B) exfoliated morphology.

4.4 Thermal properties

Dynamic mechanical analysis (DMA) performed from 30°C to 250°C was used to investigate the influence of the organoclay on the storage modulus and the Tg of the nanocomposites. In the glassy region, as shown in Figure 4.4(A), the storage modulus of the nanocomposites increases with the organoclay loading. The storage modulus at 100°C as shown in Figure 4.4(B), illustrates an increase of 35% with addition of 7.5 wt% organoclay (i.e. from 1.66 GPa to 2.24 GPa).

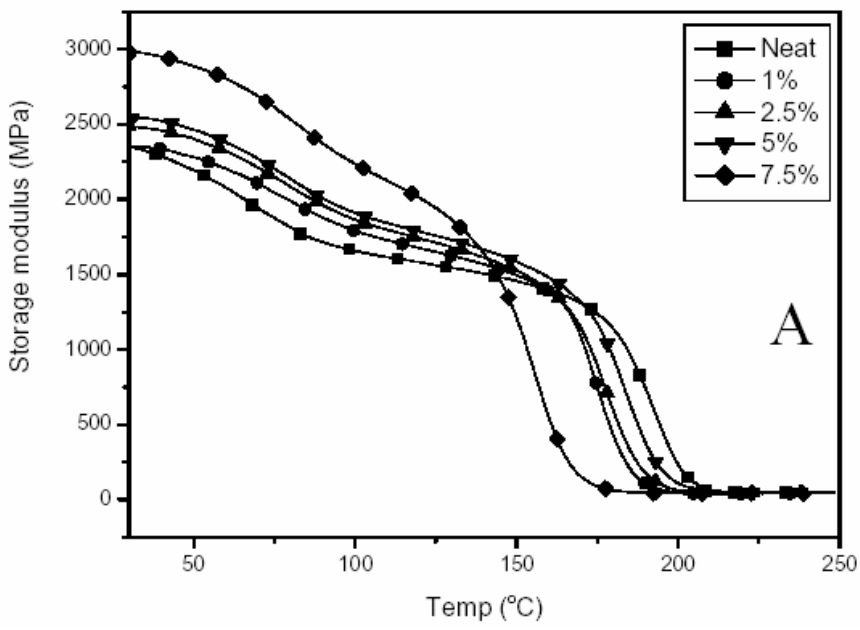

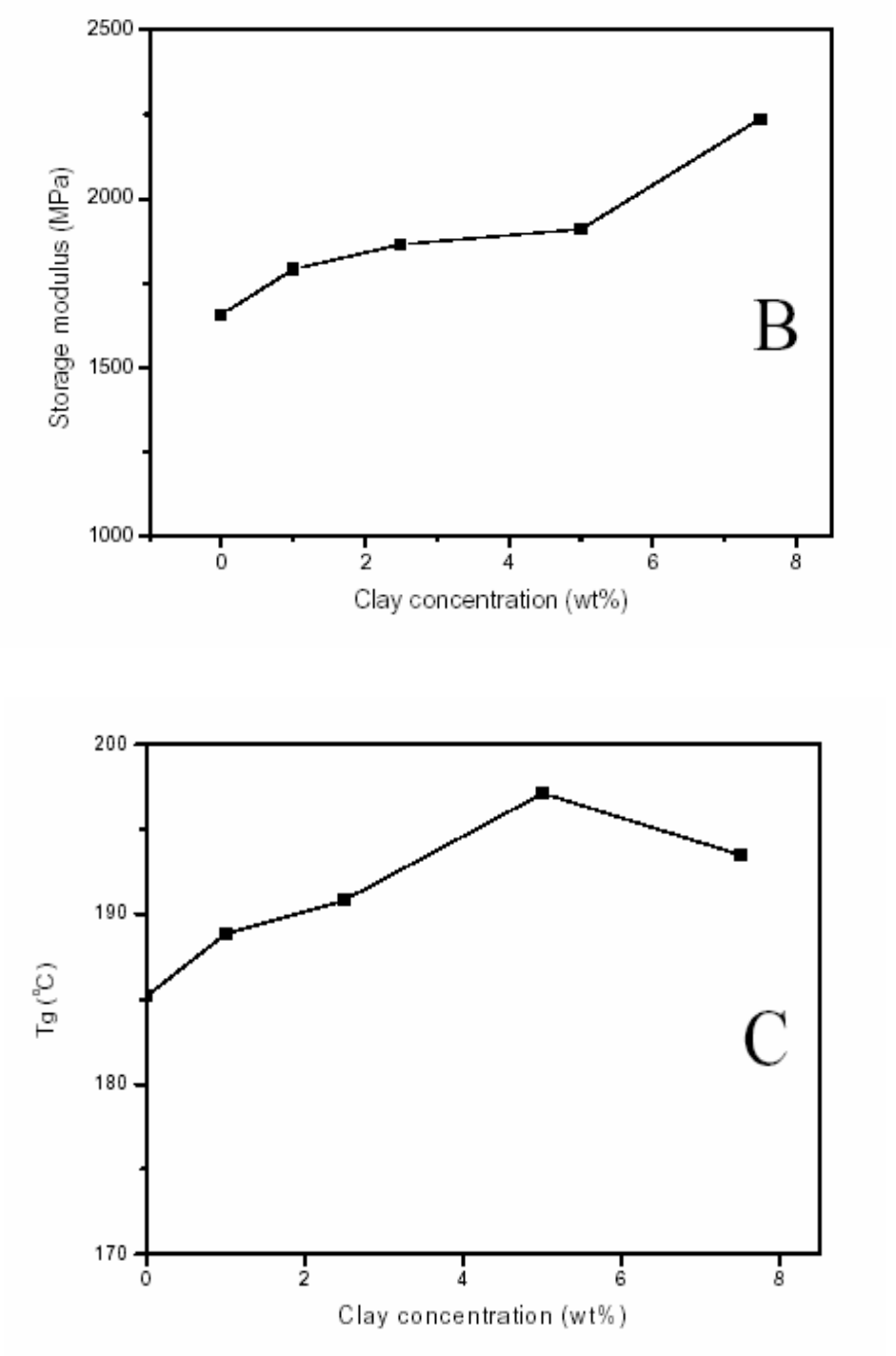

Figure 4.4. Dependence of thermal properties on clay concentration: (A) storage modulus; (B) storage modulus at 100°C; (C) glass transition temperature.

However, it can also be seen that the glass transition temperatures (Figure 4.4(C)) of the nanocomposites changes as compared to the neat epoxy, but the trend is not consistent with clay concentration. The values of Tg increased steadily with increasing organoclay concentration at the beginning, but dropped when the concentration is higher than 5 wt%. The glass transition temperatures of DGEBA-based epoxy nanocomposite systems have been investigated previously **(1-4)**. While increased glass transition temperatures were reported in some cases of intercalated nanocomposite systems **(2, 3)**, others have found a constant or slightly decreased Tg **(4, 5)**. The "absorbed layer" effect of the clay usually increases the glass transition temperature due to chains being tied down by the surface of the silicate. On the other hand, the alkyl-ammonium chains, which were introduced to the silicate layer surfaces during surface modification, lower the epoxy cross-linking density near the surfaces, thus leading to a lower Tg. This effect is more evident at high clay concentration. The observed Tg could be considered as a competitive consequence of these effects due to incorporation of organoclay. Since the system is complex, with a range of chemistries possible, it is much more difficult to identify reasons.

4.5 Mechanical properties

4.5.1 Tensile properties

The strength-strain behavior of epoxy can be categorized into brittle fracture, characterized by no yielding point. Figure 4.5(A) illustrates a region of Hookean's behavior at low strains, which was precisely recorded by extensometer. A strain range of 0.5%-1.0% was used to calculate the Young's modulus. As shown in Figure 4.5(B), the tensile modulus increases by about 20% for an organoclay concentration of 7.5 wt%.

Note that an increase of about 13% is achieved with addition of only 1 wt% organoclay. It should be recalled that for the nanocomposite with 1 wt% organoclay, WAXS showed no peak, indicating that the exfoliated clay morphology dominates. Thus, it indicates that the exfoliated structure contributes more significantly to the improvement of the tensile modulus than the intercalated one. However, the improvement is modest as compared to Lan and Pinnavaia's work **(6)**, in which the modulus of highly flexible resins was increased by approximately 500% at an organoclay concentration of 10 wt%. According to other researchers **(6, 7)**, highly flexible epoxy resins with low glass temperature below room temperature give much larger increases of stiffness in comparison to rigid, highly cross-linked epoxy resins. This effect was mainly attributed to the increased elasticity of the matrix above Tg, which allows shear deformation and stress transferring from the matrix to the platelet particles. In addition, this effect could also be explained by "rule of mixing", which illuminates that the reinforcement effect should be more significant for low modulus epoxy than high modulus epoxy. Considering the high rigidity of our epoxy matrix, the results are reasonable.

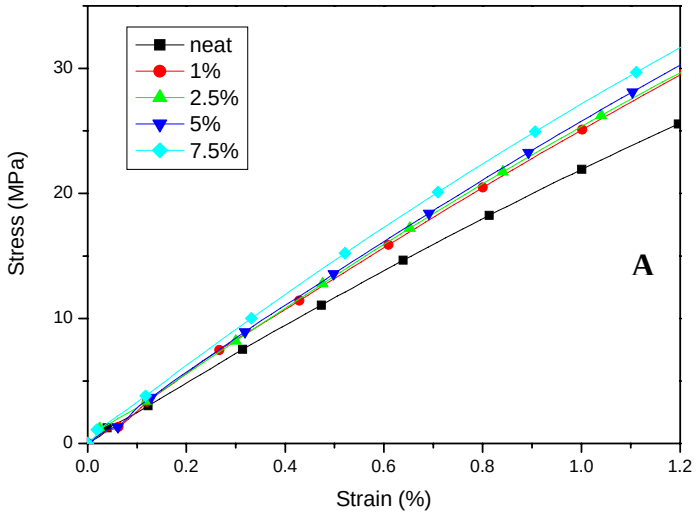

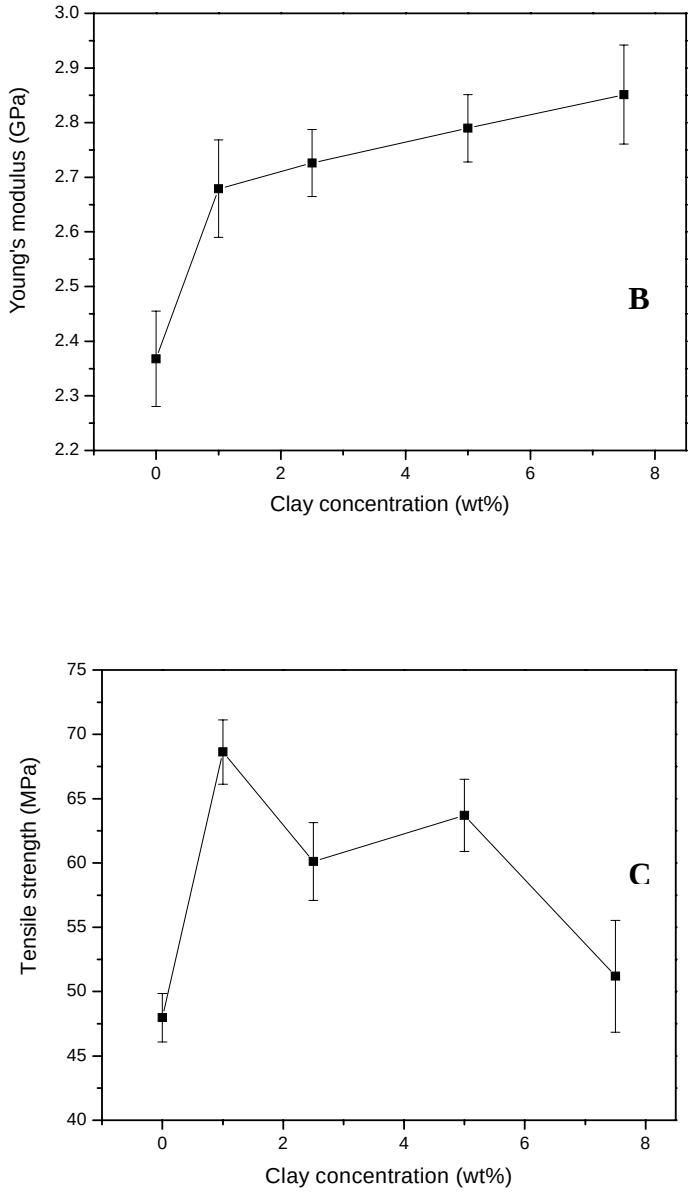

Figure 4.5. Dependence of (A) strength-strain behavior; (B) tensile modulus; (C) tensile strength on clay concentration.

The tensile strength, shown in Figure 4.5(C), increased by 44% with addition of 1 wt% organoclay, but dropped with further increasing organoclay content. On the fracture surface of every tensile sample, clay clusters were often observed, which may act as a defect center or stress concentration centers and cause the sample to fail. Since the

composites with higher clay concentration have more clay aggregates, the resulted tensile strength could not be significantly improved by incorporation of more organoclay.

4.5.2 Fracture toughness

The mode I fracture toughness, K_{IC}, as a function of the organoclay concentration (wt%) of the nanocomposites is shown in Figure 4.6(A). Whilst most toughening techniques show a loss in stiffness, such as in rubber toughened epoxy resins **(8)**, it can be seen that both toughness and stiffness have been improved through the organoclay incorporation with epoxy, as also observed by other researchers **(9)**. The fracture toughness increased linearly with organoclay incorporation and achieved a final improvement of 43% from 0.63 MPa·m$^{1/2}$ for neat epoxy resin to 0.90 MPa·m$^{1/2}$ for the nanocomposites containing 7.5 wt% organoclay.

Since the Young's modulus (E) also increases, K_{IC} may not provide a reliable parameter for the fracture toughness of the material. Therefore, there is a need to examine the critical energy release rate, G_{IC}, which is defined as the rate of energy released by the crack growth. For plain strain state, G_{IC} is related to K_{IC} by **(10, 11)**

$$G_{IC} = \frac{K_{IC}^2}{E^*},$$

where $E^* = E/(1-\nu^2)$, where ν is the Poisson's ratio. Here we only consider the normalized G_{IC} and the change of ν is negligible, so E is used instead of E^*.

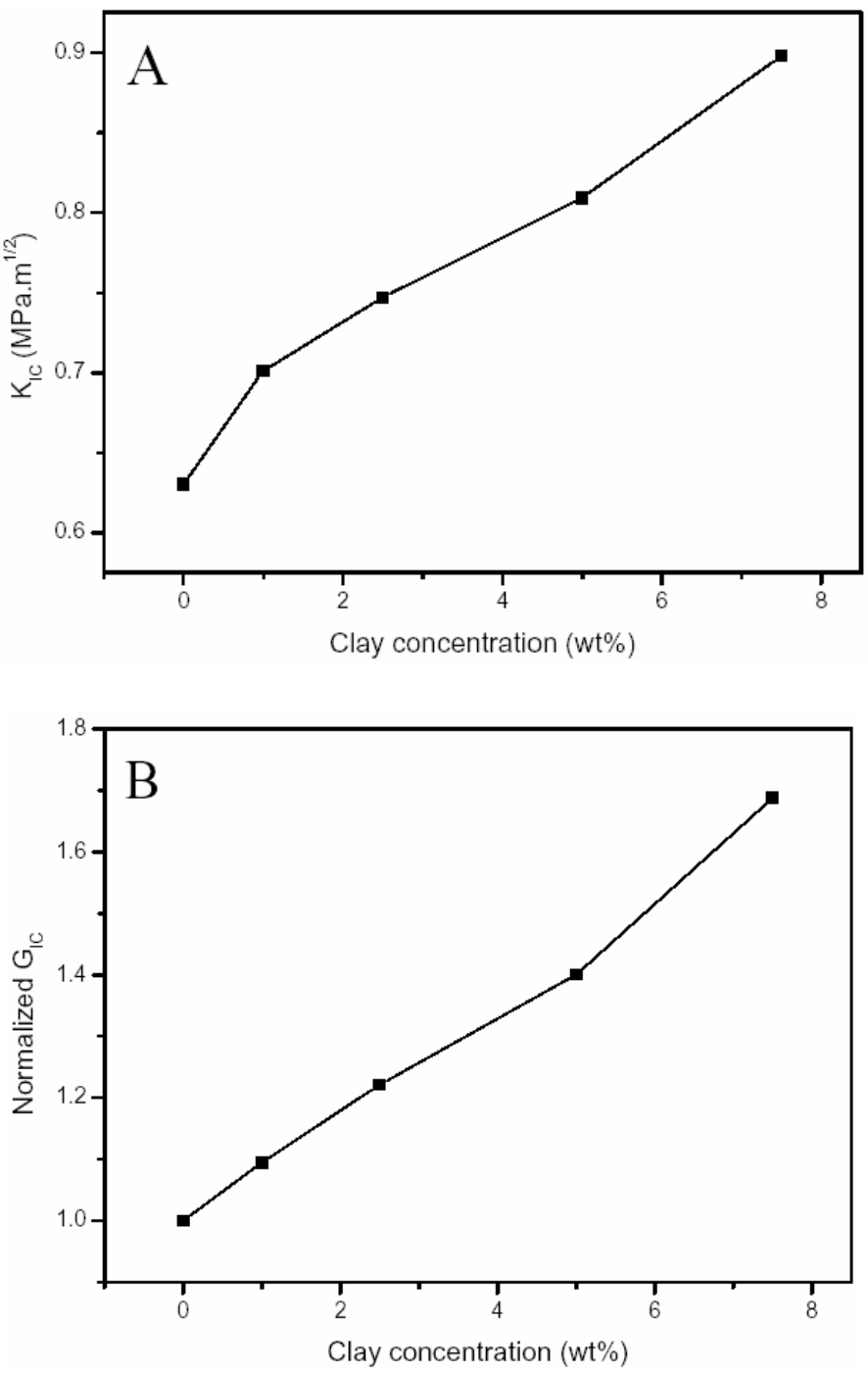

Figure 4.6. Dependence of fracture toughness on clay concentration:
(A) K_{IC}; (B) normalized G_{IC}.

The normalized G_{IC} was calculated by dividing the G_{IC} values of the nanocomposite by the G_{IC} value of the neat epoxy, which is 170 J/m^2. It can be seen in Figure 4.6(B) that the

normalized G_{IC} increased by 70% with incorporation of 7.5 wt% organoclay. Since G_{IC} represents the energy per unit area necessary to create a new surface area at the crack tip, this increase of G_{IC} indicates the fracture resistance is really improved.

4.6 Morphologies of fracture surfaces by SEM

The fracture surfaces within process zone **(12)** of organoclay filled epoxy nanocomposites were examined using SEM to investigate the fracture behavior and toughening mechanisms. Figure 4.7 shows the fracture surfaces of neat epoxy (A) and nanocomposites with 2.5 wt% (B) and 7.5 wt% (C) organoclay, where the arrows indicate direction of crack propagation. The fracture surfaces in Figure 4.7(A) are very smooth and featureless, indicating a typical brittle failure nature for neat epoxy resin. Compared with that of neat epoxy, Figures 4.7(B) and (C) exhibit rougher fracture surfaces of the composites containing 2.5 wt% and 7.5 wt% organoclay respectively, indicating that more energy was dissipated through creation of a new surface. The surface roughness significantly increases with increasing clay concentration, which is consistent with the improvement of fracture toughness.

In Figure 4.7(B), the clay aggregates with size of several μm are evidenced. The crack tip usually breaks the aggregates and propagates further. Steps parallel to the crack propagation direction are clearly observed behind the aggregates. Similar structures are often observed in fiber **(13)** and glass bead **(14, 15)** filled epoxy systems, which are the characteristic tail structures formed when two secondary crack fronts separated by a

particle meet with each other **(16-18)**. Due to the small size and large number of the clay aggregates, which cause short inter-particle distance, the steps in the systems studied here are smaller and shorter than those in fiber and glass bead filled epoxy systems **(13-15)**. The steps are highly curved and deflected from the initial crack propagation direction, which usually cause shear and tear deformation of the matrix to dissipate much energy. This effect is more evident in the specimen with high clay concentration (Figure 4.7(C)), in which almost no step texture could be identified. In addition to the step formation, other mechanisms, such as crack front bowing **(19)** as indicated by the arrows in Figure 4.7(B), may also be operative. Considering that the extent of clay exfoliation is low, it might not contribute much to the fracture toughness improvement. Therefore, the dominant mechanism may be the shear deformation of epoxy matrix induced by clay aggregates and clay particle breakage.

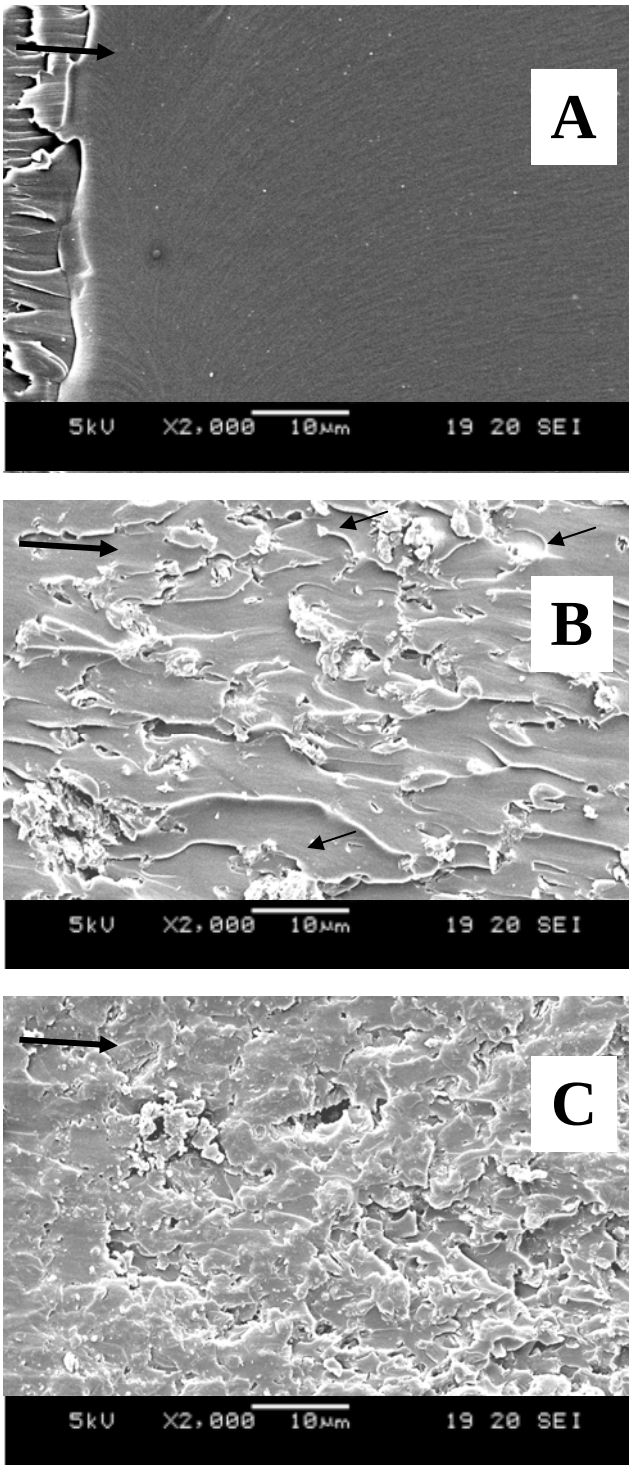

Figure 4.7. SEM micrographs of the fracture surfaces of (A) neat epoxy; nanocomposite with (B) 2.5 wt% clay; (C) 7.5 wt% clay.

4.7 Summary

Epoxy-organoclay nanocomposites with different clay loading were prepared using in-situ polymerization method. WAXS and TEM illustrated a mixed exfoliated/intercalated structure. The thermal properties and glass transition temperatures of the cured systems were determined by DMA. The storage modulus increases with clay concentration, indicating the reinforcing effect of clay. The Tg increases at low clay content, but decreases with incorporation of more organoclay, which was attributed to the interaction between the matrix and clay and the surfactant. Both toughness and stiffness of the materials were improved through the incorporation of organoclay, despite the fact that it is often found that these two properties cannot be simultaneously achieved. The fracture surfaces of the nanocomposites were investigated using SEM. Maybe due the low exfoliation fraction, the clay aggregates, not exfoliated layers, were found to be main reason for the toughening effect.

Overall, the organoclay is effective in improving thermal/mechanical properties of epoxy. Nevertheless, the poor clay exfoliation weakened the enhancement. In addition, the high content of surfactant, which lowers the effective clay concentration, compromised the reinforcing effect of clay. In the following chapter, a new approach will be proposed with an aim to improve exfoliation and eliminate the clay surface modifiers.

References:

1. Usuki A, Kawasumi M, Kojima Y, Okada A, Kurauchi T, Kamigaito O. *J. Mater. Res.*, 1993; 8: 1174-1178.
2. Lee DC, Jang LW. *J. Appl. Polym. Sci.*, 1997; 68: 1997-2005.
3. Kelly P, Akelah A, Qutubuddin S, Moet A. *J. Mater. Sci.*, 1994; 29: 2274-2280.
4. Massam J, Pinnavaia TJ. *Clay Mater. Res. Soc. Symp. Proc.*, 1998.
5. Tak GK, Sue HJ. *Preparation and mechanical properties of epoxy-clay nanocomposites. ACS Spring meeting*, 2000 San Francisco.
6. Lan T, Pinnavaia TJ. *Chem. Mater.*,1994; 6: 2216-2219.
7. Wang MS, Pinnavaia TJ. *Chem. Mater.*, 1994; 6: 468-474.
8. Sankaran S. *J. Appl. Polym. Sci.*, 1990; 39: 1635-1647.
9. Becker O, Verley R, Simon GP. *Polymer*, 2002; 43: 4365-4373.
10. Williams JG. *Introduction to linear elastic fracture mechanics*. In: Moore DR, Pavan A and Williams JG (Ed.). *Fracture mechanics testing methods for polymers, adhesives and composites*. *ESIS publication 28*, 2001, pp. 3-10.
11. Williams JG. *Introduction to elastic-plastic fracture mechanics*. In: Moore DR, Pavan A and Williams JG (Ed.). *Fracture mechanics testing methods for polymers, adhesives and composites*. *ESIS publication 28*, 2001, pp. 119-122.
12. Pearson RA and Yee AF. *J. Mater. Sci.*, 1986; 21: 2475-2488.
13. Wang L, Teh SF, Tjiu WW, Liu TX, He CB. *Polym. Compos.*, 2005; 26: 333-342.
14. Lee J, Yee AF. *Polymer*, 2000; 41: 8375-8385.
15. Lee J, Yee AF. *Polymer*, 2001; 42: 577-588.
16. Lange FF. *Philos. Mag.*, 1970; 22: 983-992.

17. Spanoudakis J, Young RJ. *J. Mater. Sci.*, 1984; 19: 473-486.

18. Spanoudakis J, Young RJ. *J. Mater. Sci.*, 1984; 19: 487-496.

19. Bagheri R, Pearson RA. *Polymer*, 2000; 41: 269-276.

Chapter 5. Microwave-assisted pristine clay system

5.1 Background

In the above chapter, we have demonstrated that in epoxy matrix, the exfoliation of organoclay is incomplete. In addition, organoclay contains large amounts of organic modifiers, which not only increase the cost but also cause the interface between the layers and matrix very complex, thus influencing the properties of the material. Therefore, there is a need to develop a new approach to disperse clay with a low or zero organic content into polymer matrix. Recently, the idea of using microwave to achieve matrix polymerization and intercalation has been employed to synthesize polymer-clay nanocomposites **(1, 2)**. In this work, we applied this idea to epoxy system and investigated the influence of raw clay on the mechanical properties of the matrix.

5.2 Preparation of epoxy-raw clay nanocomposites

Raw clay was treated in a humidity chamber for 9 hours under 90^{o}C, 100% RH. The treated clay was dispersed in epoxy resin at 30^{o}C using a stirrer at 2000 revolutions per minute (rpm). After mixed for 1 h, the epoxy-clay blend was treated with microwave for 1 min. A household microwave oven was used in this work. The samples were treated in the oven at its maximum power of 800 Watt. Then the curing agent was added and the mixture was stirred under vacuum for 1 h. The mixture was poured into a glass mould and cured for 2 h at 100^{o}C, followed by a post curing for 5 h at 180^{o}C.

5.3 Exfoliation mechanism and morphology of pristine clay

The idea of the new approach is that, if moisturized raw clay was employed as the fillers mixed with epoxy resin, and a short time microwave treatment was applied to the epoxy-clay mixture before curing, the water in the clay galleries may vaporize rapidly and generate a high internal pressure within the clay particles due to the localized intensive heating from the microwave. It was hypothesized that this "popcorn" effect may overcome the resistance forces arise from the static electrical attraction and van der Waals forces between the clay layers, leading to a high degree of clay exfoliation. The proposed mechanisms are schematically shown in Figure 5.1.

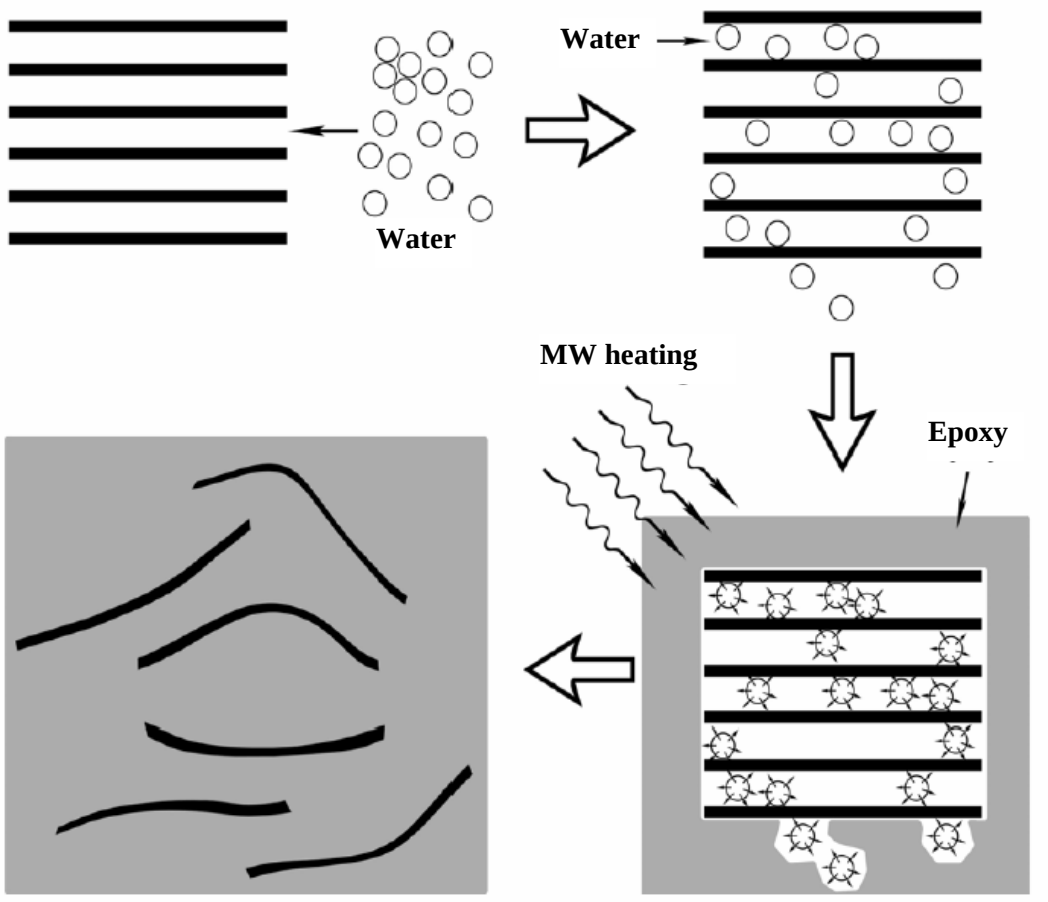

Figure 5.1. The proposed exfoliation mechanism of raw clay.

For the microwave induced "popcorn" to take place, we put the pristine clay in a moisture chamber at 100% RH and 90°C for 9 hours in order to introduce water into the clay galleries. As can be seen in Figure 5.2, water uptake of the raw clay increases rapidly in a short time and gradually levels off, which tends to saturate after 9 hours.

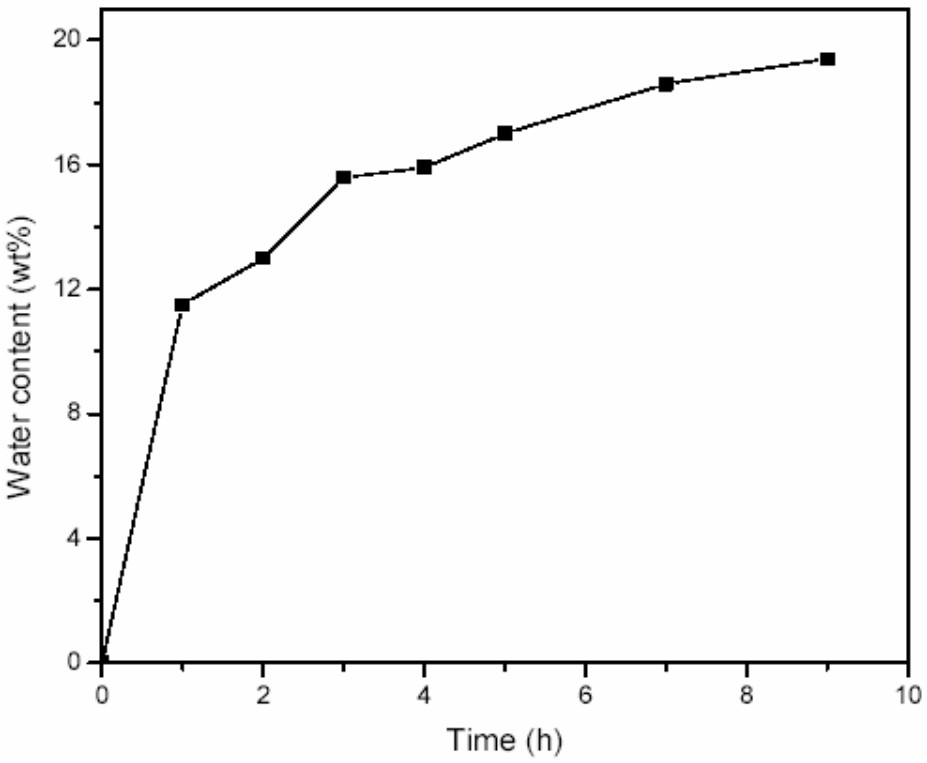

Figure 5.2. Water absorption of raw clay as a function of treatment time.

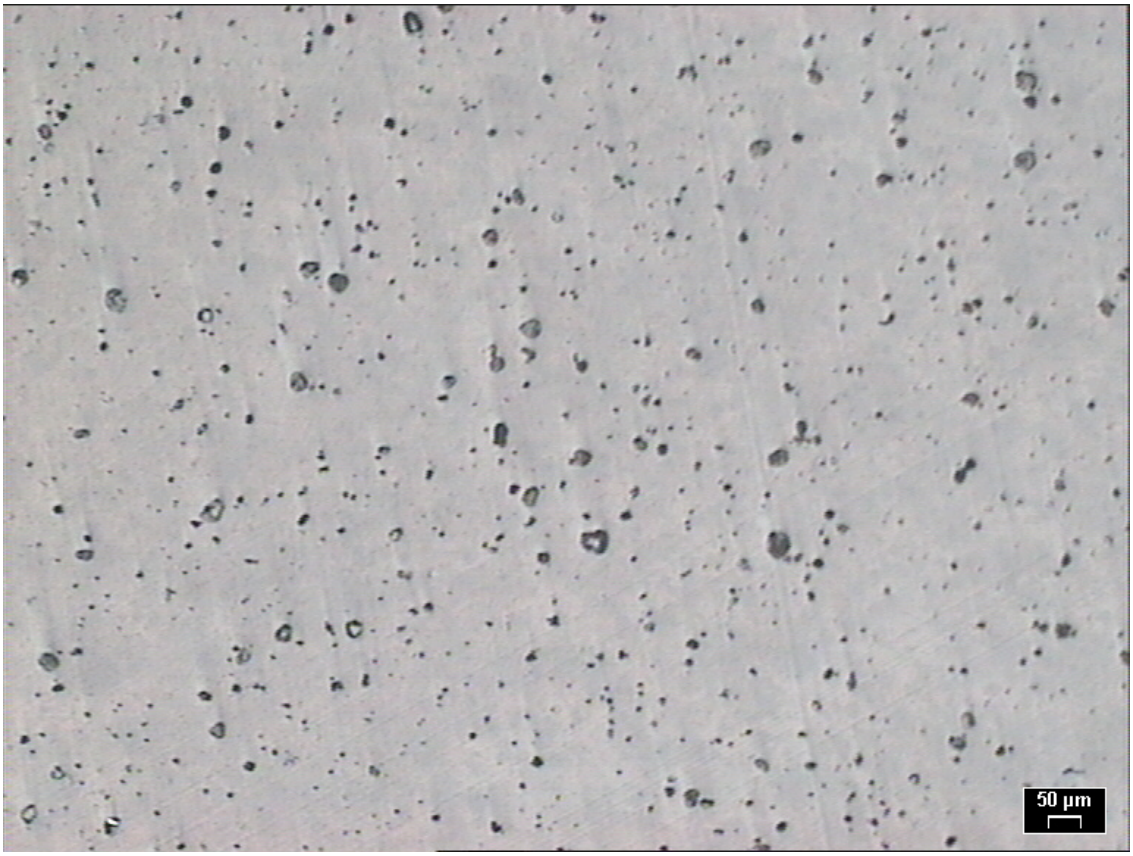

Figure 5.3. OM image of clay dispersion (5 wt% raw clay).

In this work, a wide range of epoxy nanocomposites containing 0, 2.5, 5, 7.5, 10, 12.5, 15 and 20 wt% raw clay were prepared with the new approach. The morphology of the cured samples was investigated using OM, WAXS and TEM. The optical micrograph in Figure 5.3 shows the polished surface of the nanocomposite containing 5 wt% clay, in which large particulate aggregates can be observed. This may be due to the poor compatibility between raw clay and epoxy matrix.

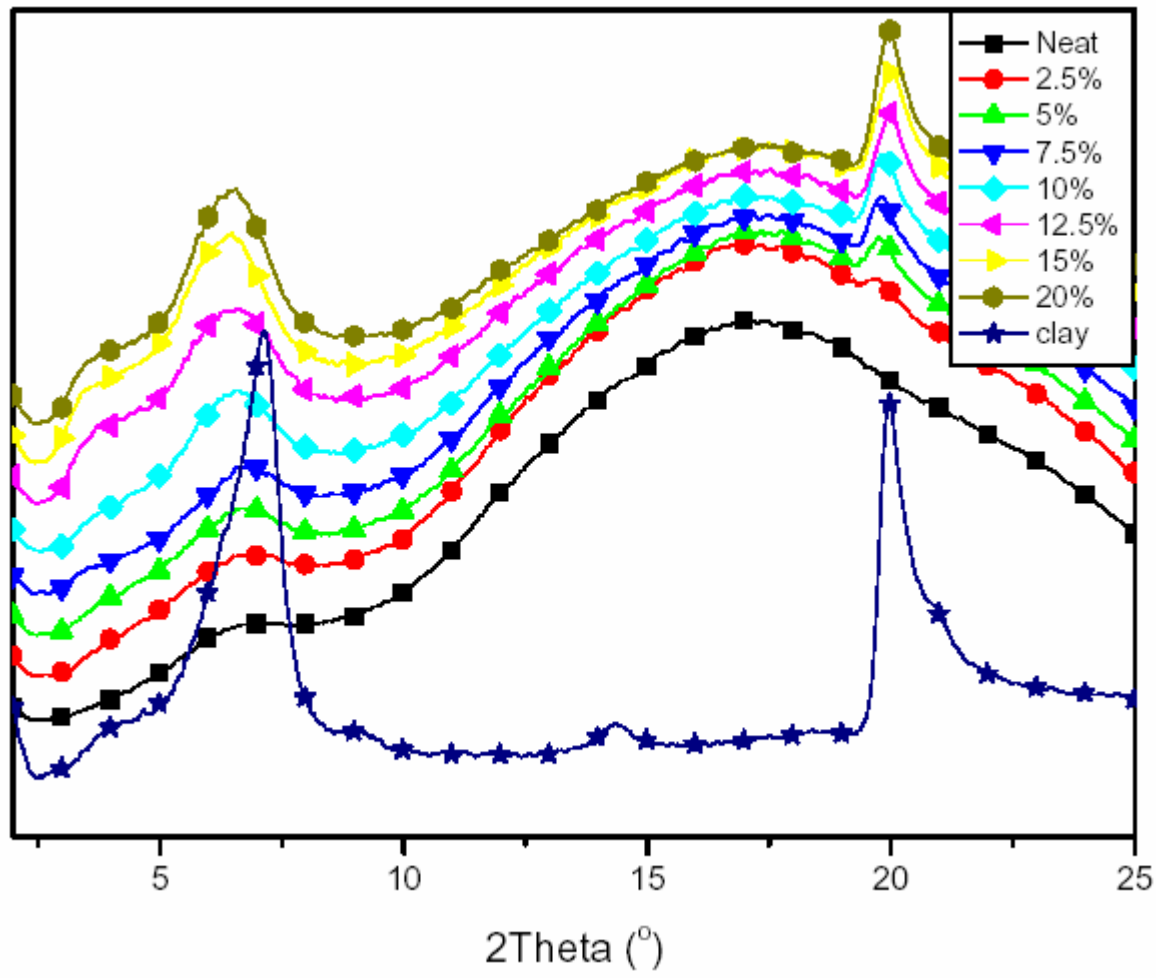

Figure 5.4. WAXS patterns of epoxy-pristine clay systems.

The WAXS diagrams for the nanocomposites with different clay concentrations are shown in Figure 5.4. By WAXS, the microstructure of the composite is not clearly illustrated. There are observed peaks for the composites, as well as a slightly shift of the scattering peaks toward lower angle, which seems to indicate the existing of intercalated structure in some areas while the original structure kept unmoved in some other areas. It should be also noted that the peak intensity of composites reduced significantly as compared to that of raw clay and the reduction is comparable with the organoclay system,

which could be due to the formation of exfoliated structure. Yet WAXS only gives a coarse image of the morphology, the fine structures still need to be confirmed by TEM.

Figures 5.5(a)-(e) show TEM images of the epoxy-raw clay sample prepared using microwave treatment. The array of clay platelets that was widely reported in literature does not seem to exist in our samples when the clay content is lower than 5 wt%. Figure 5.5(a) is one of the TEM micrographs taken from a sample with 2 wt% microwave-treated pristine clay. Clearly, the surface of the clay platelets shown in Figure 5.5(a) are parallel to the TEM micrograph surface with some of them curled up, showing the edge of the exfoliated clays no thicker than a few nanometers. When the samples with high clay contents were examined, the exfoliated clay platelets are easily seen, as demonstrated in Figure 5.5(b). Interestingly, the exfoliated clay particles are obviously highly deformed and no specific orientation of the clay platelets can be identified. It seems that the explosion of the "water bombs" in the clay galleries had opened up the clay galleries effectively. Figures 5.5(c) and (d) are from a closer TEM examination on one of the aggregates, revealed a microstructure of a porous ball, or "loss cabbage", with exfoliated and curved clay platelets as the ball surface. The enlarged TEM micrographs in Figure 5.5(e) was taken from the dark strings in Figure 5.5(d), which are bundles of clay platelets not fully exfoliated due, probably, to poor moisture penetration at this region.

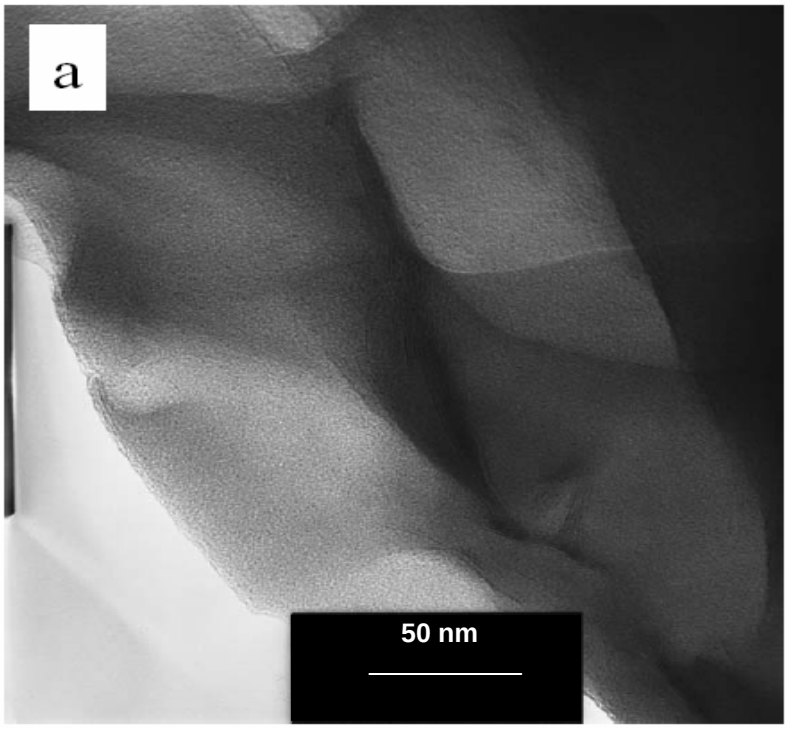
a
50 nm

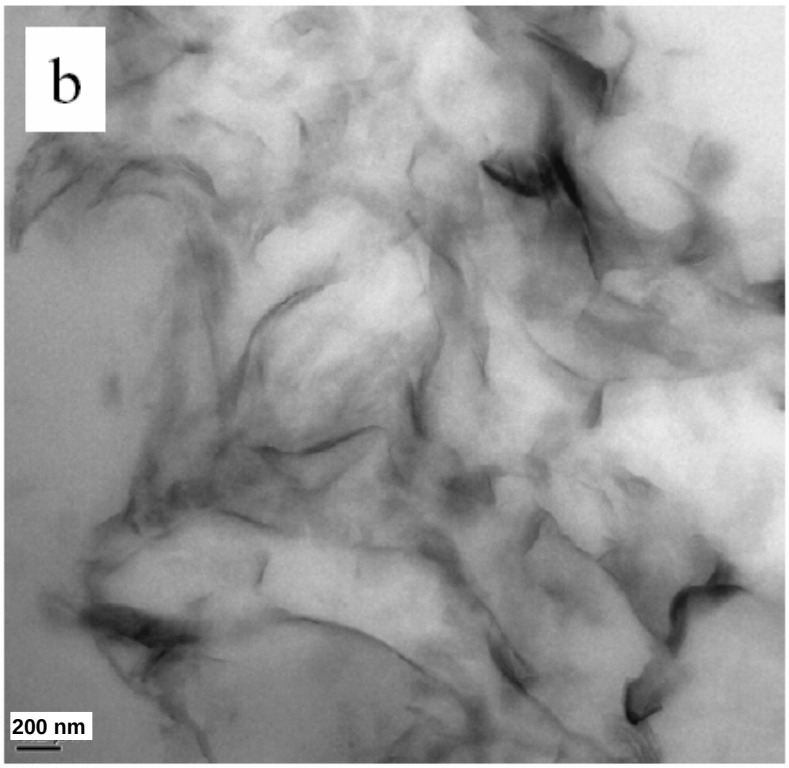
b
200 nm

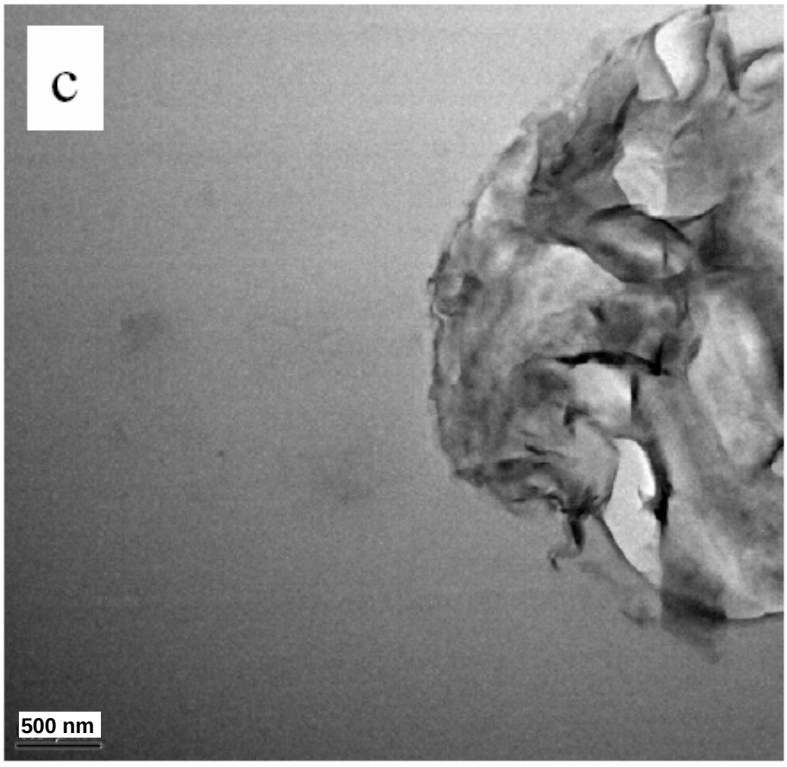
c
500 nm

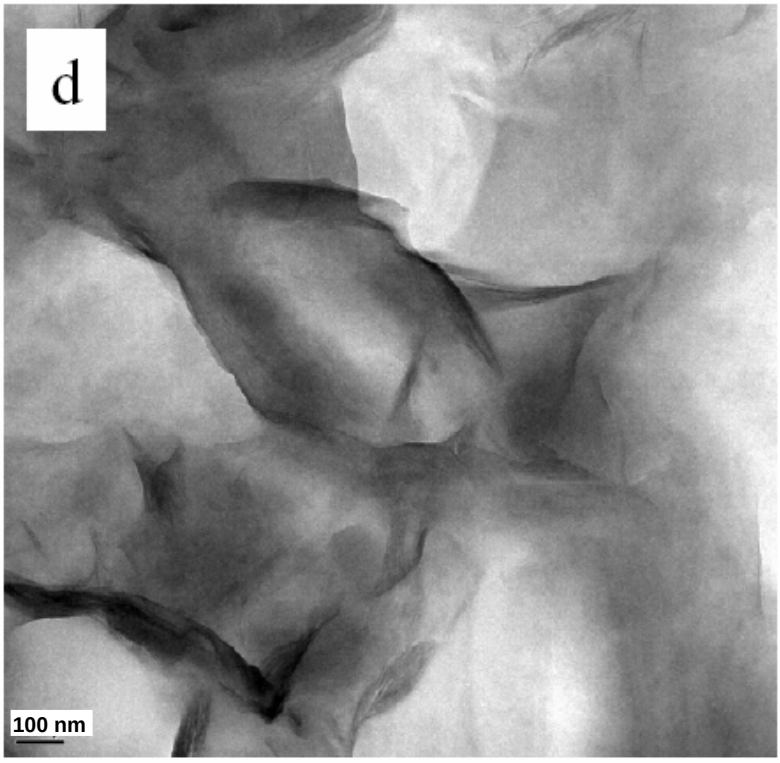
d
100 nm

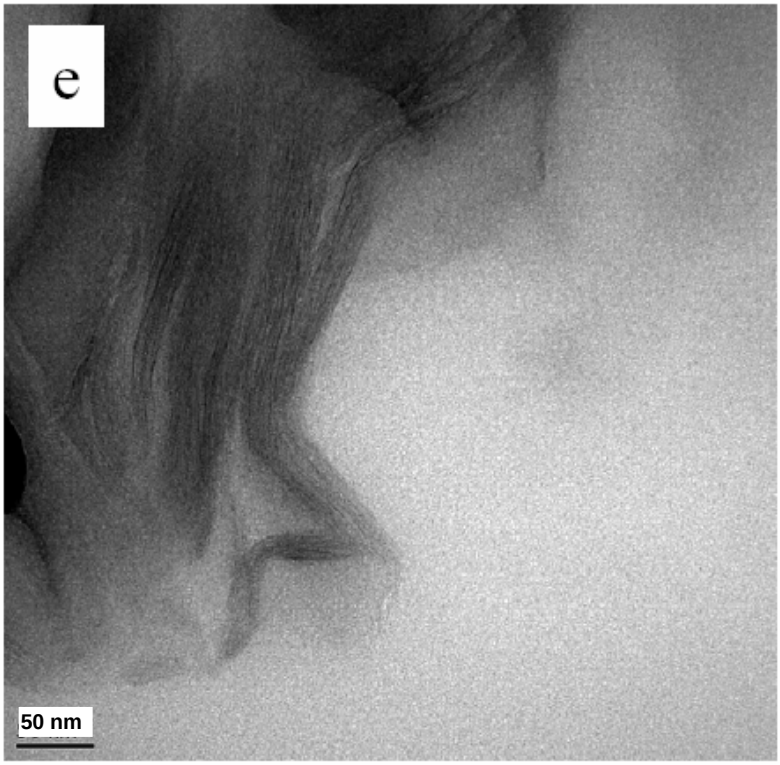

Figure 5.5. TEM observations of clay dispersion: (a) 2 wt%; (b) 15 wt%; (c) an aggregate (15 wt%); (d) an enlarged image of a location in Figure 5.5(c); (e) a black region in Figure 5.5(d).

From the above-mentioned observations, it is believed that the exfoliation of the pristine clay with microwave/moisture assistance was achieved through the mechanisms as illustrated in Figure 5.1. It is well known that a polar molecule, such as water, can be quickly heated up by microwave. When the pristine clay is treated in a moisture chamber, the clay absorbs water and stores the water in the galleries between the clay layers because the hydrophilic surfaces of pristine clay have high affinity for water. After the moisturized clay is mixed with epoxy resin and treated by microwave, the localized intensive heating by the microwave will quickly vaporize the water in the clay galleries and generate a high internal pressure. The repulsive force of this "popcorn" process will overcome the static attraction between the nanolayers; thus, facilitate the exfoliation of

the clay. Since the distribution of the repulsive force along the clay gallery may not be uniform, i.e. the force at the center of the gallery may be larger than that at two edges, or moisture penetration may not reach certain locations, therefore, the exfoliation process may cause localized deformation of the clay platelets, as already demonstrated by the TEM results.

Moreover, we also propose that the aggregates found in high clay content sample are actually clusters of exfoliated clay platelets in a "loss cabbage" structure, due to poor dispersion and distribution of the platelets in epoxy. The poor dispersion and distribution is understandable if we recall that the clay surfaces are hydrophilic and introducing water into the clay leads to an even lower miscibility between the clay and epoxy.

5.4 Thermal properties

The effect of pristine clay on the thermal mechanical properties was studied using dynamic mechanical analysis (DMA) performed from 30^{o}C to 250°C. In the glassy region, as shown in Figure 5.6(A), the storage modulus of the nanocomposites increases with the clay loading modestly. The storage modulus at 100°C (Figure 5.6(B)) illustrates an increase of 12.5% with addition of 20 wt% pristine clay (i.e. from 1.66 GPa to 1.86 GPa). This improvement is very limited as compared to the organoclay system, indicating that the pristine clay is much less effective than organoclay. Possible reasons could be non-uniform clay dispersion, weak interface and residual moisture. Poor interaction

prevents epoxy's diffusion into the clay layers, leading to inhomogeneous clay dispersion throughout the matrix although the clay layers had been delaminated by microwave, which compromised the reinforcing effect of clay. The hydrophilic nature of pristine clay caused very poor interaction between clay layers and epoxy, resulting in poor improvement. In addition, during the nanocomposite preparation, large amount of moisture was introduced into the clay galleries to facilitate delamination. After microwave treatment, the clay layers were pushed apart and the moisture was released to polymer phase. A portion of moisture resided inevitably even if the mixture was vacuumed for 1 hour. The residual water will plasticize the matrix **(1-4)** and compromise the reinforcing effect of clay further.

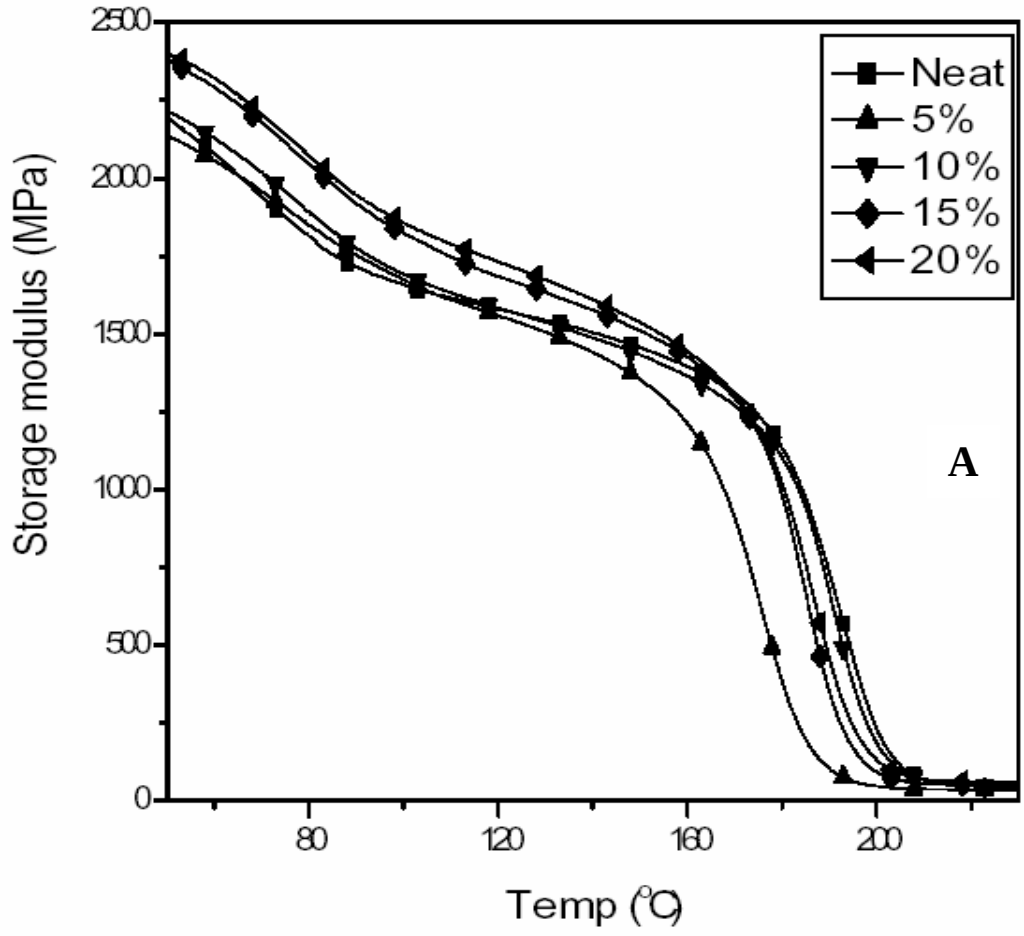

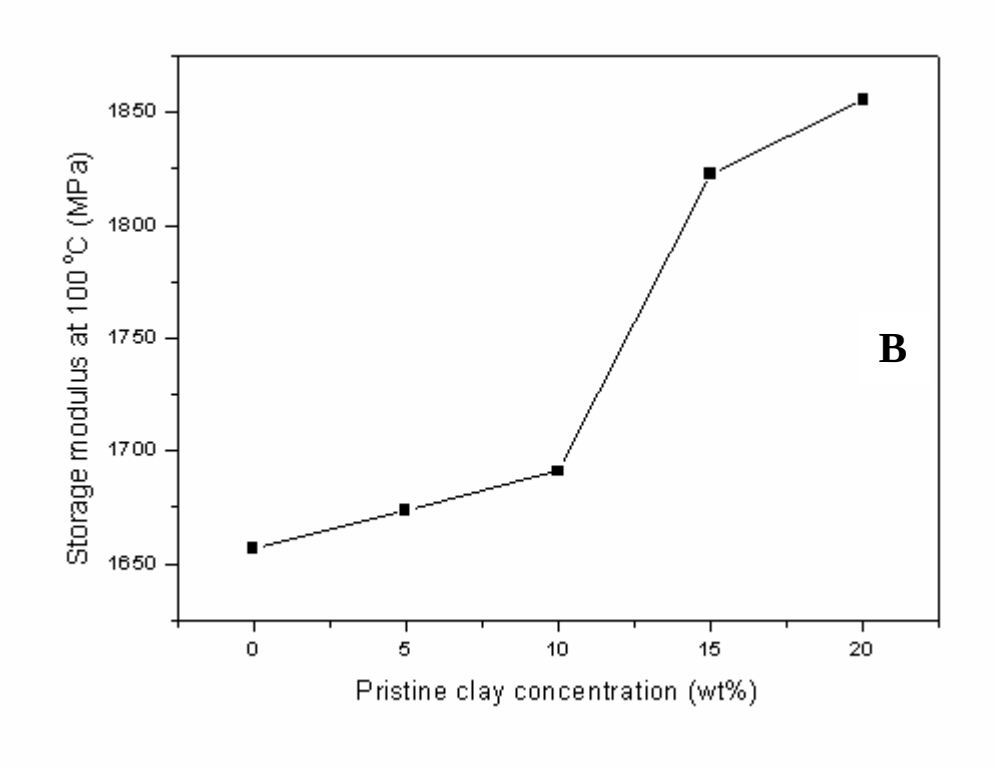

Figure 5.6. Dependence of thermal properties on clay concentration: (A) storage modulus; (B) storage modulus at 100°C.

5.5 Mechanical properties

5.5.1 Tensile properties

Figure 5.7(A) is the strength-strain behavior of epoxy-pristine clay composites, where a linear range between 0.5% and 1.0% was used to calculate the Young's modulus. As shown in Figure 5.7(B), the Young's modulus of the epoxy-clay nanocomposites is dependent on clay concentration and increases about 50% with a raw clay concentration of 20 wt%. Considering the high rigidity of the matrix studied here and the weak interaction between the raw clay and epoxy, this improvement is quite significant. The tensile strength increased 24% with addition of 5 wt% clay, but dropped with further

addition of raw clay (Figure 5.7(C)). On the fracture surface of tensile samples, some defects (clay clusters or bubbles) could be observed, which could have acted as defect centers and initiated the failure of the samples. Since the composites with a higher clay concentration have more clay aggregates, the resulted tensile strength could not be significantly improved by incorporating clay.

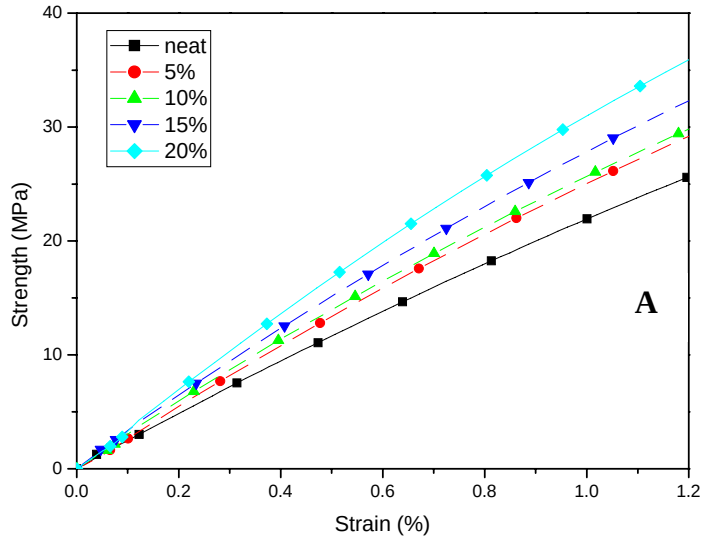

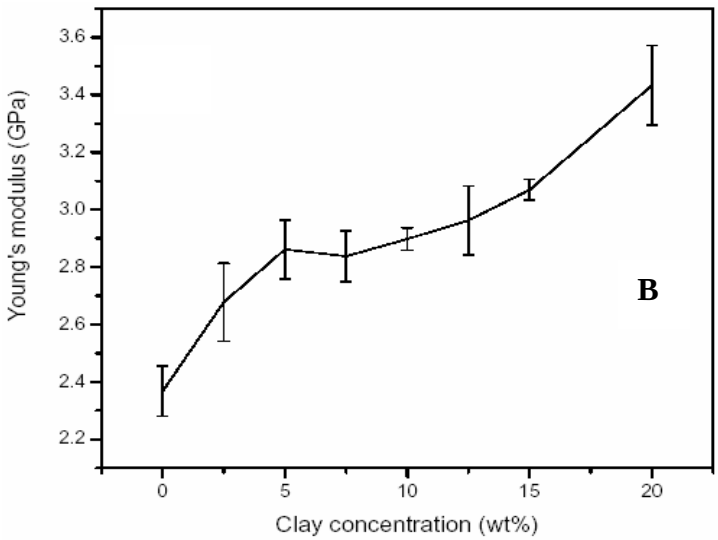

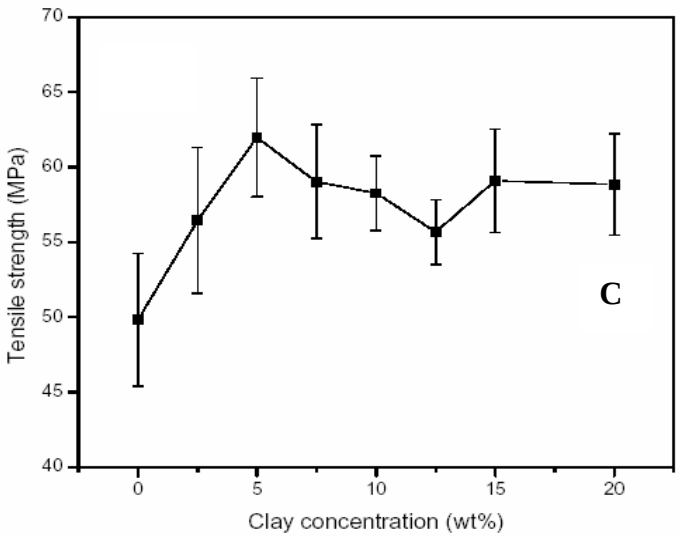

Figure 5.7. Dependence of (A) strength-strain behavior; (B) Young's modulus; (C) tensile strength on clay concentration.

5.5.2 Fracture toughness

The mode I fracture toughness, K_{IC}, as a function of the raw clay concentration (wt%) is shown in Figure 5.8(A). The K_{IC} increased by about 105% with addition of 20 wt% raw clay, i.e. from 0.63 MPa·m$^{1/2}$ to 1.29 MPa·m$^{1/2}$.

The normalized G_{IC} was calculated by dividing the nanocomposite G_{IC} values through the G_{IC} of the neat epoxy (170 J/m^2). From Figure 5.8(B), it can be seen that the G_{IC} increased 200% with incorporation of 12.5 wt% raw clay. Since G_{IC} represents the energy per unit area necessary to advance the crack at the crack tip, such a significant increase of G_{IC} means the fracture resistance is subsequently improved. The value of G_{IC}, however, decreased slightly with further addition of raw clay. Similar situation was also observed in organoclay filled polymer systems **(5-7)**, in which the fracture toughness/Young's modulus increased with clay concentration at first, but dropped when the concentration

higher than certain values. These behaviors could be attributed to the microstructure of the composite. At a low volume fraction, the silicate layers can be completely intercalated or well exfoliated, but at a relatively high volume fraction, only a certain amount of silicate layers can be intercalated or exfoliated in the composite whereas the others exist in the original form without intercalation, which contributes little to the mechanical properties and even forms defect centers in the matrix, causing the sample to fail under stress. In our organoclay system (Figure 4.6), this was not observed mostly due to the clay concentration not reacheding the threshold value.

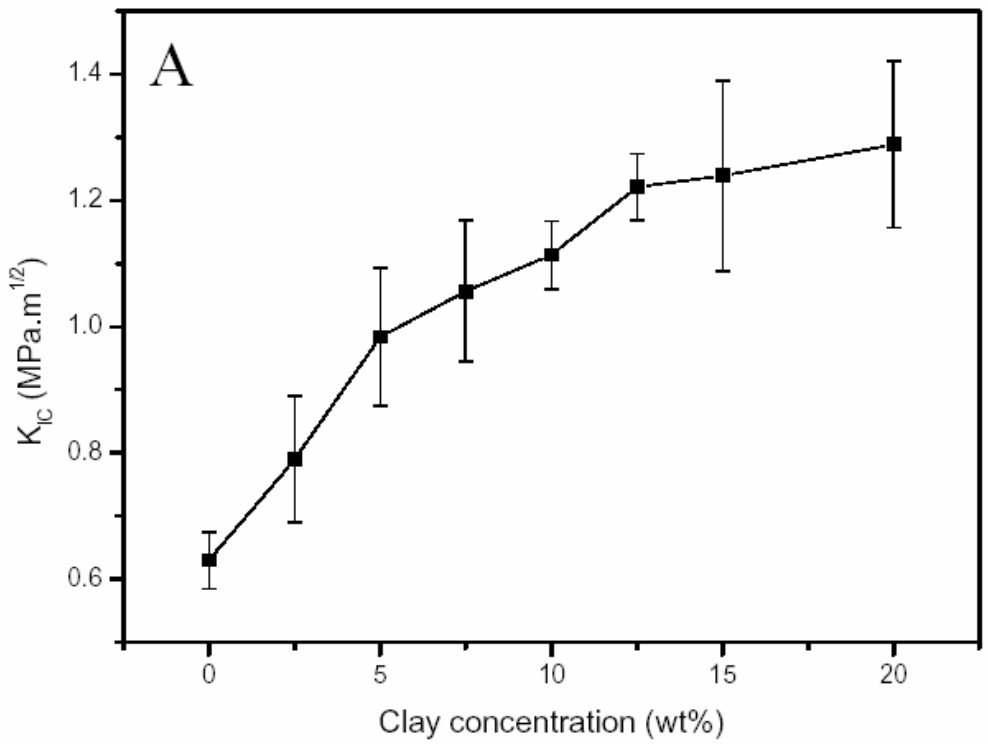

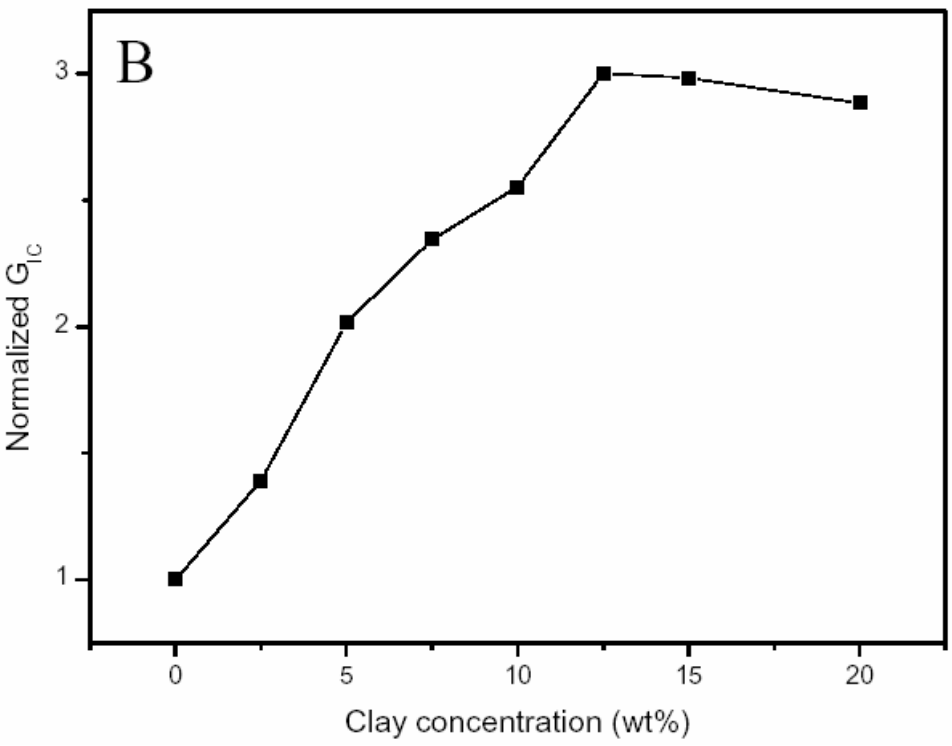

Figure 5.8. Dependence of (A) K_{IC}; (B) normalized G_{IC} on clay concentration.

5.6 SEM morphology of the fracture surface

The process zones on the fracture surfaces of raw clay filled epoxy were examined using SEM to investigate the toughening mechanisms. It can be seen that in Figure 5.9(A) the fracture surface of neat epoxy is very smooth and featureless, showing the typical brittle failure nature for neat epoxy resin. Nevertheless, Figures 5.9(B), (C) and (D) illustrate the rougher fracture surfaces of the composites containing 5 wt%, 10 wt% and 20 wt% raw clay in epoxy matrix respectively at the same magnifications, which reveals that more energy was dissipated through creation of new surface. The surface roughness increases with clay concentration. This is consistent with fracture toughness improvement.

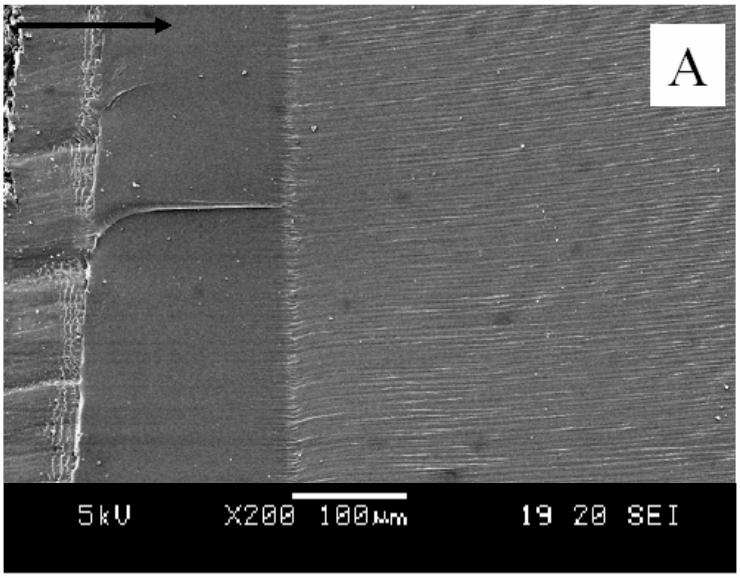
A
5kU X200 100µm 19 20 SEI

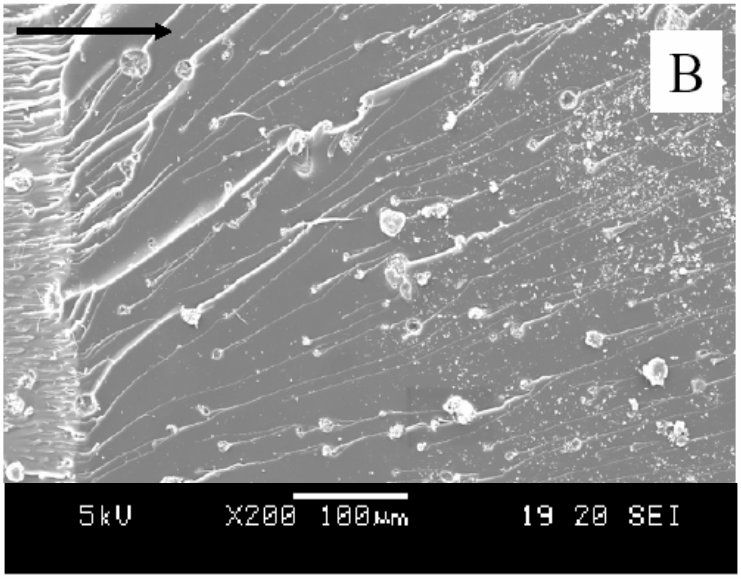
B
5kU X200 100µm 19 20 SEI

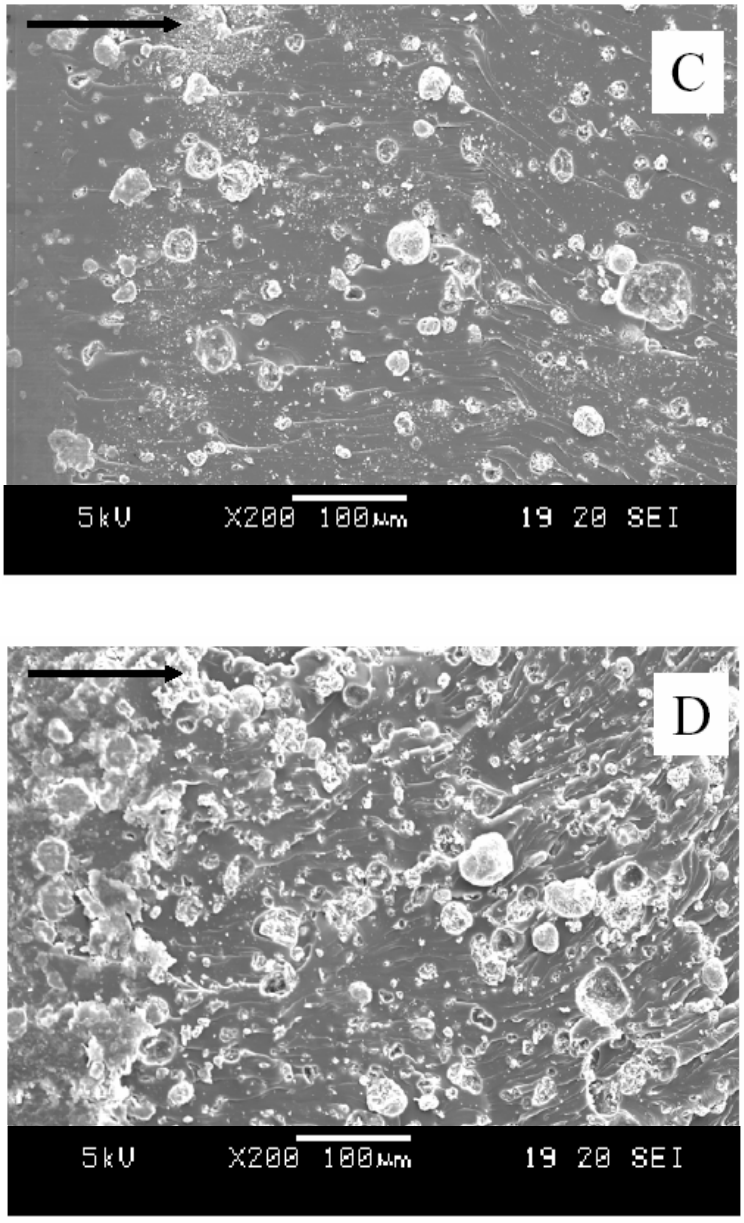

Figure. 5.9. SEM morphology of the fracture surface of (A) neat epoxy; nanocomposites with (B) 5 wt% raw clay; (C) 10 wt% raw clay; (D) 20 wt% raw clay.

Under SEM, the fracture surface of raw clay nanocomposite is quite different with organoclay filled epoxy nanocomposites but similar as glass bead **(8, 9)** toughened epoxy. As shown in Figure 5.9, large amount of aggregates with diameter around 10 μm to 50

μm are evidenced, which were formed due to the poor interaction between raw clay and epoxy. Inside the aggregates, clay exists in exfoliated or intercalated structure as revealed by TEM. In Figures 5.9(B), (C) and (D), the crack tip usually breaks these aggregates and propagates further. Steps parallel to the crack propagation direction are clearly observed behind the aggregates. Similar structures are often observed in fiber **(10)** and glass bead **(8, 9)** filled epoxy systems, which are the characterized tail structure formed when two secondary crack fronts separated by a particle meet with each other **(11-13)**. With the raw clay concentration increasing, the number of aggregation increases and the inter-particle distance decreases, causing the neighboring secondary crack fronts interact with each other. As a result, the steps are highly curved and deflect from the crack propagation direction, which can cause shear and tear deformation of the matrix to dissipate energy. Yet the fracture mechanisms are still under investigation, more work still need to be done to fully understand the fracture and toughening behavior of the above system.

5.7 Summary

Pristine clay nanocomposites were synthesized successfully using microwave method. Characterizations of the microstructure show that a mixed exfoliated/intercalated structure was formed in the nanocomposite, together with some large clay clusters. It has been shown that both toughness and stiffness of the materials were improved through the incorporation of raw clay. The fracture surface of the nanocomposites was investigated using SEM. The aggregates of epoxy and clay were found to be the main reason of the toughening effect. Yet due to the incompatibility between pristine clay and epoxy matrix, uniform dispersion was not achieved, which in turn compromised the enhancement of

clay. Residual moisture was also supposed to be a negative role in the material properties. Nevertheless, this approach provides an opportunity to prepare clay nanocomposites without surfactant, which is ideal for scientific study and economic for commercial applications.

In the following chapter, a novel approach will be presented to synthesize epoxy-nanoclay composites with reduced surface modifier and excellent exfoliated morphology.

References:

1. Yoo YJ, Choi KY, Lee JH. *Macromol. Chem. Phys.*, 2004; 205: 1863-1868.
2. Aranda P, Mosqueda Y, Perze-cappe E, Ruiz-hitzky E. *J. Polym. Sci.: Part B*, 2003; 41: 3249-3263.
3. Browning CE. In: Browning CE and Seferis JC (Ed.). *Processing and structural properties of composites*. *New York: Plenum press*, (1983).
4. Mohd Ishak ZA, Tengku Mansor TSA, You BN, Ishiaku US, Karger-Kocsis J. *Plast. Rubber. Compos.*, 2000; 29: 263-270.
5. Ishak ZA, Berry JP. *Polym. Compos.*, 1994; 15: 223-230.
6. Clark Jr RL, Craven MD, Kander RG. *Composites A*, 1999; 30: 33-48.
7. Zerda AS, Lesser AJ. *J. Polym. Sci.: Part B,* 2001; 39: 1137-1146.
8. Liu LM, Qi ZN, Zhu XG. *J. Appl. Polym. Sci.*, 1999; 71: 1133-1138.
9. Yang Y, Zhu ZK, Yin J, Wang XY, Qi ZE. *Polymer*, 1999; 40: 4407-4414.
10. Lee J, Yee AF. *Polymer*, 2000; 41: 8363-8373.
11. Lee J, Yee AF. *Polymer*, 2001; 42: 577-588.

12. Wang L, Liu TX, Tjiu WC, Teh SF, He CB. *Polym. Compos.*, 2005; 26:333-342.

13. Lange FF. *Philos. Mag.*, 1970; 22: 983-992.

14. Spanoudakis J, Young RJ. *J. Mater. Sci.*, 1984; 19: 473-486.

15. Spanoudakis J, Young RJ. *J. Mater. Sci.*, 1984; 19: 487-496.

Chapter 6. Solvent-assisted silane-modified clay system

6.1 Process and mechanisms

6.1.1 Background

From our experiences in the above two chapters, the poor clay dispersion observed in epoxy-clay nanocomposites is mainly due to the preparation process and the intercalation/exfoliation mechanisms involved. In organoclay system, the main resistance forces to fully exfoliation are extragallery viscous force and van der Waals forces, while in microwave-assisted pristine clay system, the incompatibility serves a hurdle after the resistance forces were overcome by microwave. In order to overcome the drawbacks in these two methods, we developed in this study a new approach in preparing epoxy nanocomposites with silane-modified clay using a "hydro-compounding" technique. This technique leads to a better clay exfoliation with only a very low concentration of organic modifier (< 5 wt%).

6.1.2 Sample preparation

4 g of pristine clay was dispersed into 120 ml of deionized water to form a suspension, in which clay concentration is 3.2 wt%. The suspension was stirred at room temperature for 24 h and sonicated for 30 min, and then poured in 800 ml of acetone and stirred vigorously for 5 min. A white precipitate formed, which was filtered and washed with acetone for 3 times. The wet product was added with 80 ml of acetone to form clay/acetone slurry. 0.2 g of silane was added into the slurry and stirred for 10 h and

sonicated for 30 min at room temperature. Afterwards, the slurry was mixed with epoxy resin at 50ºC and stirred for 2 h. Acetone was evaporated by drying the mixture in a vacuum oven at 50ºC for 48 h. Then stoichiometric quantity of the curing agent was added, and the mixture was stirred and degassed under vacuum at 75ºC for 60 min. Finally the mixture was cured at 100ºC for 2 h and post-cured at 180ºC for 5 h. The method is referred as a "hydro-compounding" process because the dispersion and exfoliation of clay were achieved in the presence of water. Hereafter, the epoxy nanocomposites prepared using the "hydro-compounding" process are designated as EHC nanocomposites.

6.1.3 A "hydro-compounding" process

It is well known that pristine clay is hydrophilic and can form a stable suspension in water, in which clay is dispersed as isolated sheets or small domains consisting of a few sheets. It would be an ideal way to maximize the exfoliation if the dispersion state of clay in water can be successfully transferred to epoxy matrix. Based on this concept, a new approach to achieve epoxy-nanoclay composites was designed as described in the experimental section. A schematic illustration is shown in Figure 6.1. There are two purposes for exchanging water with acetone in the second step. One is to avoid excessive oligomerization of silane during surface modification since the condensation reaction can be catalyzed by existence of water; another one is to facilitate a better exfoliation and dispersion of modified clay in epoxy prepolymer in the following step, because the latter is soluble in acetone. Furthermore, the low boiling point acetone can be easily removed before curing starts.

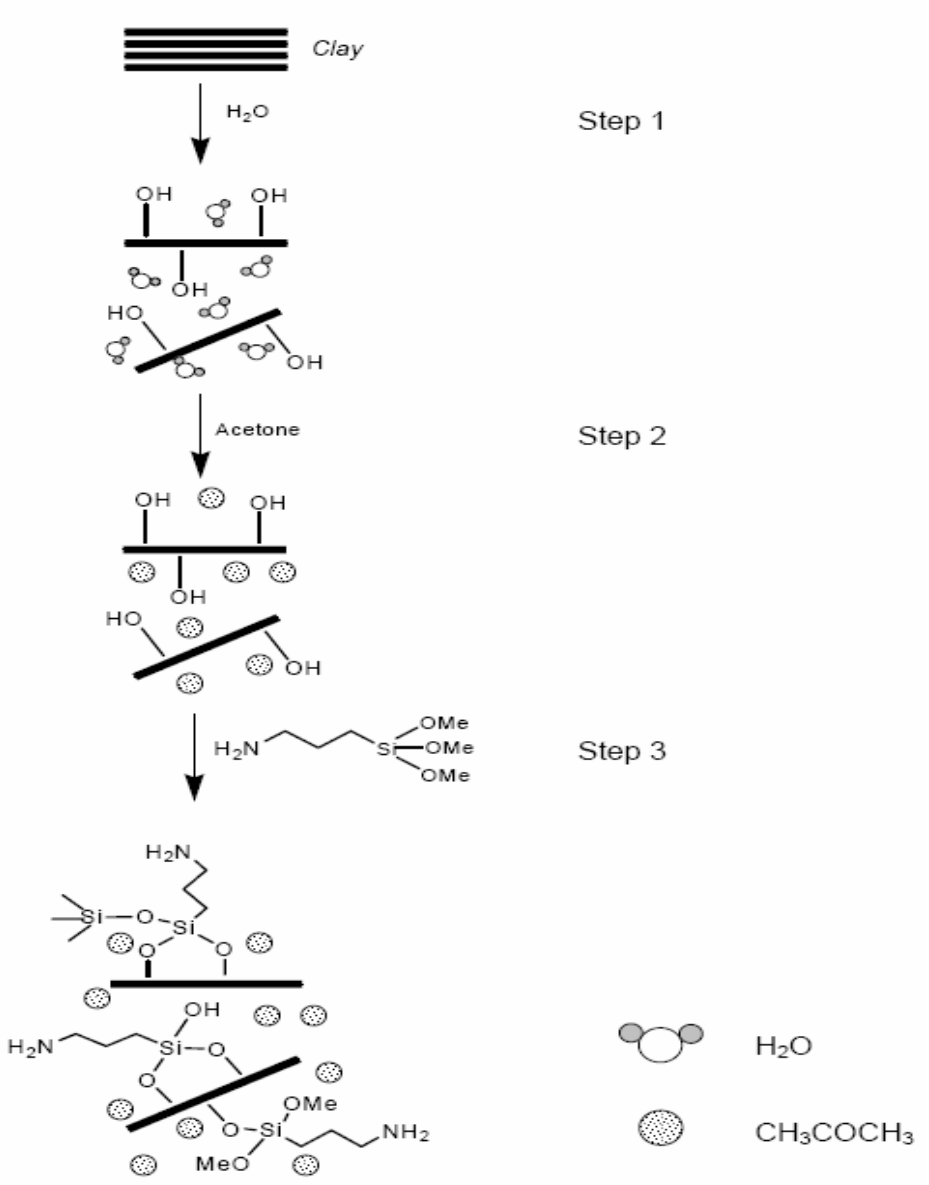

Figure 6.1. Schematic representation of clay modification.

The change of morphology of clay during each stages of processing was monitored using WAXS. For clay/water suspension and clay/acetone slurry, glass capillaries (Hampton Research, HR6-194) were used to carry the liquid samples. The WAXS diagrams of pristine clay, empty glass capillary, clay/water suspension, precipitated clay in acetone, modified clay/acetone slurry, as well as dried modified clay are collected in Figure 6.2.

The glass capillary is specially manufactured for X-ray experiments, which does not show any peak in the range of $2\theta = 2.5$ to 10^{o} (curve 2). The morphology of pristine clay resembles smectic liquid crystals which give rise to a low angle scattering in WAXS, representing the interlayer distance of the clay aggregated as shown in curve 1 in Figure 6.2. The d-spacing of the peak is about 1.2 nm which is typical for pristine clay. For clay/water suspension with clay concentration of 3.2 wt%, the absence of (001) scattering is significant, which indicates that clay has been exfoliated/dispersed by water. This implies that either the layer structure of the clay has been totally destroyed/distorted or the clay layers are swollen to a d-spacing > 4.5 nm (curve 3) which is out of range of our WAXS. In fact, a systematic study reported by Morvan et al **(1)** has shown that the interlayer distance can be 15 nm in a clay/water suspension with 8.5 wt% of clay. When the clay/water suspension was mixed with acetone, clay precipitated to form loose sediments. A weak and broad peak is observed at $2\theta = 5.24^{o}$ (1.68 nm) in the corresponding WAXS curve (curve 4), indicating that some of the clay platelets may reassembly to form a layer structure or the interlayer distance for some the swollen galleries reduced due to the removal of water. It is worth mentioning however that the d-spacing of clay in the slurry is bigger than that of pristine clay (1.21 nm) reveals that clay was swollen by acetone or residual water although some of the clay platelets aggregate together. The d-spacing difference is about 0.5 nm and it is estimated that there may be a single molecular layer between each clay layer. The dispersion state of clay is likely similar to that of clay in salt solution **(1)**. That is to say, clay platelets are not uniformly dispersed in the whole sample and two types of domain coexist: small nematic domains consisting of a few paralleling clay platelets and pores of mainly acetone with numerous

individual clay platelets. The modification with silane did not affect the microstructure much because the (001) scattering of modified clay/acetone slurry appears at the same position as that before modification (curve 5). After drying, the modified clay shows a peak at $2\theta = 7.20^{o}$ (1.22 nm, curve 6), which is very close to that of pristine clay, indicating that almost no modifier molecules intercalated into the clay galleries. This is understandable because the silane is preferentially grafted at the edge of the clay platelets rather than the surface of the clay platelets due to existence of hydroxyl group at the edge of the clay platelets. However, event with such minimal modification, the resulting epoxy nanocomposites exhibit a much better exfoliation morphology.

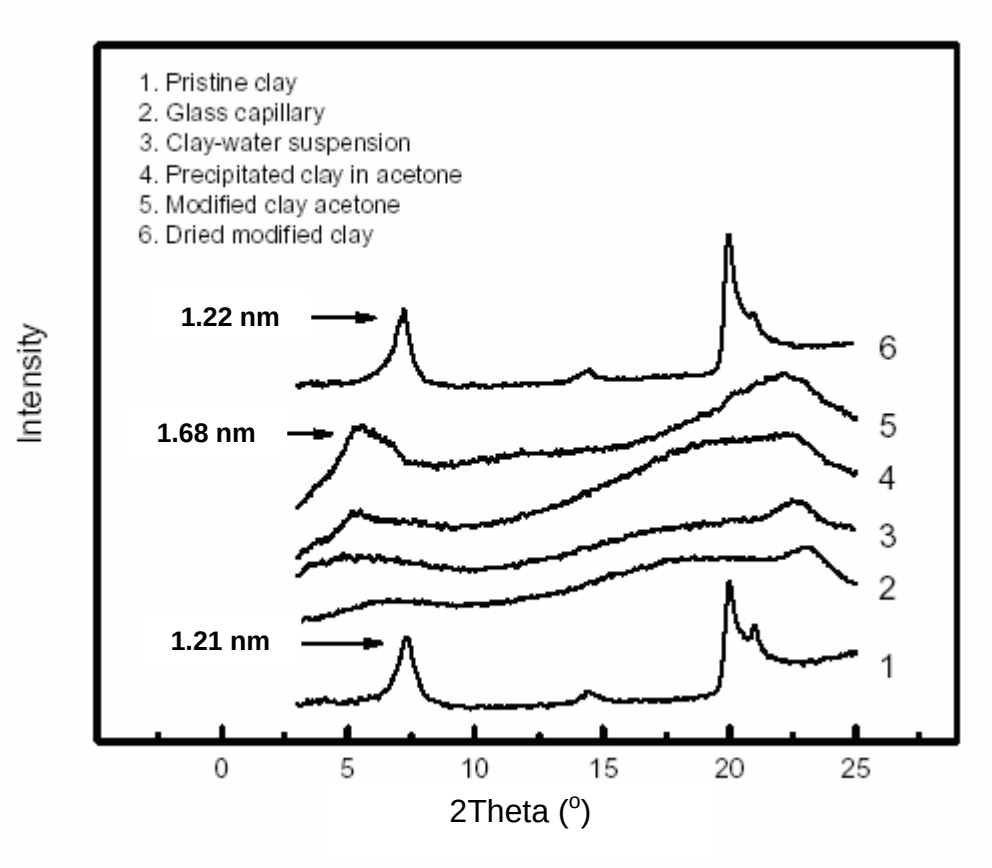

Figure 6.2. WAXS diagrams of (1) pristine clay; (2) glass capillary; (3) clay/water suspension; (4) precipitated clay in acetone; (5) modified clay in acetone; (6) dried modified clay.

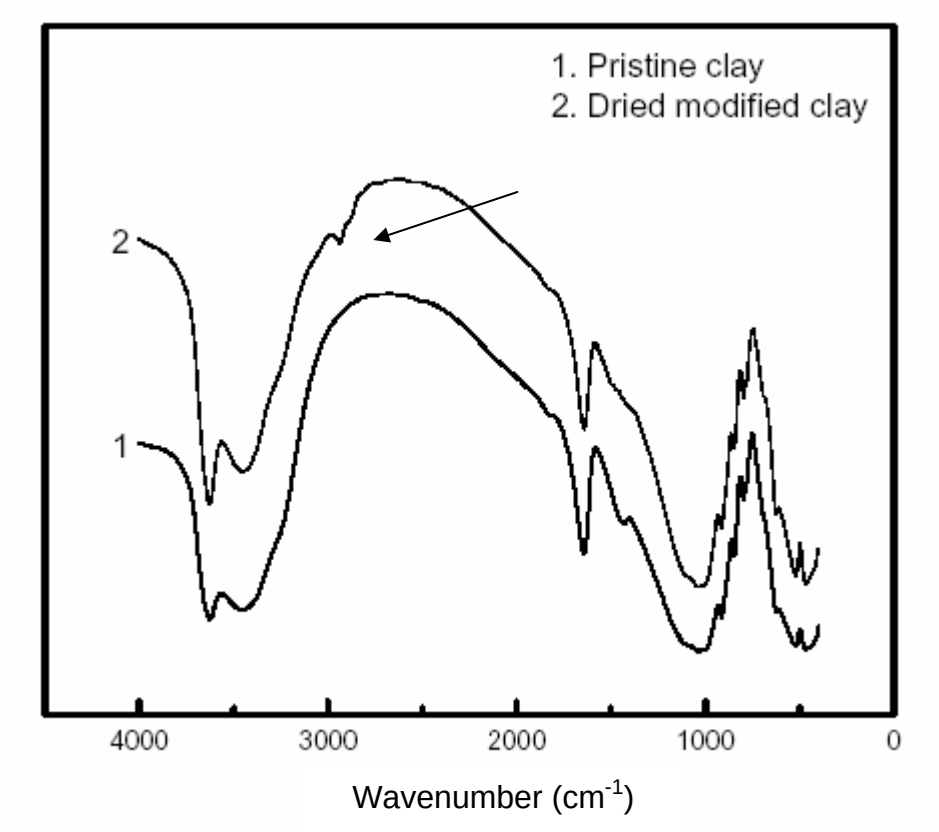

Figure 6.3. FTIR spectra of (1) pristine clay; (2) dried modified clay.

The evidence for the reaction between the silane and clay platelets comes from FTIR and ToF-SIMS studies. The FTIR spectrum of pristine clay (Figure 6.3) displays typical –OH stretching (3634 cm^{-1}) absorbance, and broad bands at 3447 and 1640 cm^{-1} attributed to adsorbed water molecules **(2)**. The bands at 1116, 1035 and 914 cm^{-1} can be collectively attributed to Si–O stretching vibrations **(3)**. The spectrum of silane-modified clay displays almost the same pattern as that of pristine clay except a new band of –CH stretching at 2937 cm^{-1}, which indicates the grafting of organic groups on the clay mineral surface.

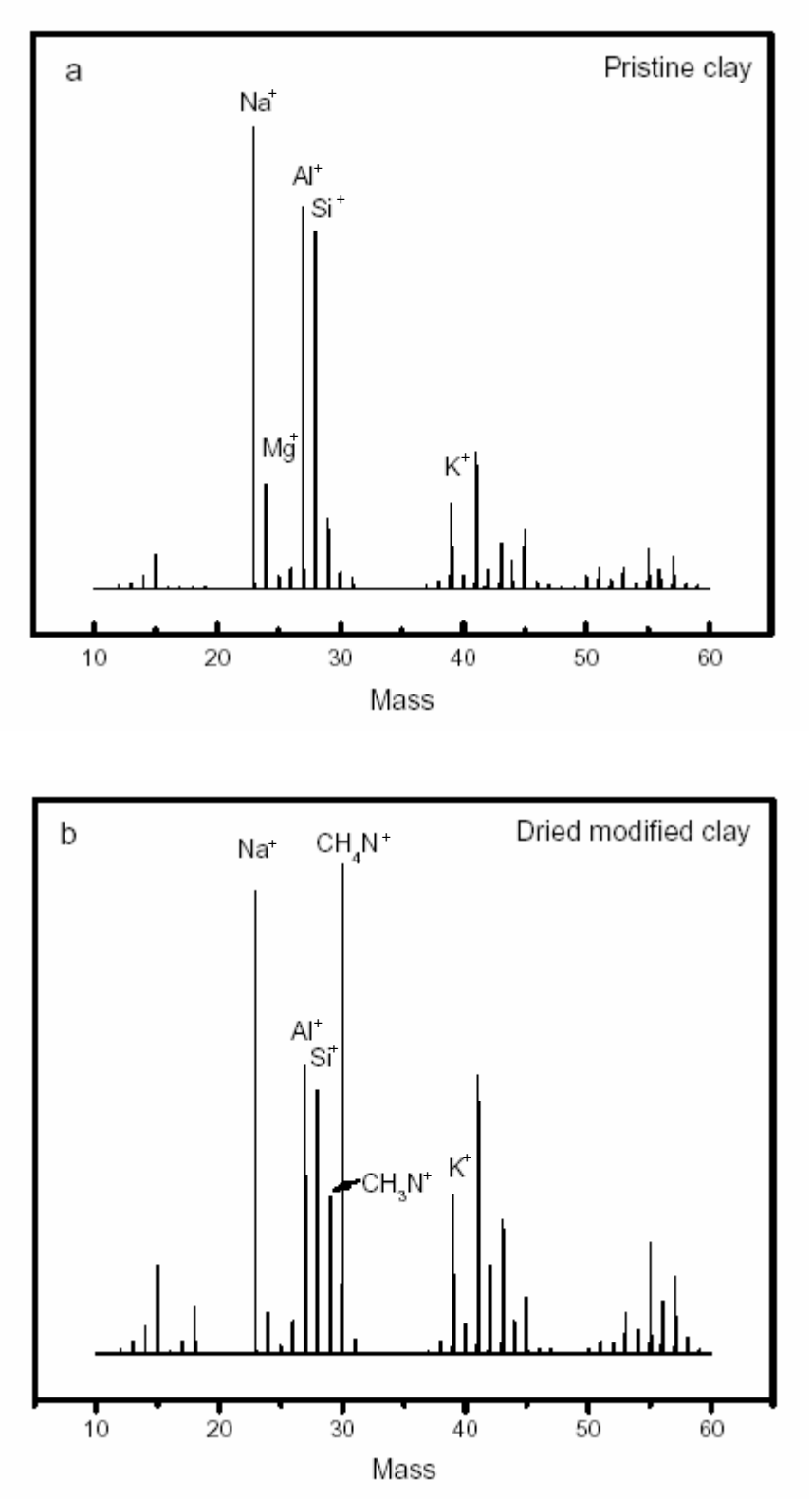

Figure 6.4. ToF-SIMS spectra of (a) pristine clay; (b) dried modified clay.

ToF-SIMS spectra of pristine clay and the modified clay are shown in Figure 6.4. For the pristine clay, abundant Na+, Al+ and Si+ are observed, which is consistent with the natural composition of the sodium montmorillonite. Lower abundance cations corresponding to K+ and Mg+ are also observed, which are components of the pristine clay. In addition, the presence of organic adsorbates is observed as well. Relatively abundant example is observed at m/z 41, similar as the organic ions reported by Groenewold and co-workers with clay **(4)**. When the clay was modified with silane, new ions with m/z 29 and 30 are observed in the ToF-SIMS spectrum, which correspond to elemental compositions of CH_3N+ and CH_4N+ respectively. Evidently, they are derived from the amine group of silane molecules. Since the samples were washed with acetone for 3 times and dried before subjected to characterization, the silane existed in the modified clay was supposed to be chemically bonded to the layers.

In summary, the highly exfoliated structure of clay in water was partially transferred into acetone media, in which small swollen clay tactoids and single clay platelets coexist. The modification reaction mainly takes place on the surfaces or edges of the single platelets and the tactoids rather than inter-galleries. It is expected that the nematic and pore structure will be transferred into epoxy in the following steps.

6.1.4 Microstructure of EHC nanocomposites

To prepare the EHC nanocomposites, epoxy prepolymer was mixed extensively with the modified clay/acetone slurry, and subsequently the solvents were removed. The mixtures

are transparent up to 5 wt% clay, indicating good dispersion of clay in epoxy matrix. The WAXS curve 6 in Figure 6.5 represents the typical structure of such epoxy/clay mixtures before curing, in which a weak peak was observed at $2\theta = 6.56^{o}$ (1.35 nm). By comparing this scattering (curve 6 in Figure 6.5) with curves 5 in Figure 6.2, it is obvious that the layers collapsed slightly but not completely after the removal of solvents, and some of the epoxy molecules had intercalated into the clay galleries. The scattering in curve 6 in Figure 6.5 is in contrast to curve 6 in Figure 2 where a very intense, sharp peak appears at low angle with intensity comparable to the crystalline peak at $2\theta = 20^{o}$ when the modified clay was dried without addition of epoxy.

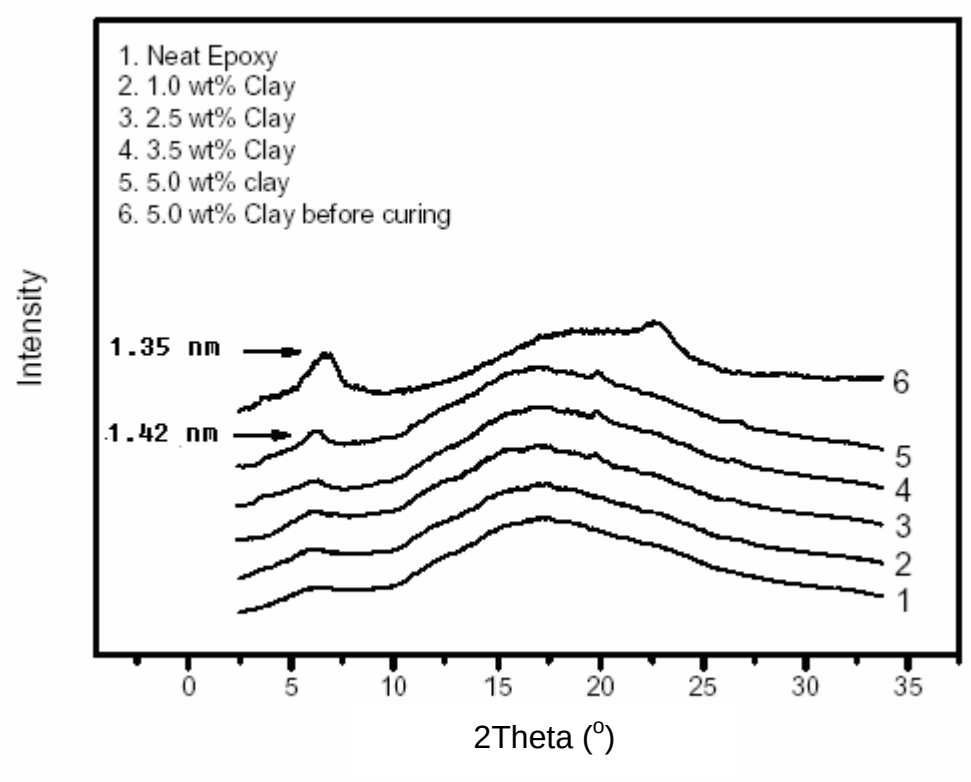

Figure 6.5. WAXS diagrams of EHC nanocomposites with different clay content.

During curing, the tactoid galleries were expanded further. For samples with 1.0 and 2.5 wt% clay, the (001) scattering peak is almost invisible (curves 2 and 3 in Figure 6.5), revealing that a high degree of exfoliation has been achieved in these samples. For the samples containing more than 3.5 wt% clay, a weak scattering peak occurs with a slight large d-spacing of 1.42 nm, while the intensity decreases considerably (weaker than the amorphous halo). Evidently, the morphology is determined in the preparation steps before curing, whereas the curing step doesn't affect the microstructure significantly. Optical micrograph shows that, in the EHC nanocomposite, clay particles are uniformly dispersed in the matrix and the visible aggregate size is smaller than 3 μm (Figure 6.6(a)), much smaller than that of organoclay and pristine clay system. Figures 6.6(b) and (c) present TEM micrographs showing that the clay is exfoliated into single layers or thin tactoids that consist of 5 to 10 clay layers. These single layers and thin tactoids disperse uniformly and randomly in the matrix, indicating that our new approach is very effective in promoting both the exfoliation and dispersion of clay.

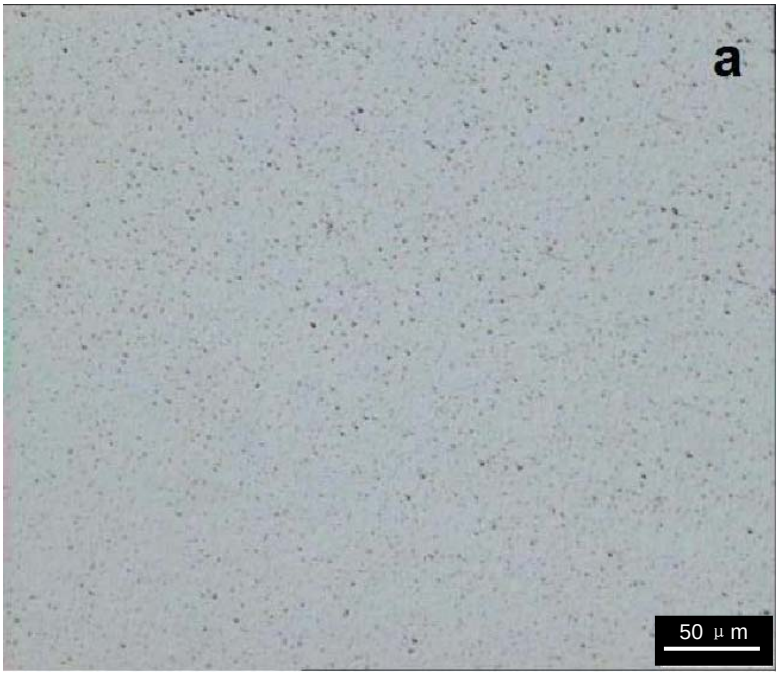

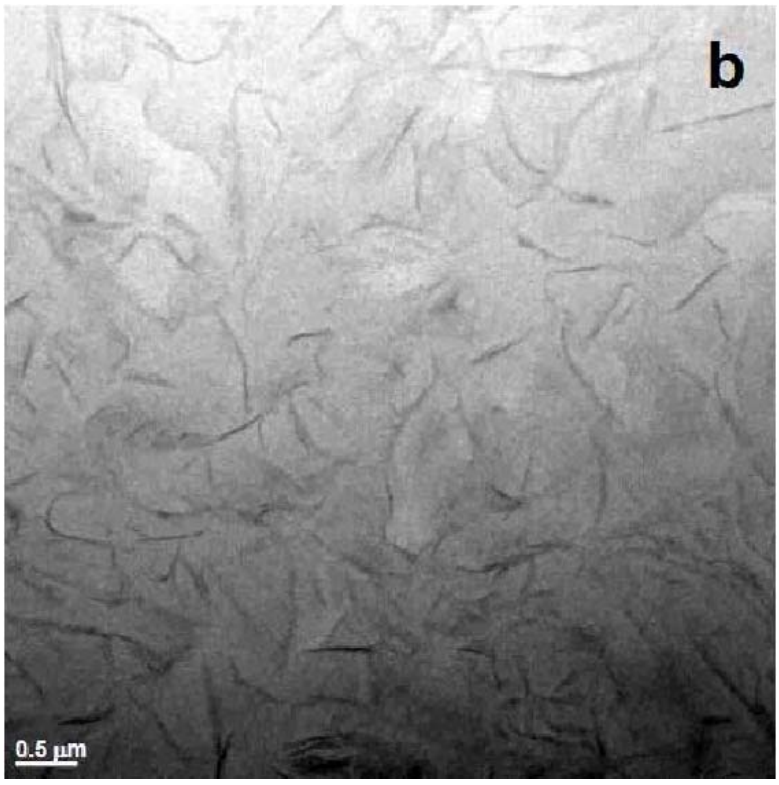

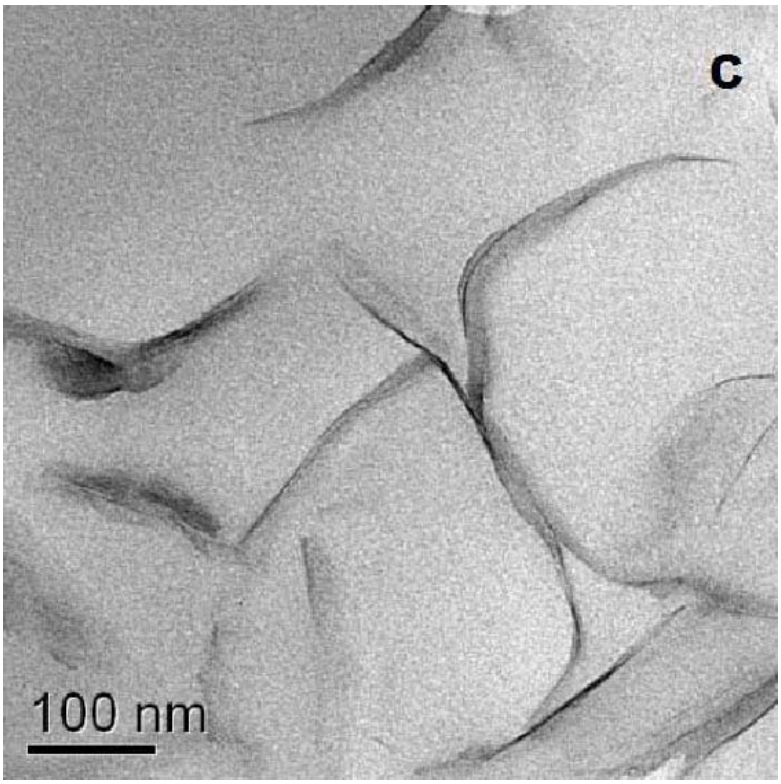

Figure 6.6. Morphology of EHC nanocomposite containing 2.5 wt% of pristine clay. (a) optical micrograph; (b) and (c) TEM micrographs.

It is interesting to see that the final microstructure of our nanoclay composites is quite similar to the microstructure reported by Morvan et al (**1)** for clay/water suspensions added with brine. It is understandable because acetone is not as effective as water in swelling clay due to the lower polarity of the former. When the water in the swollen clay is exchanged by acetone, the clay precipitates from the solution and interlayer distance is likely to decrease, just as it happens when brine is added in clay/water solution (**1)**.

It is clear that the dispersion and exfoliation mechanisms in our new approach are different from that in widely used epoxy-organoclay systems. In the new approach, most of the exfoliation and dispersion process occur before curing. The key point is "hydro-processing", i.e. the dispersion and exfoliation state of modified clay in the clay/acetone slurry was directly transferred into epoxy. The final microstructure depends on the state of dispersion and exfoliation of clay in water and acetone, and how much it can be maintained in epoxy with the aid of silane modification. During the curing stage, more epoxy molecules intercalate into clay galleries and help clay to exfoliate further, but this is not crucial to the final morphology. This is in contrast to epoxy-organoclay systems in which the curing stage is the most important step.

Compared with most of the commercialized organoclays, in which the amount of organic modifier is between 25 wt% to 45 wt%, the concentration of silane used in the new approach is much lower (5 wt% of pristine clay). Meanwhile, the acetone solvent could be easily recycled. These could be very important for commercialization in terms of cost and the properties of the final product.

6.2 Thermal/Mechanical properties

In this work, bulk samples containing 1, 2, 3 and 4 wt% SMC were prepared for thermal/mechanical characterization. Due to the ultra high viscosity in the process, higher concentration samples always contain defects, bubbles for example, thus were not subjected to the tests.

6.2.1 Thermal mechanical properties

The dynamic mechanical analysis (DMA) was performed to investigate the influence of the silane-modified clay (SMC) concentration on the storage modulus and the α-transition (tanδ) of the EHC nanocomposites. In the glassy region, as shown in Figure 6.7(A), the storage modulus increases with the clay loading. The storage modulus at 100^{o}C (Figure 6.7(B)) increases 20% with addition of 4 wt% SMC (i.e. from 1.66 Gpa to 2.00 GPa). On the other hand, glass transition temperatures identified from tanδ of the nanocomposites remains constant with addition of SMC (Figure 6.7(C)). As mentioned before, the silane is preferentially grafted at the edge of the clay platelets rather than at the surface of the clay platelets due to existence of hydroxyl group at the edge of the clay platelets. The amine end group of silane will react with the epoxide group of the resin to form chemical bond, which could lead to hindered relaxation mobility in the polymer segments at near edge areas. This leads to an increase of Tg. However, at the surface of the clay platelets, there still lacks of surrounding entanglements and the cross-link density may also reduce, which will result in a lower Tg. Yet the effect of clay on glass transition of polymer is still under investigation. It is hard to identify the dominant mechanisms unless precise characterization of the polymer/clay interface is achieved.

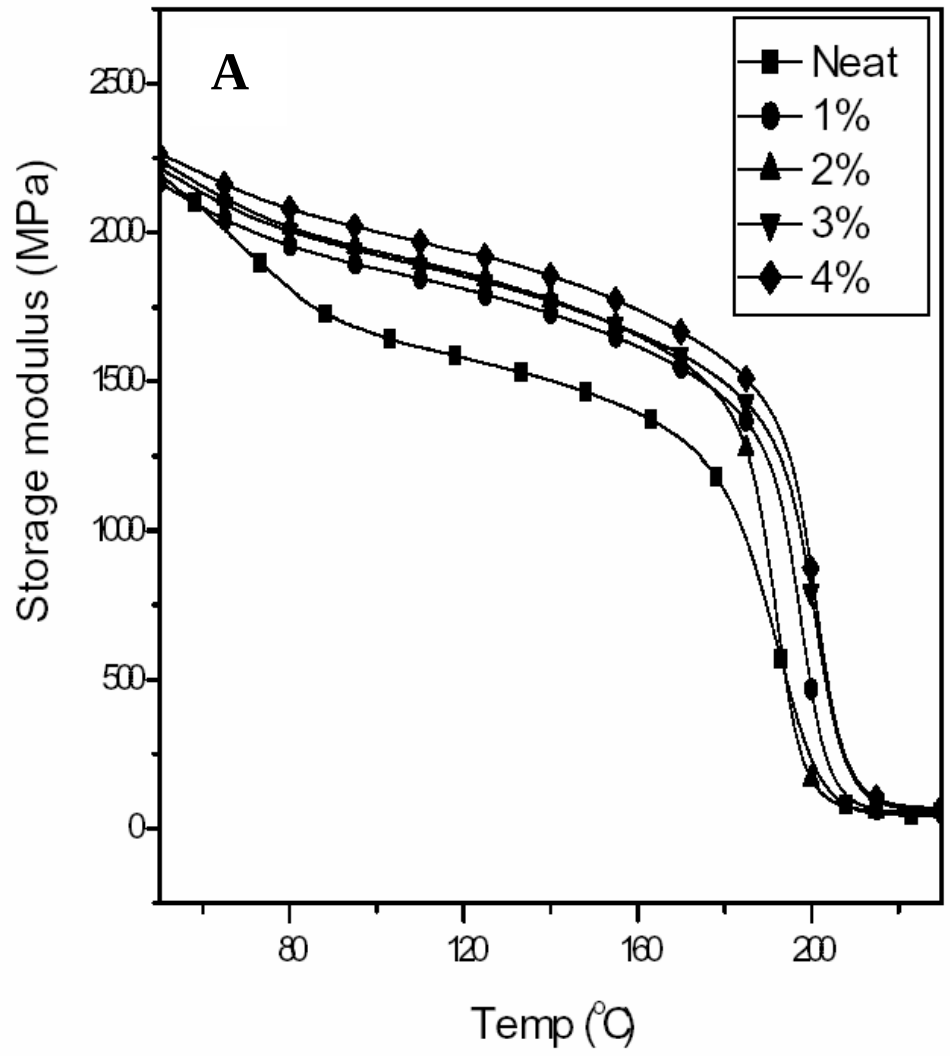
A
Neat
1%
2%
3%
4%
Storage modulus (MPa)
2500
2000
1500
1000
500
0
80
120
160
200
Temp (°C)

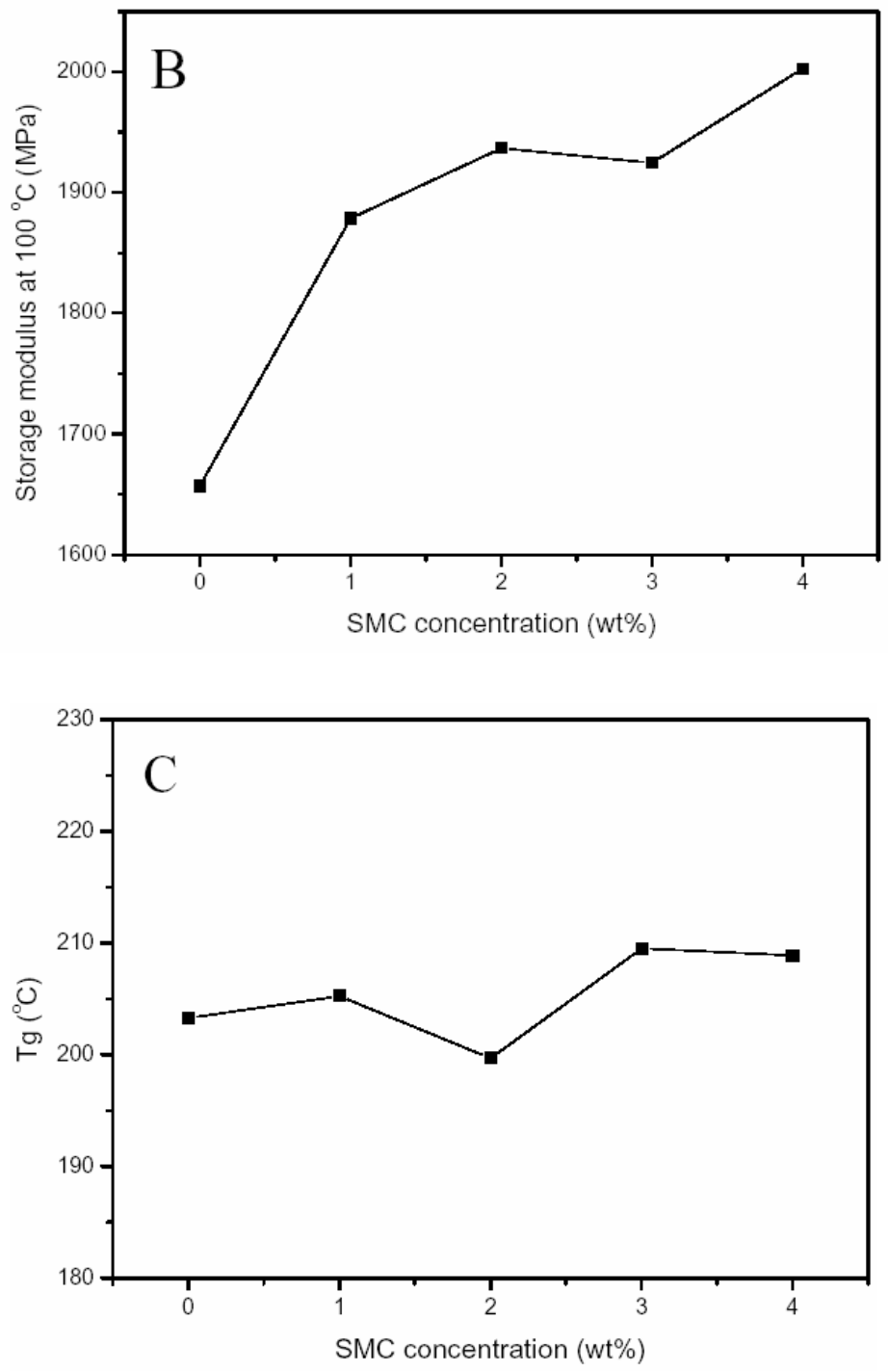

Figure 6.7. Dependence of (A) storage modulus; (B) storage modulus at 100°C; (C) glass transition temperatures on clay concentration.

6.2.2 Tensile properties

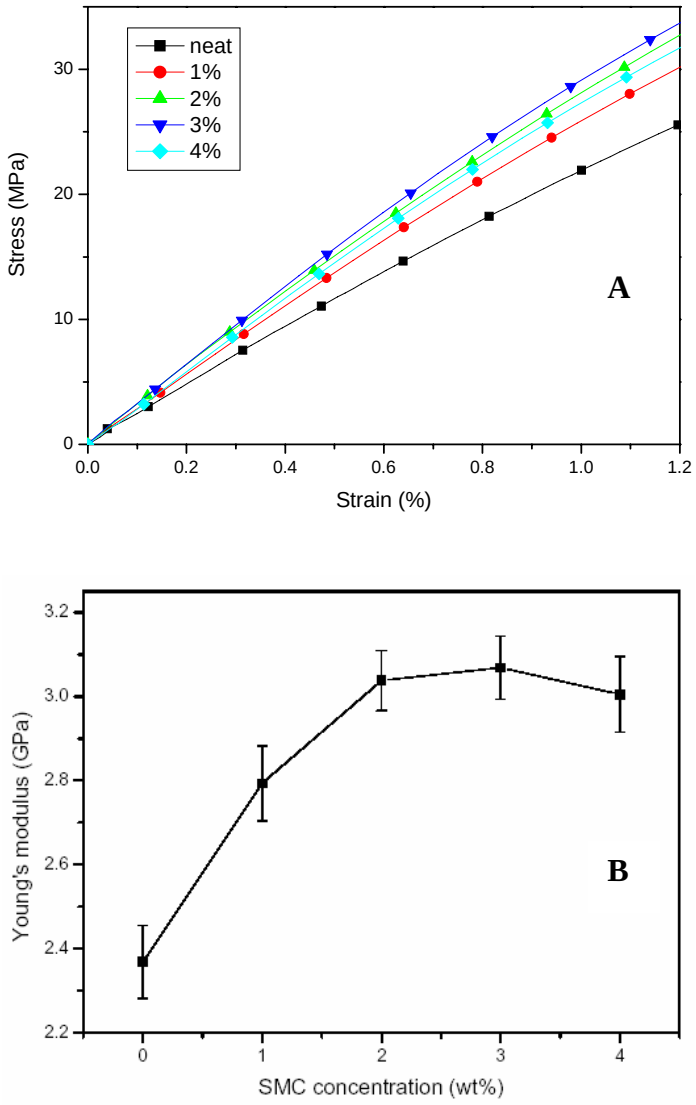

Figure 6.8. Dependence of (A) strength-strain behavior; (B) Young's modulus on clay concentration.

Tensile properties of the neat epoxy and the nanocomposites are shown in Figure 6.8. An elastic strength-strain behavior of epoxy-SMC nanocomposites was shown in Figure 6.8(A). Young's modulus was calculated within a strain range of 0.5%-1.0%. As plotted in Figure 6.8(B), a linear increasing in tensile modulus with respect to SMC content is

evident at low concentration. This result is typical of polymeric systems in which nano-scale clay dispersion is prevalent **(5-7)**. This was expected since the clay particles inherently possess high modulus and would strengthen the polymeric matrix when dispersed in the nano-scale level. The modulus increases 27% with incorporation of only 2 wt% SMC, which is quite significant as compared to organoclay and pristine clay systems at the same clay content. This result appears to confirm that the clay exfoliation is better in this SMC system. However, EHC nanocomposites suffered a compromise in the Young's modulus with addition of more SMC. This should be also related to the relative poor clay dispersion at high concentration.

6.2.3 Fracture toughness

The mode I fracture toughness, K_{IC}, determined by 3-point bend method, is shown in Figure 6.9(A) as a function of the SMC concentration (wt%). It is notable that the stress intensity factor K_{IC} also exhibits an upper limit at the SMC concentration of 2 wt%. K_{IC} increased by about 46% and 67% from 0.68 MPa·m$^{1/2}$ for the neat epoxy resin to 0.92 MPa·m$^{1/2}$ and 1.06 MPa·m$^{1/2}$ for the nanocomposites containing 1 wt% and 2 wt% SMC respectively, but dropped to 0.98 MPa·m$^{1/2}$ and 1.00 MPa·m$^{1/2}$ when clay concentration increased to 3 wt% and 4 wt% respectively.

The normalized G_{IC} was calculated by dividing the G_{IC} values by the G_{IC} of the neat epoxy (170 J/m^2). As shown in Figure 6.9(B), G_{IC} increased by 80% and 120% with incorporation of just 1 wt% and 2 wt% SMC clay respectively. Since G_{IC} represents the

energy per unit area necessary to advance the crack at the crack tip, such a significant increase of G_{IC} reveals that the fracture resistance is remarkably improved. SMC clay exhibited splendid performance in improving mechanical properties in this system. The value of G_{IC}, however, dropped with further addition of clay. This trend is consistent with the K_{IC} data and confirms the observation by our group in a different epoxy-clay system prepared using the same approach **(8)**.

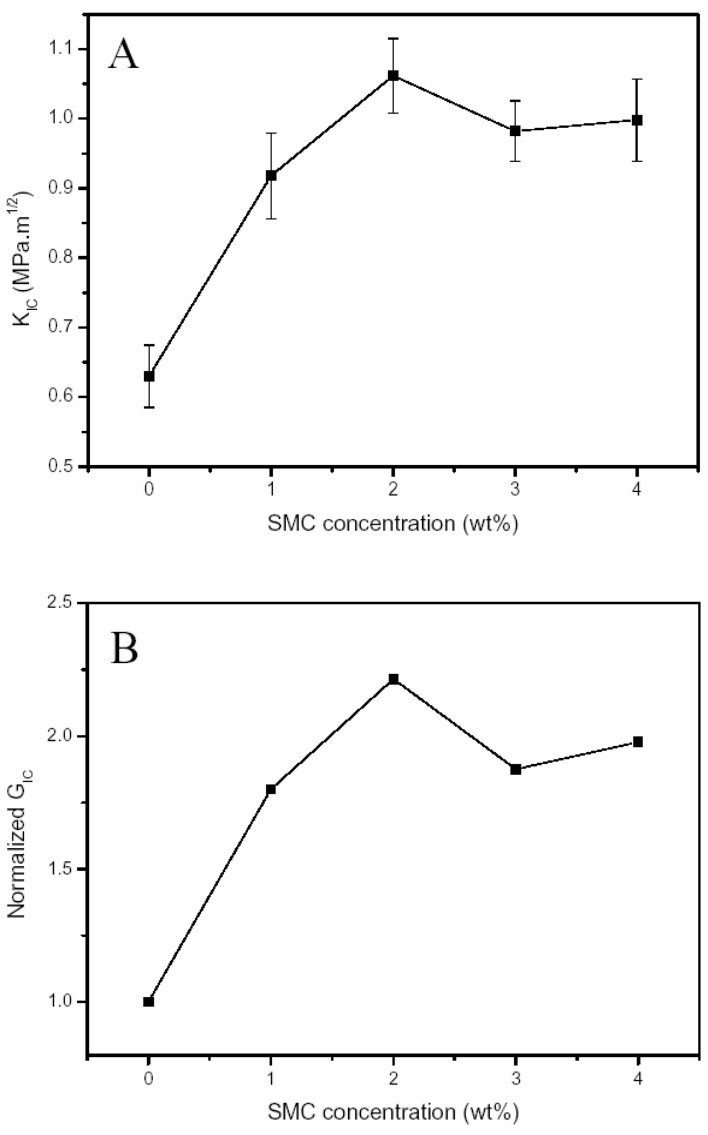

Figure 6.9. Dependence of fracture toughness on clay concentration: (A) K_{IC}; (B) normalized G_{IC}.

In order to elucidate the reasons for the fracture behavior, the fracture surfaces within process zone were examined using SEM. Figure 6.10 shows the SEM micrographs of the fracture surfaces for the neat epoxy (Figure 6.10(A)), the nanocomposites with 1 wt% (Figure 6.10(B)), 2 wt% (Figure 6.10(C)) and 4 wt% (Figure 6.10(D)) clay at magnification of 2000； and the nanocomposites with 1 wt% (Figure 6.10(E)) and 4 wt% (Figure 6.10(F) and (G)) clay at magnification of 5000. The fracture surface of neat epoxy (Figure 6.10(A)) is smooth and featureless due to its brittle nature. On the contrary, Figures 6.10(B), (C) and (D) show rougher fracture surfaces of the nanocomposites, which account for the improvement on fracture toughness. The fracture surfaces of the nanocomposites with 1 wt% and 2 wt% clay appear similar under 2000 magnification (Figures 6.10(B) and (C) except that the roughness seems to increase. However, the surface morphology of the nanocomposites with 4 wt% clay is much different (Figure 6.10(D)) by showing cluster structures, which appears to indicate that the clay dispersion is different and fracture mechanisms varies. The higher magnification images illustrate the difference. With low SMC content (Figure 6.10(E)), the fracture surface shows numerous micro-cracks, which could have been generated at the interface of exfoliated clay layers and epoxy matrix. The micro-cracks propagate along the clay platelets and result in a highly tortuous fracture surface. On the other hand, in high SMC concentration nanocomposites, as shown in Figure 6.10(F) and (G), clay clusters are observed and typical tail structures behind aggregates are also evidenced. The tail structures are often observed in hard particle filled epoxy systems, which are caused when two secondary crack fronts separated by a particle meet with each other **(9, 10)**. The change in fracture surface morphology suggests that the dominant toughening mechanisms are different at

low and high clay concentrations. This might be responsible for the sharp drop in the fracture toughness of the 3 wt% SMC composite (Figure 6.9). It should be mentioned that mixture of epoxy and SMC is of high viscosity after evaporation of acetone solvent. Therefore, clay aggregation is unavoidable and will increase with clay concentration. These aggregates may be prevalent enough to change the dominant fracture mechanisms at high concentration. Quantitative comparison of these mechanisms cannot yet be made since it requires careful experimental evaluation of various microstructural parameters associated with them. More work needs to be done to fully understand the fracture and toughening behavior of the above system.

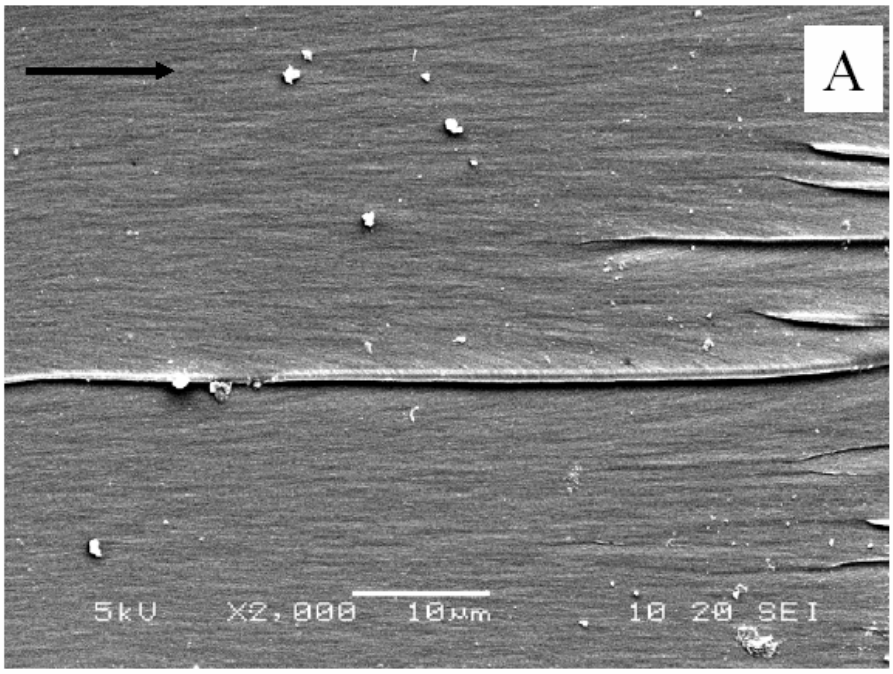

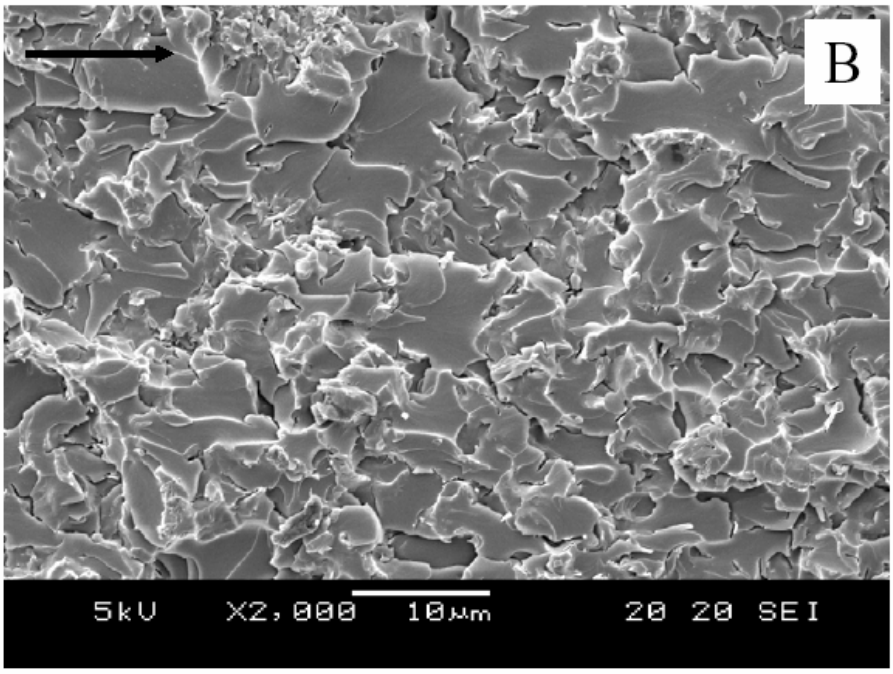
B
5kV X2,000 10µm 20 20 SEI

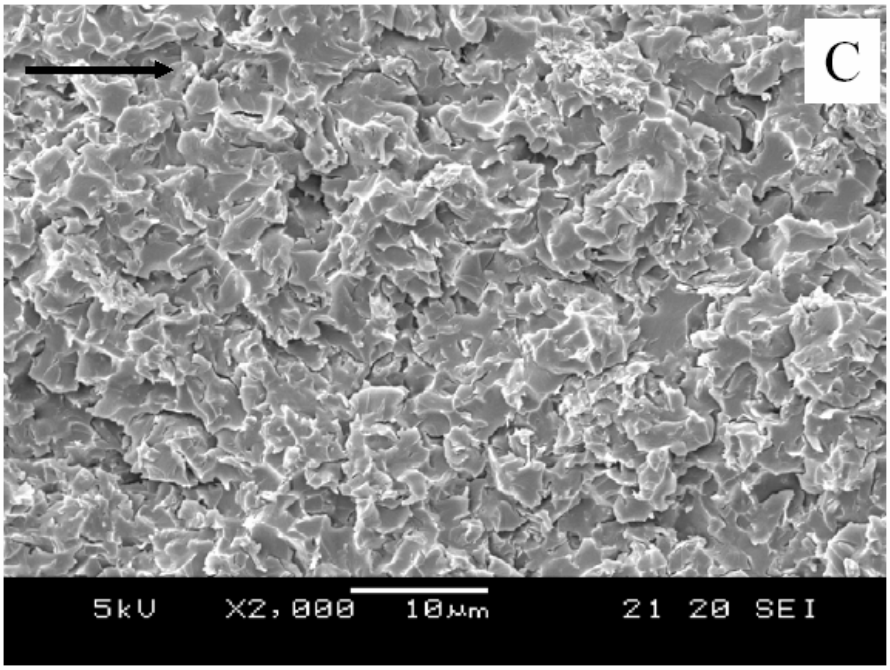
C
5kV X2,000 10µm 21 20 SEI

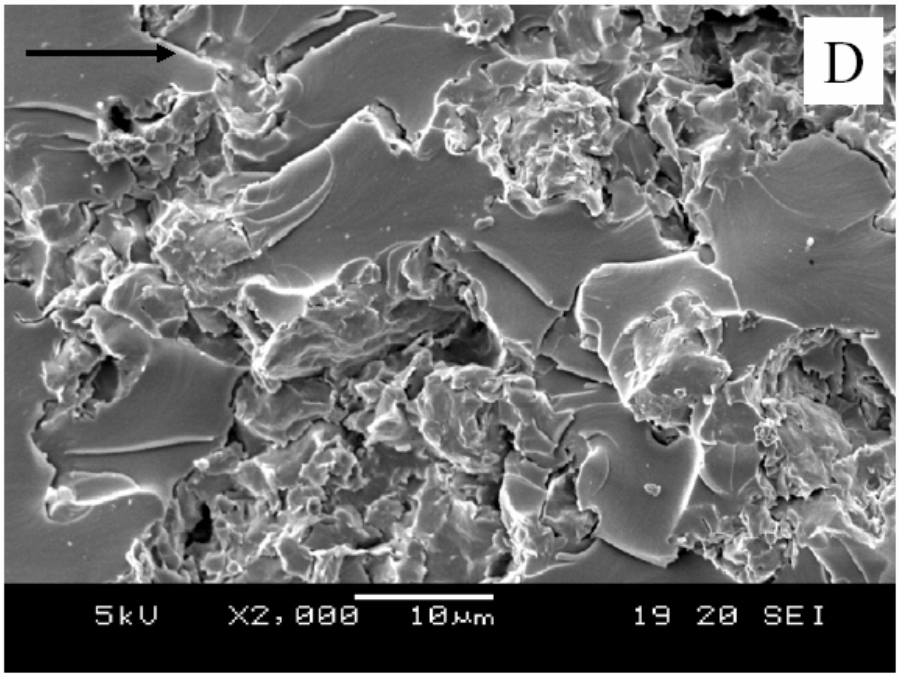
D
5kV X2,000 10µm 19 20 SEI

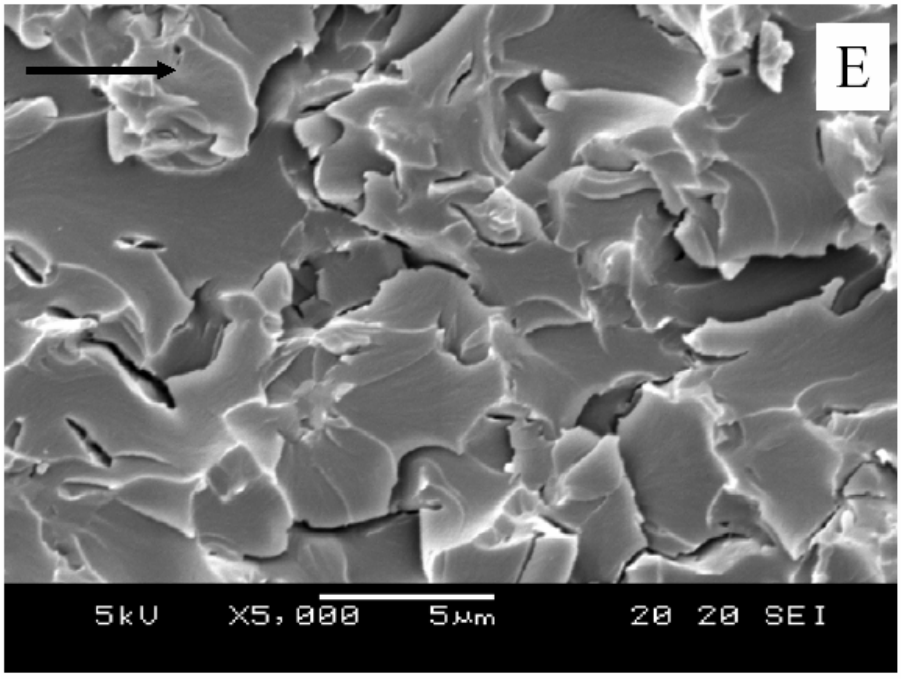
E
5kV X5,000 5µm 20 20 SEI

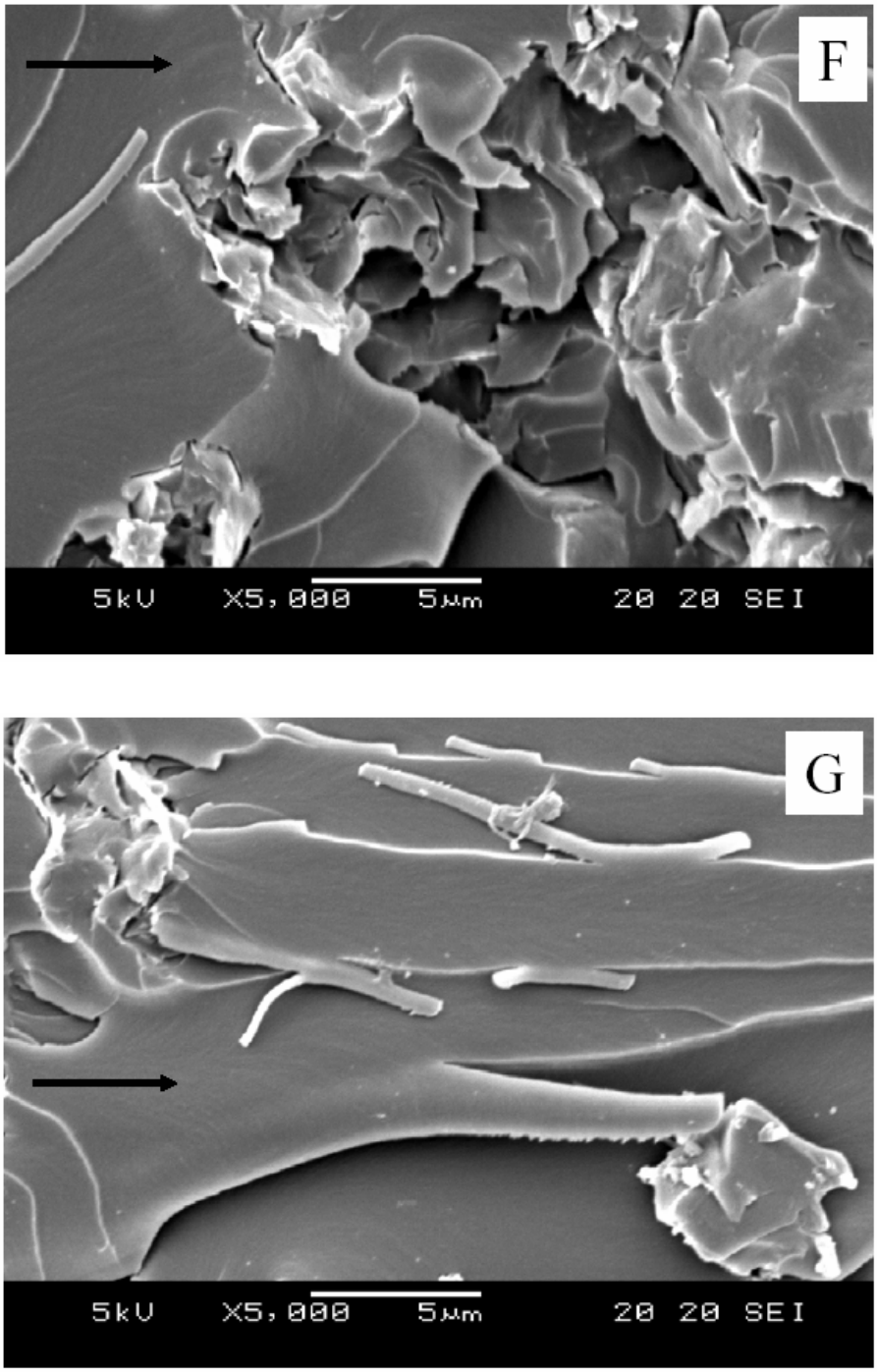

Figure 6.10. SEM micrographs of the fracture surfaces for (A) neat epoxy; nanocomposites with (B) 1 wt%; (C) 2 wt%; (D) 4 wt% clay at a magnification of 2000 and (E) 1 wt%; (F), (G) 3 wt% clay at 5000

6.3 Hydrothermal effects on the material properties

6.3.1 Background

Epoxy resins have been widely used as matrices of polymer composites with carbon fiber, polymer fiber and glass sphere as the reinforcements **(11-16)**, due to their excellent engineering properties, such as high stiffness and strength, creep resistance and chemical resistance. In the past decades, the structure-property relationships of epoxy-based composites have been studied extensively. One of the major concerns is the moisture-induced degradation of performance. Due to existence of polar groups, epoxies and their composites tend to absorb moisture from the environment and consequently their thermal/mechanical properties may change considerably **(17-20)**. It is well recognized that many polymers including epoxy resins suffer substantial losses in their thermal/mechanical properties during hydrothermal ageing (refers to the ageing process which involves the combination of water and temperature). In particular, the glass transition temperature of epoxy is lowered by the absorbed moisture through plasticization **(20-22)**. Since many applications cannot accept the moisture sensitive nature of epoxy-based composites, intensive research work has been undertaken to modify epoxy-based composites with reduced moisture absorption but without compromising their performance.

Recently, growing interests have been paid to epoxy nanocomposites with layered silicates as fillers. Numerous efforts have been made to achieve highly exfoliation of the layered silicates in epoxy and to study the thermal, mechanical and fracture behavior of the epoxy-layered silicate nanocomposites **(23-27)**. Nevertheless, currently there is little

information regarding the effects of water absorption on the thermal/mechanical properties of epoxy-layered silicate nanocomposites. Therefore another objective of this research is to investigate the hydrothermal ageing behavior of epoxy-clay nanocomposites under controlled condition.

The epoxy-clay nanocomposites containing 2.5 wt% SMC clay were prepared through the "hydro-compounding" method, in which clay is highly exfoliated and uniformly dispersed as shown in section 6.1. The neat epoxy sample and the epoxy-clay nanocomposite sample with 2.5 wt% clay were cut and machined to different dimensions for tensile, fracture and dynamic mechanical analysis respectively. The specimens were immersed in deionized water bath at 60^{o}C for a period of one month. The moisture absorption was recorded every day. The specimens were periodically taken from the water bath and subjected to different characterization.

6.3.2 Water absorption

The moisture absorption experiments of the neat epoxy and the epoxy nanocomposite with 2.5 wt% SMC clay in hydrothermal condition was performed in an oven. Figure 6.11 shows the percentage of water absorbed by the neat epoxy and the epoxy-SMC nanocomposite as a function of time. A similar behavior for the two samples was observed: the water uptake increased rapidly during the initial stage (1-10 days), and then levelled off. After about 30 days, the water uptake approached an maximum value, the saturate point. The saturated amount of absorbed water is 1.60% and 2.25% for the neat

epoxy and the epoxy-SMC nanocomposite respectively. Note that the saturate point in the nanocomposite is 0.65% higher than that of the neat counterpart, which contrasts with previous published work **(28, 29)**, where lower water absorption was observed polymer-organoclay nanocomposites. The difference is possibly due to the different clay surface modifications, i.e. the type and amount of organic modifiers used. In the reported systems **(28, 29)**, the modifiers are usually alkyl-ammonium salts, which often occupy more than 25-45 wt% of the modified clay (known as organoclay). In the present system, the surface modifier is silane, which is less hydrophobic. Moreover, the amount of silane is less than 5 wt% of clay, which mainly reacts at the edge of the clay rather than occupying the clay surface, hence leads to a less hydrophobic nature of the surface. Since the modified clay is still partially hydrophilic, the clay surface may absorb moisture molecules and thus a higher water uptake is observed.

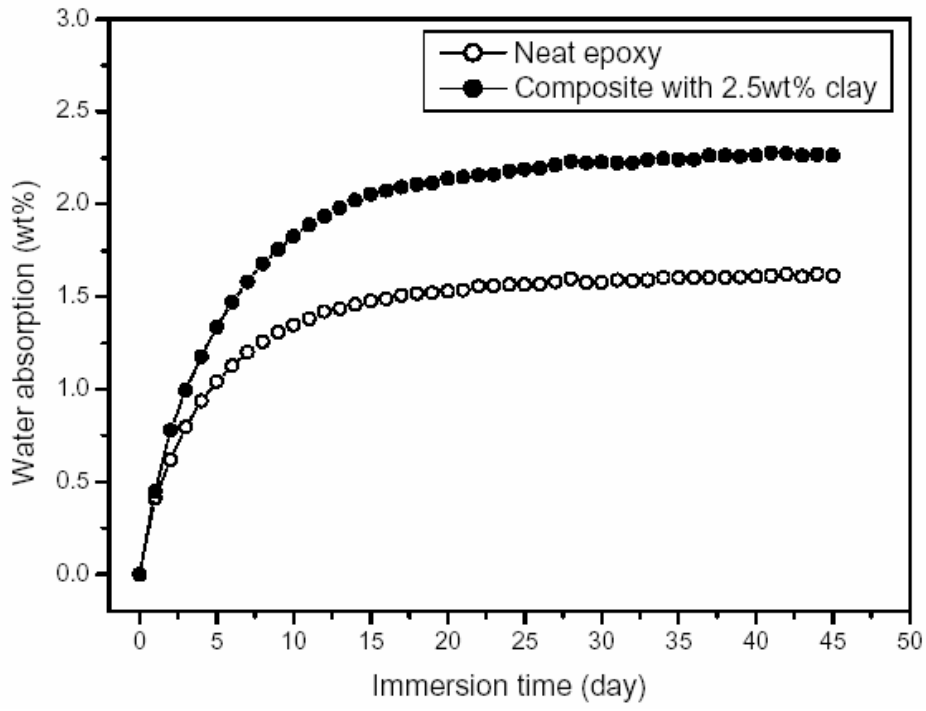

Figure 6.11. Water absorption of neat epoxy and nanocomposite with 2.5 wt% clay as a function of immersion time.

6.3.3 Mechanical properties

The effects of ageing time on mechanical properties of the neat epoxy and the epoxy-SMC nanocomposite were illustrated in Figures 6.12 and 6.13. Normally the most significant result of moisture absorption in composite materials is the plasticization effect to the matrix, which renders the matrix softer and weaker. However, in the present systems, the values of fracture toughness, K_{IC} (Figure 6.12), and tensile modulus (Figure 6.13(A)) were not influenced by moisture absorption within the experimental error. The same trend was documented in Kevlar fiber filled epoxy system, showing that moisture uptake caused no change in the elastic modulus **(19)**. Recently, Hodzic reported that the initiation value of the fracture toughness of polyester-glass composites remained a constant value after 11 weeks of water ageing **(30)**. It is worth noting that those non-deteriorated properties are all within elastic scope. One interpretation of this is that the elastic properties are dominated by the "framework" and reinforcement. They are not adversely affected by resin plasticization induced by water absorption. This explanation appears to be supported by the fact that the fracture toughness and tensile modulus were not badly influenced by moisture in epoxy-clay nanocomposite although it absorbed much more water than neat epoxy.

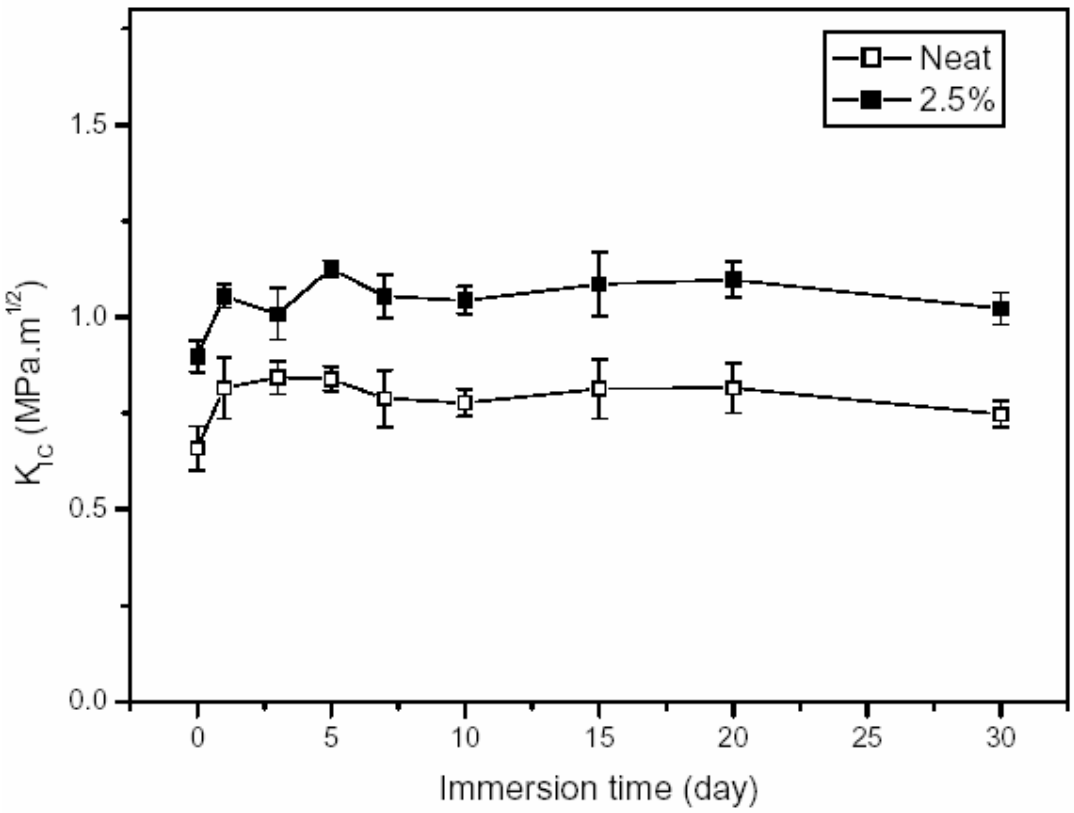

Figure 6.12. Dependence of fracture toughness on immersion time.

Figures 6.13(B) and (C) show the changes in tensile strength and strain as a result of moisture uptake. The tensile strength of the neat epoxy (Figure 6.13(B)) remained constant after the water absorption while that of the epoxy-clay nanocomposite decreased. This can be attributed to the interaction between water molecules and clay. Moisture is more likely to diffuse along the epoxy/filler interface and destroy the interfacial bonding rather than diffuse through the matrix (a slow and temperature dependent process). Thus the tensile strength decreased with the exposure time because the failure in composites is greatly influenced by the property of interface region.

The changes in the strain at break with hydrothermal ageing are more complex. Water molecules act as a plasticizer in composite materials and may lead to an increase of the maximum strain **(31)**. As shown in Figure 6.13(C), such an increase was evidenced in neat epoxy immersed in water. In the epoxy-clay system, the strain at break increased gradually till 10 days (water content 1.8 wt%) with the increase of water uptake, and decreased rapidly with the prolongation of immersion time. The same behavior has hbeen observed in PMMA system **(32)**, which is attributed to the formation of water clusters that act as fillers in the matrix. In our system, a water content of 1.8 wt% seemed to be a threshold. When moisture content higher than the threshold, water clusters grow to a high level to affect the tensile strength. These clusters act as stress concentrators and initiate early fracture. Moreover, these clusters may also account for the decrease of tensile strength at high moisture level. For neat epoxy, the saturated point (1.6 wt%) is lower than the threshold 1.8 wt%, so no such effect was observed.

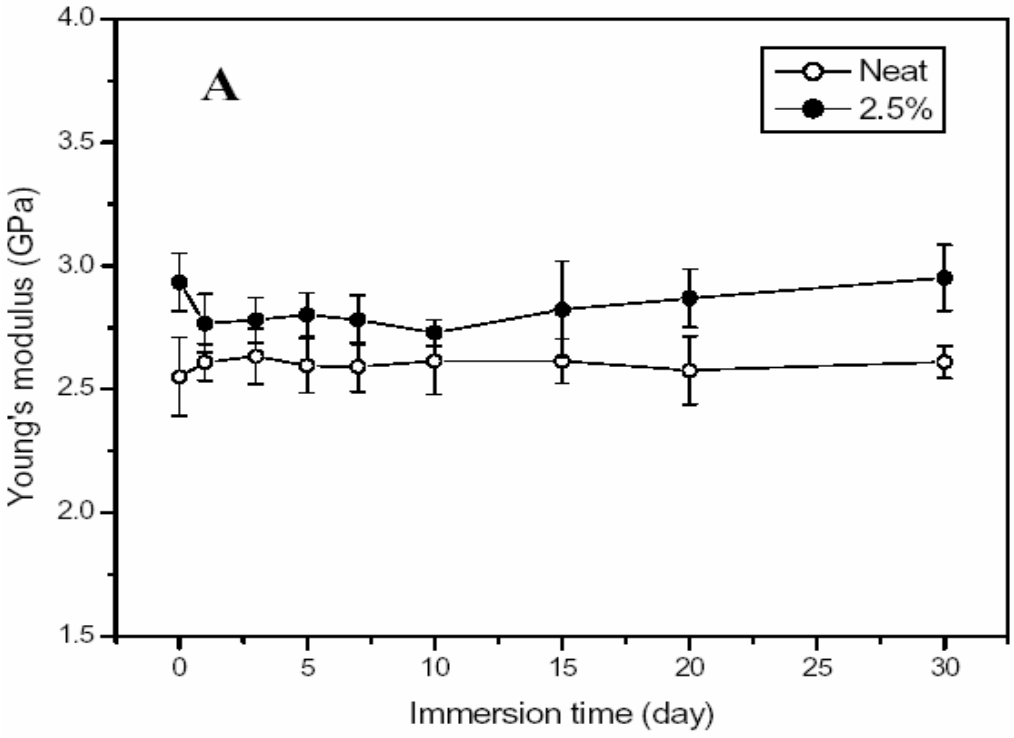

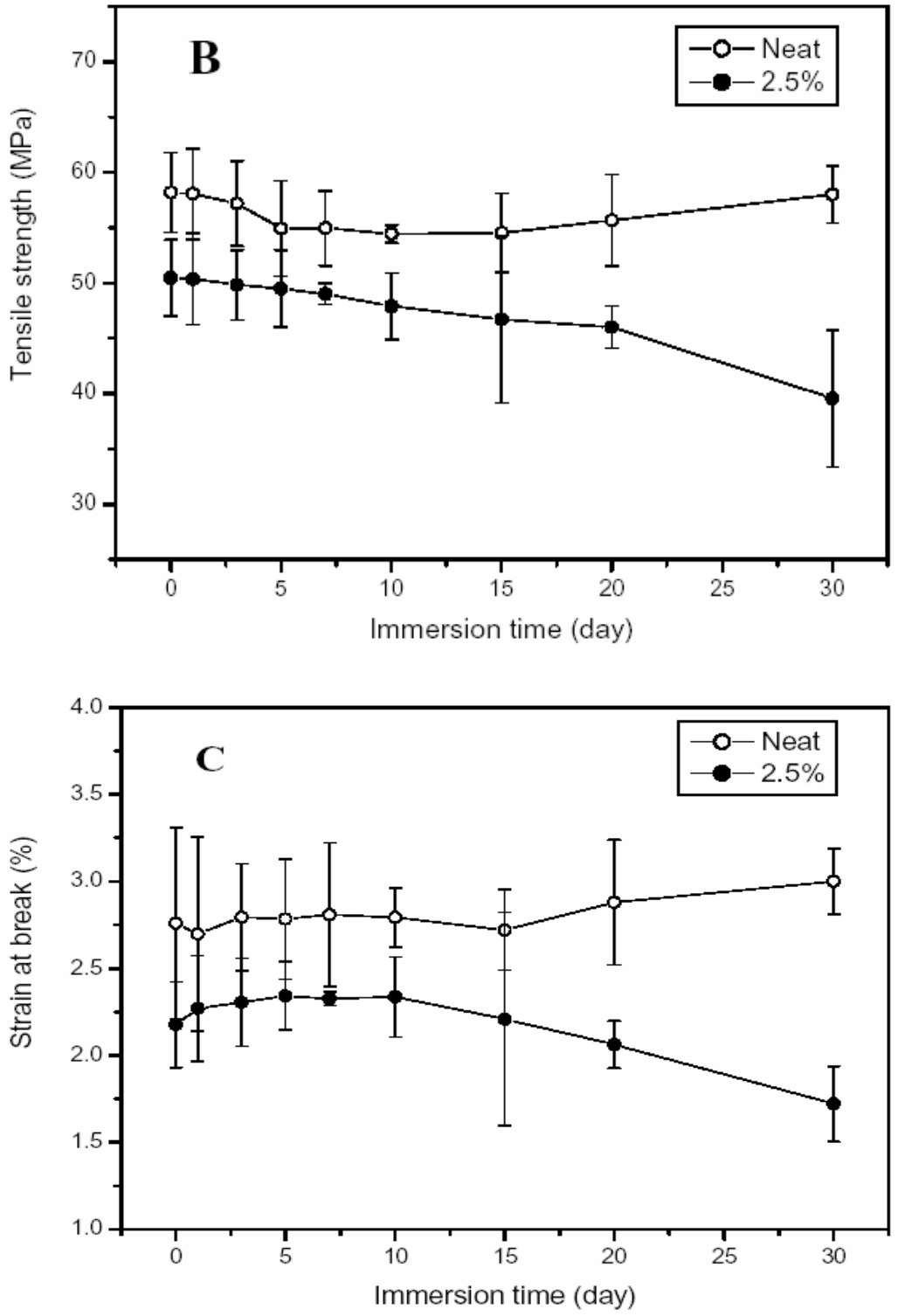

Figure 6.13. Dependence of (A) tensile modulus; (B) tensile strength; (C) strain at break on immersion time.

6.3.4 Thermal mechanical properties

Figure 6.14 shows the variations of the storage modulus of the neat epoxy and the epoxy-clay nanocomposite upon exposure time to distilled water at 60^{o}C. Both systems exhibit similar response to moisture uptake. In low temperature range (below 80^{o}C), the change of storage modulus with water absorption is insignificant. This result is consistent with the tensile tests, where Young's modulus remained constant with increased water absorption. In high temperature range (> 80^{o}C), the dependence of storage modulus on water uptake became more significant and showed a monotonic decrease with the increase of water uptake, as can be seen in Figure 6.15. At 150^{o}C, the storage modulus of the neat epoxy deteriorated by about 18% (from 1624 MPa to 1330 MPa) after 30 days immersion with a water uptake of 1.6 wt%. The epoxy-clay nanocomposite suffered an even larger decrease (22%, from 1744 MPa to 1361 MPa) due to its higher water uptake (2.2 wt%) as compared with the neat epoxy.

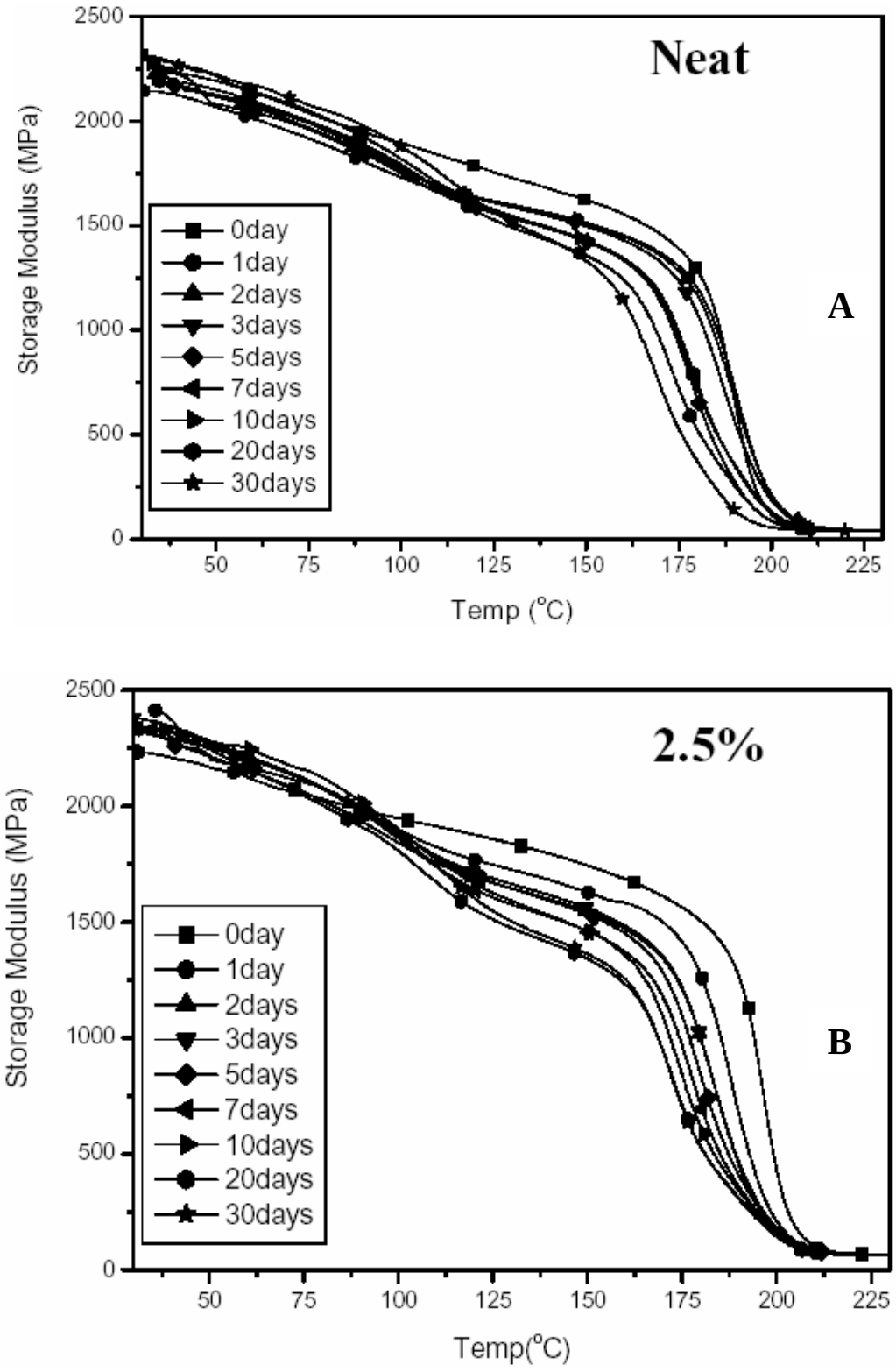

Figure 6.14. Variations of storage modulus on immersion time: (A) neat epoxy; (B) nanocomposite with 2.5 wt% SMC.

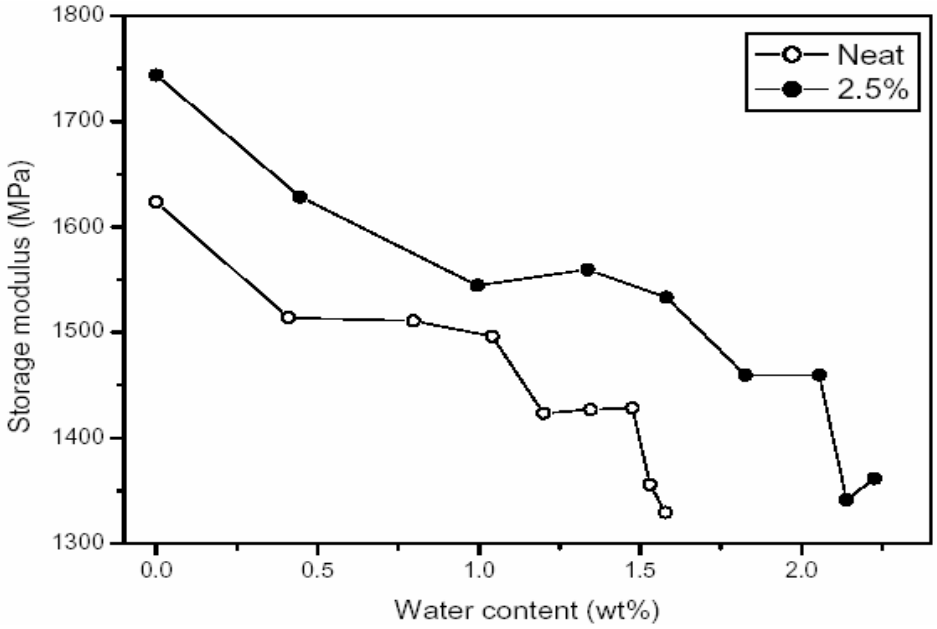

Figure 6.15. Dependence of storage modulus on water content at 150 ºC.

Exposing the specimen to hot water greatly influences the relaxation behavior of the materials. The variations of the α-relaxation upon water immersion time were presented in Figure 6.16. The following phenomena were observed: (a) the glass transition temperature (Tg, peaks in the tanδ curve) decreased gradually with water uptake; (b) the shift of α-relaxation towards lower temperature was accompanied by an increased broadening of the peak width; (c) the intensity of the α-relaxation decreased and, after longer immersing times, a shoulder peak emerged at the lower temperature side and it shifted towards lower temperature. As was previously reported for fiber composites, moisture acts as a plasticizer and makes the glass transition shift to lower temperatures **(33, 34)**. The reduction of the intensity and the broadening of the peak width are due to uneven plasticization throughout the samples. It is well known that the cured epoxy contains regions with different cross-link density. The incorporation of clay filler makes the system more complex. The clay filler can affect the diffusion of the molecules during

curing and result in heterogeneity in the composite. Also clay fillers are more hydrophilic than the matrix does. Obviously the water preferentially located in areas of low cross-link density and nearby clay particles. Thus the appearance of two distinct relaxations possibly indicates the presence of two regions in the material: a more plasticized region which affords for the shoulder peak in relaxation spectrum, and a less plasticized region that gives rise to the main peak. Yet this relaxation transition behavior is still under argument **(19, 35-38)**, further investigation is needed.

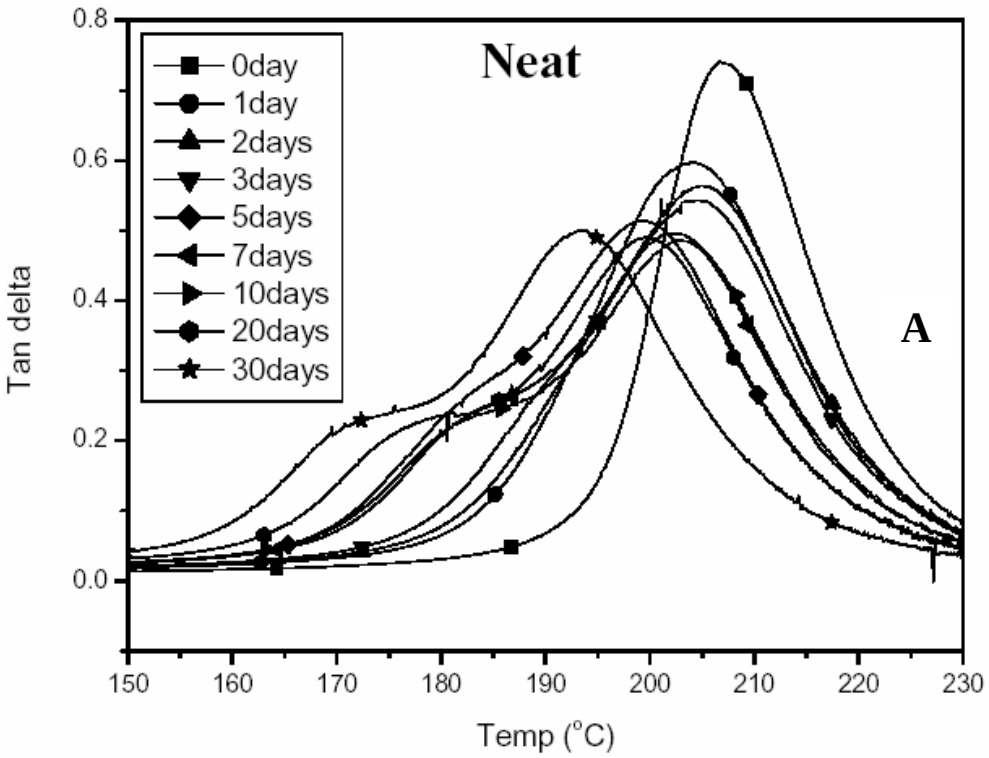

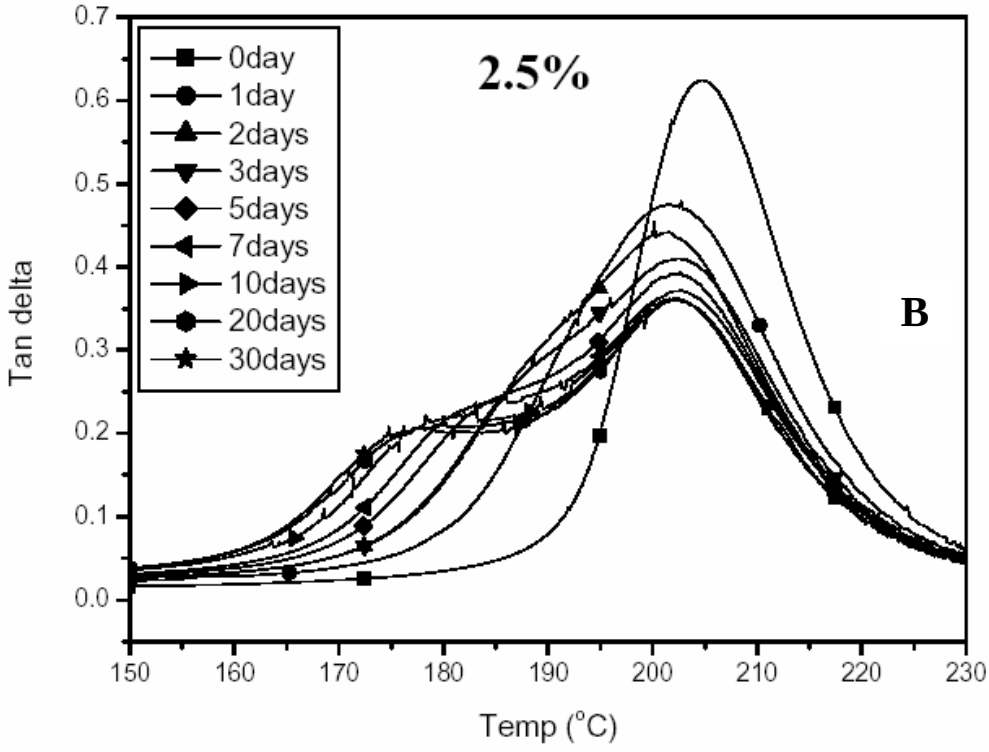

Figure 6.16. Variations of α-transition on immersion time: (A) neat epoxy; (B) nanocomposite with 2.5 wt% SMC.

6.4 Summary

A "hydro-compounding" approach has been developed for epoxy-clay nanocomposite preparation using pristine clay, which involves a new exfoliation mechanism. With this approach, the dispersion state of clay in water has been transferred into epoxy matrix by a solvent exchange step and a surface modification step. The critical step is the replacement of water with organic solvent, which facilitates the surface modification and dispersion of modified clay in epoxy matrix. The most significant feature of the new technique is that very little amount of organic modifier is required to facilitate the high exfoliation and well-dispersion of the clay. Although the reported work is based on the epoxy-clay

system, the technique may also be utilized in melt extrusion processes, thus opens up potential applications to thermoplastic polymer systems with cost effectiveness.

The storage modulus increases monotonically with clay content in glass region, and a 20% improvement was achieved with addition of 4 wt% SMC. The Tg remains constant with clay concentration, which can be attributed to the interactions between the matrix and SMC (clay and silane). An increase of Tg should be expected by improving the interactions. SMC exhibited marked effect in enhancing the Young's modulus and fracture toughness, which could be attributed to good clay dispersion. SEM investigation on the fracture surface of nanocomposites revealed that the dominant toughening mechanisms changed with an increase in clay concentration. Clusters formed in the processing were proposed to be accounted for the difference.

The hydrothermal effect on the thermal/mechanical properties of neat epoxy and epoxy-clay nanocomposite was studied. The moisture uptake significantly affects the modulus at high temperature, the tensile strength and the α-relaxation behavior. On the other hand, at low temperature, the modulus and fracture toughness was not strongly influenced. The matrix plasticized by water was proposed to be responsible for the decrease of storage modulus and the changes of relaxation behavior. As the moisture content increases, there is a reduction in strain at break for the epoxy-clay nanocomposite while that of the neat epoxy remains constant. This effect was attributed to epoxy/clay interface debonding induced by water and formation of water cluster fillers that act as defects in the composite.

References:

1. Morvan M, Espinat D, Lambard J, Zemb Th. *Colloids and Surfaces*, 1994; *A*82: 193-203.
2. Katti DR, Katti KS, Shanmugasundaram V. *Mater. Res. Soc. Symp. Proc.*, 2002; 704: 257-262.
3. Wypych F, Schreiner WH, Mattoso N, Mosca DH, Marangoni R, da S. Bento CA. *J. Mater. Chem.*, 2003; 13: 304–307.
4. Groenewold GS, Avci R, Karahan C, Lefebre K, Fox RV, Cortez MM, Gianotto AK, Sunner J, Manner W L. *Anal. Chem.*, 2004; 76: 2893-2901.
5. Lan T and Pinnavaia TJ. *Chem. Mater.*, 1994; 6: 2216-2219.
6. Liu TX, Liu ZL, Ma KX, Shen L, Zeng KY, He CB. *Polym. Compos.*, 2003; 6: 331-337.
7. Delozier DM, Orwoll RA, Cahoon JF, Johnston NJ, Smith Jr JG, Connell JW. *Polymer*, 2002; 43: 813-822.
8. Wang K, Chen L, Wu JS, Toh ML, He CB, Yee AF. *Macromolecules*, 2005; 38: 788-800.
9. Lange FF. *Philos. Mag.*, 1970; 22: 983-992.
10. Spanoudakis J, Young RJ. *J. Mater. Sci.*, 1984; 19: 487-496.
11. Carfagna S, Meo G, Nicolais L, Giamberini M, Priola A, Malucellis G. *Macromol. Chem. Phys.*, 2000; 201: 2639–2645.
12. Lee J, Yee AF. *Polymer*, 2000; 41: 8375-8385.
13. Teh, SF, Liu TX, Wang L, He CB. *Composites A*, 2005; 36: 1167-1173.

14. Wang L, The SF, Tjiu WWC, Liu TX, He CB. *Polym. Compos.*, 2005; 26: 333-342.
15. Bagheri R, Pearson RA. *Polymer*, 2000; 41: 269-276.
16. Bennet JA, Young RJ. *Comp. Sci. Technol.*, 1997; 57: 945-956.
17. Ellyin F, Maser R. *Comp. Sci. Technol.*, 2004; 64: 1863-1874.
18. Wood CA, Bradley WL. *Comp. Sci. Technol.*, 1997; 57: 1033-1043.
19. Akay M, Kong Ah Mun S, Stanley A. *Compos. Sci. Technol.*, 1997; 57: 565-571.
20. Karad SK, Attwood D, Jones FR. *Composites A*, 2002; 33: 1665-1675.
21. Browning CE. In: Browning CE and Seferis JC (Ed.). *Processing and structural properties of composites. New York: Plenum press*, (1983).
22. Mohd Ishak ZA, Tengku Mansor TSA, You BN, Ishiaku US, Karger-Kocsis. *J. Plast. Rubber. Compos. Process. Appl.*, 2000; 29: 263-270.
23. Giannelis EP. *Appl. Organomet. Chem.*, 1998; 12: 675-680.
24. LeBaron PC, Wang Z, Pinnavaia TJ. *Appl. Clay. Sci.*, 1999; 15: 11-29.
25. Gilman JW. *Appl. Clay. Sci.*, 1999; 15: 31-49.
26. Kojima Y, Usuki A, Kawasumi M, Okada A, Kurauchi T, Kamigaito O. *J. Polym. Sci.: Polym. Chem.*, 1993; 31: 983-986.
27. Wang L, Liu TX, Tjiu WWC, He CB. *Scientific Israel-Technological Advantages (SITA-Journal)*, 2005; Issue 7, in press.
28. Liu XH, Wu Q. *J. Macromol. Mater. Eng.*, 2002; 287: 180-186.
29. Becker O, Varley RJ, Simon GP. *Eur. Polym. J.*, 2004; 40: 187-195.
30. Hodzic A, Kim JK, Lowe AE, Stachurski ZH. *Compos. Sci. Technol.*, 2004; 64: 2185-2195.

31. Joseph PV. *Compos. Sci. Technol.*, 2002; 62: 1357-1372.

32. Shen J, Chen CC, Sauer JA. *Polymer*, 1985; 26: 511-518.

33. Ishak ZA, Berry JP. *Polym. Compos.*, 1994; 15: 223-230.

34. Clark Jr RL, Craven MD, Kander RG. *Composites A*, 1999; 30: 33-48.

35. Mijovic J, Lin KF. *J. Appl. Polym. Sci.*, 1985; 30: 2527-2549.

36. KeNeve B, Shanahan MER. *Polymer*, 1993; 34: 5099-5105.

37. Barton JM, Greenfield DCL. *Br. Polym. J.*, 1986; 18: 51-56.

38. Chateauminois A, Chabert B, Soulier JP, Vincent L. *Polym. Compos.*, 1995; 16: 288-296.

Chapter 7. Conclusions

The initial objective of this project, that is, to prepare epoxy-clay nanocomposites with reduced and eliminated surface modifiers, has been successfully achieved. Novel approaches were developed to disperse pristine clay and silane-modified clay (SMC) into epoxy matrix. Exfoliation mechanisms were proposed and examined by WAXS and TEM techniques.

The morphology of clay in the nanocomposites was characterized by OM, WAXS and TEM, and the results were compared with the conventional organoclay nanocomposites. In organoclay filled epoxy nanocomposites, the majority retained their face-to-face orientation (intercalated structure) although a small amount of clay does indeed exfoliate. The clay platelets existed in a mixed structure of intercalation and exfoliation throughout the matrix, as also proven by other researchers. In raw clay epoxy system, unique domain morphology was observed while the array of clay platelets that was widely reported in literature did not exist in these composites. Many aggregates formed in the matrix and which was revealed by TEM to be actually clusters of exfoliated clay platelets in a "loss cabbage" structure. The miscibility between epoxy and clay due to the hydrophilic nature of raw clay surface and the water introduced to the gallery accounted for the formation of this structure. Finally, highly exfoliated morphology was achieved in silane-modified clay-epoxy nanocomposites, while the amount of surfactant was reduced. The WAXS patterns of SMC-epoxy nanocomposites did not include any (001) scattering peak after

curing and TEM micrographs elucidated that the SMC nanolayers lost their ordered stacking structure and are exfoliated in the epoxy matrix.

Batches of nanocomposites were prepared using commercial organoclay (Southern clay 93A), silane-modified clay and pristine clay, and the effects of clay concentration on the mechanical properties of the nanocomposites were analyzed. It was shown that both toughness and stiffness were improved in all these three systems, despite the fact that it was often found that these two properties could not be simultaneously achieved. The dependence of the mechanical properties on the clay concentration varied with approaches, which could be attributed to clay dispersion. SMC showed remarkable performance in improving mechanical properties of the material. In respect of the normalized G_{IC}, an increase of 100% was achieved with incorporation of just 2 wt% SMC. However, the value of G_{IC} dropped with further addition of clay due to cluster formation at high clay concentration. In organoclay system, incorporation of 7.5 wt% clay led to 75% improvement in G_{IC}. In raw clay system, G_{IC} increased 170% with incorporation of 12.5 wt% clay, but decreased slightly with further addition of raw clay.

The process zones on the fracture surface of the neat epoxy and nanocomposites were examined using SEM to investigate the deformation behavior and toughening mechanisms. It was found that although the fracture surface morphologies of the organoclay-epoxy and pristine clay-epoxy were different, yet the underlying mechanisms were similar, which were crack pinning, shear deformation of epoxy matrix induced by clay aggregates and clay clusters breakage. But in SMC-epoxy system, the situation was quite different. In high SMC concentration nanocomposites, the fracture surface

morphology and toughening mechanisms were similar to organoclay-epoxy system. In low SMC content nanocomposites, however, the fracture surface illustrated a much finer morphology, and the fracture behavior was likely to be dominated by the clay platelets instead of the aggregates. In this situation, numerous micro-cracks generated through interface or inside gallery debonding of clay and matrix, and the micro-crack fronts propagated along the clay and resulted in a highly tortuous fracture surface. Nevertheless, quantitative comparison of these mechanisms cannot be made since it requires careful experimental evaluation of various microstructural parameters associated with them.

Chapter 8. Future work

Through the comparative study of the three different systems, the effectiveness of each approach on the clay dispersion has been verified, while each approach showed its own merits as well as drawbacks.

In organoclay system, the normally used in-situ intercalation method was employed. This approach leads to composites with a mixed structure of intercalation and exfoliation, which has been extensively proved. In addition, large amounts of organic surface modifiers are necessary to render the clay organophilic, which were observed to affect the composite properties, especially at high organoclay concentration.

In microwave-assisted pristine clay system, microwave was applied to facilitate clay dispersion. Characterization results show that a mixed intercalation and exfoliation structure was formed, and the improvements in mechanical properties were comparable with organoclay system. Nevertheless, this approach provides a new idea for preparation of epoxy-clay nanocomposite, in which no organic surfactant is used. By further improving the clay dispersion and eliminating the residual moisture, these pristine clay nanocomposites may meet the scientific need to investigate reinforcing effect of clay layers and offer commercial potential to produce high performance materials.

In silane-modified clay system, a "hydro-compounding" approach was developed to achieve clay exfoliation. With this approach, highly exfoliated clay morphology was achieved by using very little amount of surface modifier. The exfoliated clay shows remarkable improvement in mechanical properties as compared to the organo and pristine clay systems. The reinforcement is still expected to further increase by fine tune the surface chemistry of clay layers. This approach is also applicable to other thermosetting or thermoplastic systems after small modification. However, the methods are not perfect, tiny aggregates exist in high clay concentration samples, which largely influence the properties of the material.

The fracture behavior study in this work helps to explain the improvement on the mechanical properties. Yet the reinforcing effect of nanoclay layers, i.e. the nano-effect, is not clear. Therefore, future research should be focused on further improving the clay dispersion and fracture mechanisms study to understand the nano-effect of clay on the mechanical properties.

The future work includes

(1) improving the clay dispersion in microwave system, to study the effects of pristine clay on properties of epoxy nanocomposites;

(2) optimizing SMC system and study the influence of interfacial interaction on the properties and toughening mechanisms of epoxy-clay nanocomposites;

(3) applying our new methods to other polymer systems.